SILICA PRECIPITATION FROM ANALCIME DISSOLUTION

by

Elizabeth Ann Gorrepati

A dissertation submitted in partial fulfillment
of the requirements for the degree of
Doctor of Philosophy
(Chemical Engineering)
in the University of Michigan
2009

Doctoral Committee:

Professor H. Scott Fogler, Chair
Assistant Professor Joerg Lahann
Associate Professor Christian M. Lastoskie
Professor Johannes W. Schwank

To my Raja,
whose love, faith, and support,
ever-present,
mere words can never describe.

ACKNOWLEDGEMENTS

First and foremost, I wish to thank Professor H. Scott Fogler for being my advisor. I have learned so much from being his student: my problem-solving skills have grown exponentially, my data analysis skills greatly improved, and my communication skills have most definitely developed under his guidance during these last few years. He is not just a great advisor, but an incredible teacher. Under his guidance, so many other students have grown in different ways due to his great strength in teaching others. Part of being a great teacher is also sometimes having patience and understanding for students, which he has shown to me, and for which I am so very grateful.

I would like to thank my mother and father, two incredibly resilient, caring, and intelligent people, for years of encouragement and inspiration. I would like to thank my sisters, Diana and Sarah, whose love has kept me grounded for so long. A more recent addition to my family, I would like to thank my mother-in-law and father-in-law for believing in me for the last ten years. And finally, I would also like to thank my brother-in-law, Uday, who has given me happiness by welcoming me as his sister.

To my groupmates – thank you for the many times you have made me laugh and for the fun adventures we have had together. Good luck in all you undertake; I will miss every one of you.

A warm thank you to my committee members, Joerg Lahann, Christian Lastoskie, and Johannes Schwank, for their valuable input.

Finally, thank you and much love to Raja, Dan, Katie, and Kirby, without whom I would never have accomplished so much.

TABLE OF CONTENTS

LIST OF FIGURES

LIST OF TABLES

LIST OF APPENDICES

Appendix:

CHAPTER I

INTRODUCTION

Matrix acidization is a common technique used to improve recovery from petroleum wells. Acidization treatments may be very effective; production may increase to several times its former level after acidization. Because of potential production gains, over 200 millon dollars per year are spent on acidization in the U.S.

Despite widespread use of acidization, design of treatments is based on field experience and empirical rules that are not sufficient in all cases, contributing to a failure rate of 32% observed for acidization. For example, acidization of offshore wells in the Gulf of Mexico resulted in a large production decline which occurred simultaneously with the appearance of a white, powdery, precipitate. There was subsequently an overhaul of standard completion and stimulation practices[1].

Further investigations revealed that the Gulf of Mexico sandstone formations were extensively cemented with the zeolite analcime. The acid dissolution of analcime resulted in silicate species, which then precipitated in the formations. Consequently, there is a need to investigate the mechanisms and kinetics behind zeolite dissolution and simultaneous silicate precipitation. Furthermore, acid dissolution of any aluminosilicate may also result in silicate precipitation. Thus, fundamental knowledge gained from investigating silicate precipitation during zeolite dissolution may be applied to dissolution of other aluminosilicates as well.

With establishment of silicate precipitation kinetics and mechanisms, effective methods of precipitation inhibition may be developed.

Motivation for This Research

Oil-production companies are currently turning more and more towards stimulation of existing wells, rather than drilling of new wells. This results in high revenues for the oil well services industry, which carries out well stimulation procedures such as matrix acidization and hydraulic fracturing for the oil-production companies. In 2005, the oil well services industry accounted for 14% (approximately $1/7^{th}$) of the New York Stock Exchange's energy sector[2].

Matrix acidization is relatively low-tech and low-cost in comparison to hydraulic fracturing. Thus, of the stimulation treatments available, the one carried out the most often is matrix acidization. In 1994, 79% of well stimulation treatments by ARCO were acid jobs; however, the acid treatments accounted for only 20% of the total cost of well stimulation treatments for ARCO[3]. *That is, acidization is the most economical way to generate extra production capacity*. For example, a Dutch oil and gas company acidized 16 wells, increasing production from 1.5 million m^3/day to 3.6 million m^3/day at a cost of $600,000 USD. This is compared with the cost of $7.5 million USD for drilling new wells for a similar production increase[4].

However, the lower cost of matrix acidization treatments results in less time and research spent on their design, which results in a ~32% failure rate for matrix acidization treatments[3]. A different estimate by Nitters *et al.* puts the failure rate of acidization treatments at 60-70%[4]. The primary reason for these failures is poor fluid selection and

placement within a well[4,5]. It is clear that better-designed matrix acidization treatments can drastically and economically increase production from existing wells. Thus, in this research we tackle the specific problem of silica precipitation that sometimes occurs during matrix acidization. This problem has been observed in Gulf of Mexico reservoirs and is documented by Underdown[6].

There is a lack of literature to explain what happens when silica is dissolved from minerals in very acidic conditions. Most studies on silica precipitation use commercially available silica compounds and sols, and do not use minerals as the source of silica. Furthermore, most silica studies are in circum-neutral pH conditions. Thus, in our research, our aim was to describe the fundamental reactions and mechanisms that govern silica precipitation from mineral dissolution in solutions of pH < -0.3. With a fundamental understanding of reactions and mechanisms of silica precipitation, more effective matrix acidization treatments may eventually be designed.

Background

Reservoir Stimulation

Well stimulation treatments fall into two main categories: fracturing and matrix acidizing. Hydraulic fracturing involves splitting formation rock by applying pressure to a borehole. Matrix acidizing, on the other hand, involves injecting acid formulations into the wellbore at a pressure less than that required for fracturing. The acid dissolves or bypasses damage and therefore increases permeability in the wellbore area.

Matrix acidization is carried out when fracturing is ineffective, as in soft chalk formations[7]. Matrix acidization is also carried out when fracturing would extend through zone boundaries and increase undesired water and gas production[7]. The most common acid formulation is known as mud acid, a mixture of hydrochloric and hydrofluoric acid. Acidization of sandstone typically dissolves damage in the sandstone formation as opposed to creating new flow channels.

However, it is estimated that 32% of matrix acidization treatments fail to increase permeability, and in fact, the treatments often-times decrease permeability of formations. One of the main reasons for these failures is cited as poor treatment fluid selection. An example of poor fluid selection occurred during acidization of Gulf of Mexico reservoirs that contain analcime, a common, naturally-occuring zeolite[1]. Analcime reacts with hydrochloric acid to form silicon reaction products, which subsequently polymerize, precipitate, and damage formations. Our studies focus on describing the fundamental reactions and phenomenon that govern analcime dissolution and the subsequent silicon precipitation.

Zeolites

Zeolites are crystalline, microporous materials that are a subclass of aluminosilicates. The microporous nature of zeolites has found use in numerous applications such as water purification, heterogeneous catalysis, dehydration of gases, removal of sulfur from gasoline, and separation of air into nitrogen and oxygen.

Natural zeolites are found worldwide, and are formed from the chemical alteration of both igneous and sedimentary rock after deposition. Zeolites are formed in several different geological environments involving aluminosilicates and water, such as the interaction of basalt and water under hydrothermal conditions. Synthetic zeolites are manufactured from aluminosilicates under hydrothermal conditions.

The zeolite framework consists of silicon, aluminum, and oxygen atoms. The silicon and aluminum atoms form the basis of the zeolite framework, and are each tetrahedrally coordinated to four oxygen atoms. The oxygen atoms form bridges between the basis atoms, forming –Si-O-Si-, or –Si-O-Al- linkages. No –Al-O-Al- linkages are found due to the fact that aluminum atoms in zeolites carry a -1 charge (Loewenstein's rule). Also, the number of -Al-O-Si-O-Al- linkages in zeolites are minimized (Dempsey's rule).

Because aluminum atoms in zeolites carry a net charge of –1, counterions of alkali, alkali earth, or transition metal cations are chemisorbed in zeolites. The cations within the micropores may be easily exchanged for other cations, modifying the pore diameters of the zeolite. Also, water is rapidly and reversibly physisorbed in zeolite pores.

Analcime

Analcime is a zeolite with notable occurrences in Canada, Italy, Iceland, the US, Nova Scotia, and Switzerland, with a hydrated pore diameter of 2.6Å. The typical unit cell composition[8] of hydrated analcime is $Na_{16}[(AlO_2)_{16}(SiO_2)_{32}] \bullet 16\ H_2O$, sometimes alternatively written as $Na_2O{\cdot}Al_2O_3{\cdot}4SiO_2{\cdot}2H_2O$. Note the Si/Al ratio of analcime is 2 for an ideal crystal.

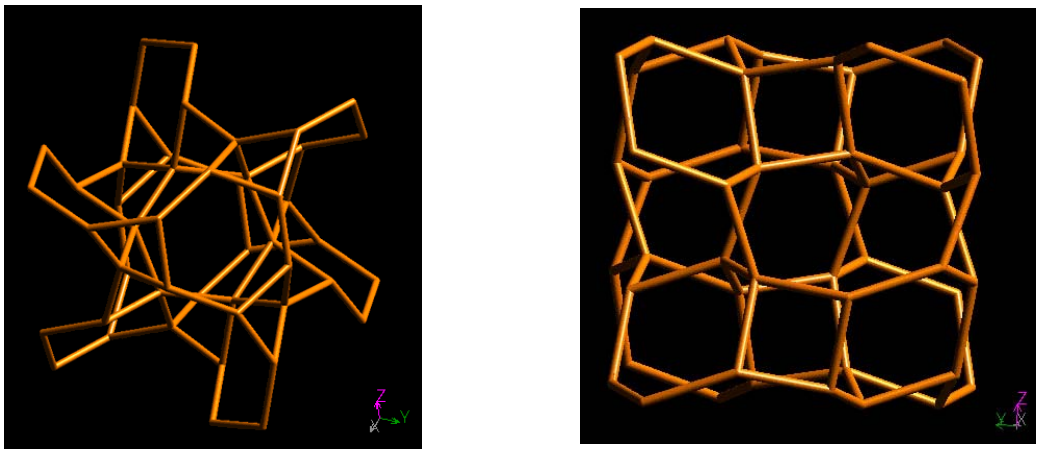

(a) (b)

Figure 1.1: Structure of analcime (a) viewed along the [111] axis (b) viewed along the [100] axis[9]. Vertices represent a Si or Al atom. Edges represent O atoms.

Dissolution of analcime in hydrochloric acid is thought to follow the reaction:

$$Na_2O{\cdot}Al_2O_3{\cdot}4SiO_2{\cdot}2H_2O + 8HCl + 2H_2O \rightarrow 2AlCl_3 + 4Si(OH)_4 + 2NaCl\ ,$$

where the products are aluminum chloride, sodium chloride, and monosilicic acid[10]. Once dissolved, the silicon can form a precipitate which could in turn block pore spaces in formations during acidization treatments.

Silica Nucleation, Precipitation, and Gelation

Monosilicic acid, $Si(OH)_4$, polymerizes in solution to form a sol, a precipitate, or a gel, depending on reaction conditions. Gels are three-dimensional, volume-spanning networks, whereas precipitates are not.

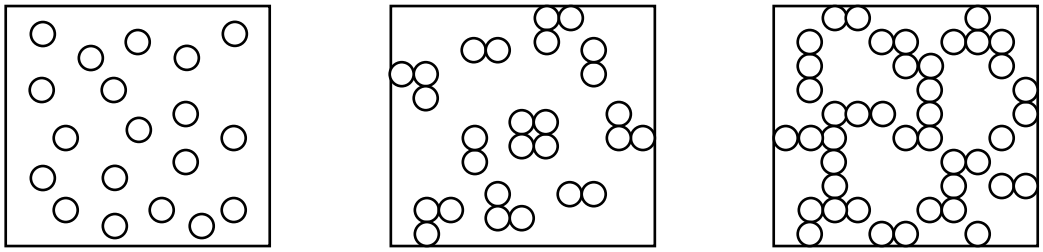

(a) (b) (c)

Figure 1.2: Two-dimensional representation of silica (a) sol (b) precipitate (c) gel (adapted from Iler[11]).

The polymerization and subsequent gelation/precipitation of silicate occurs in three steps[11]:

1) Formation of particle nuclei: monomers polymerize and cyclize to form nuclei.
2) Growth of particles: addition of monomer to particles and/or Ostwald ripening
3) Coagulation/Flocculation of particles, forming a gel or precipitate

Primary factors affecting precipitation and gelation of silicate are pH, temperature, presence of ions, and supersaturation ratio. Particles formed at pH < 7 are generally smaller than particles formed at pH 7-10. At low pH, the surfaces of silicate particles are mostly silanol –Si-OH groups. At higher pH, the silicate particles exhibit charged $–Si-O^-$ groups at the surface, which prevent coagulation and flocculation by electrostatic

repulsion. Thus, the particles formed at high pH are able to grow to larger sizes by monomer addition and Ostwald ripening. The presence of salt at high pH facilitates coagulation and flocculation by weakening the repulsion between particles.

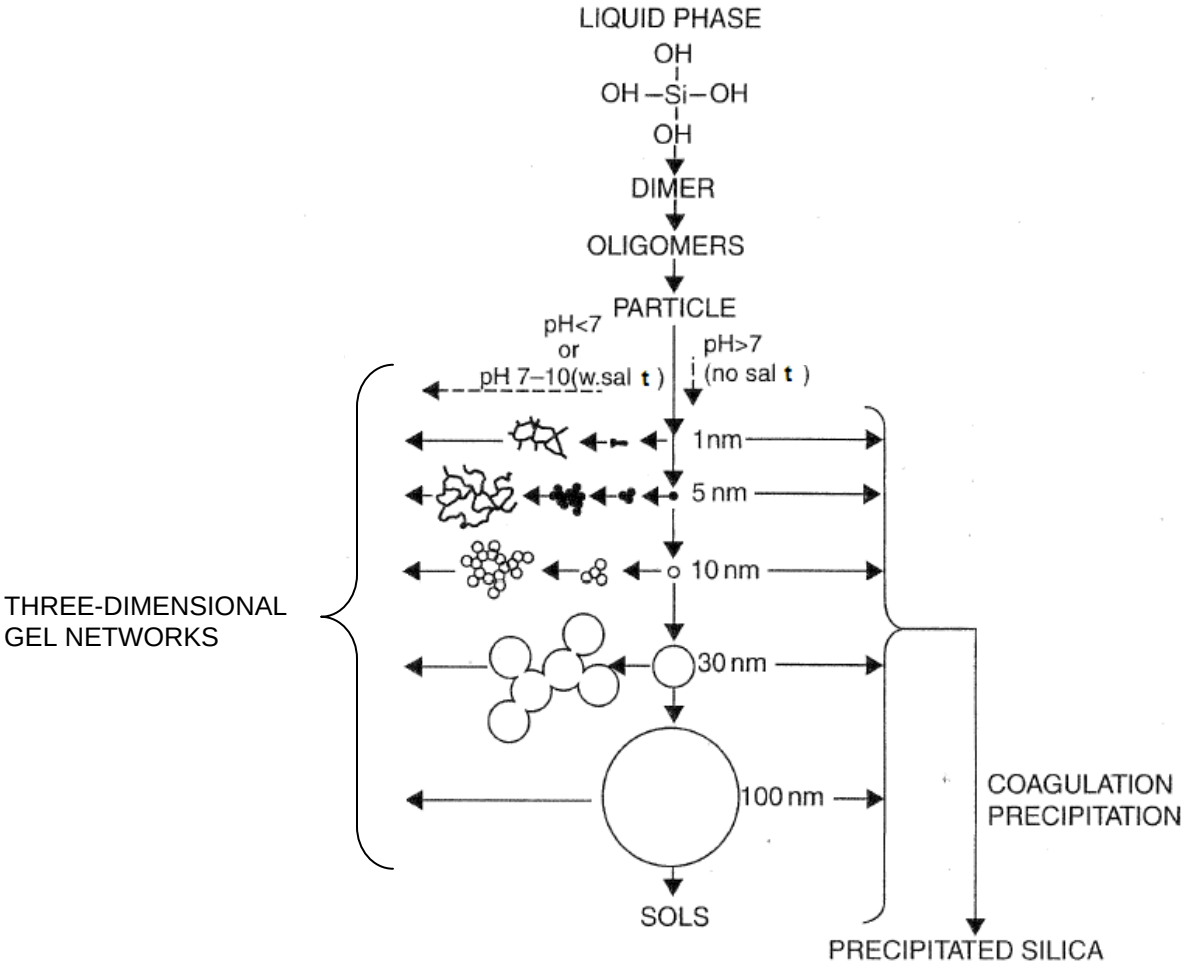

Figure 1.3: Polymerization pathways of silica (adapted from Iler[11]).

Above a pH value of 7, silica particles grow to 5-10 nm in diameter at ordinary temperature. However, at low pH, where the rate of dissolution and deposition is slower,

silica particles grow to about 2-4 nm in diameter, after which particle growth is negligible[11].

The rate of particle growth and gelation of silica sols is a minumum around pH 2, their isoelectric point, contrary to expected behaviour. Even at low concentrations of silica, 1% silica or less, silica sols may form a weak and continuous gel network[11].

Literature Survey

Dissolution of Aluminosilicates in Acid

Aluminosilicates dissolve completely and stoichiometrially in hydrofluoric acid. The dissolution of various aluminosilicates (kaolinite, sodium montmorillonite, pyrophyllite, muscovite, talc, and blotite) in HF has been shown to follow a Langmuir-Hinshelwood rate law[12]. Dissolution of analcime in hydrochloric acid was also shown follows a Langmuir-Hinshelwood rate law[13]. It has been shown that the amount and stoichiometry of zeolite dissolution in hydrochloric acid strongly depends on the initial Si:Al ratio in the zeolite.

That is, silica is removed from zeolite framework only when aluminum is removed; in other words, zeolite dissolution is aluminum-facilitated[14,15]. It is shown in Figure 4 that a higher amount of aluminum in a zeolitic framework (lower Si:Al ratio) results in a greater amount of "breaking-up" of the zeolite framework[15].

(a) Analcime

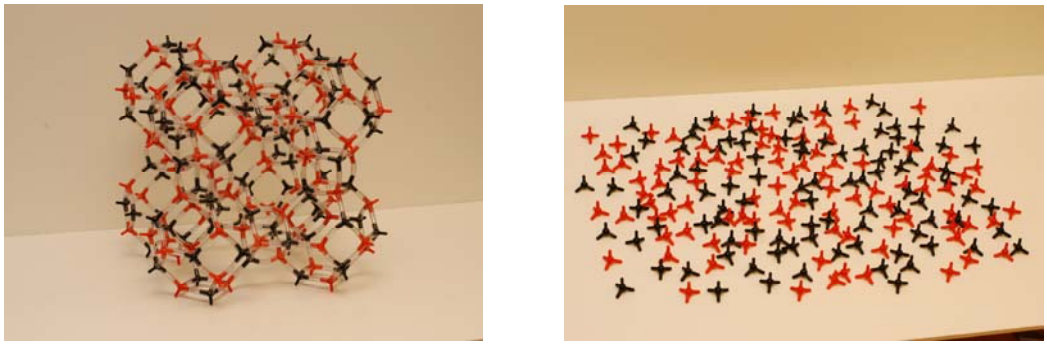

(b) Type A

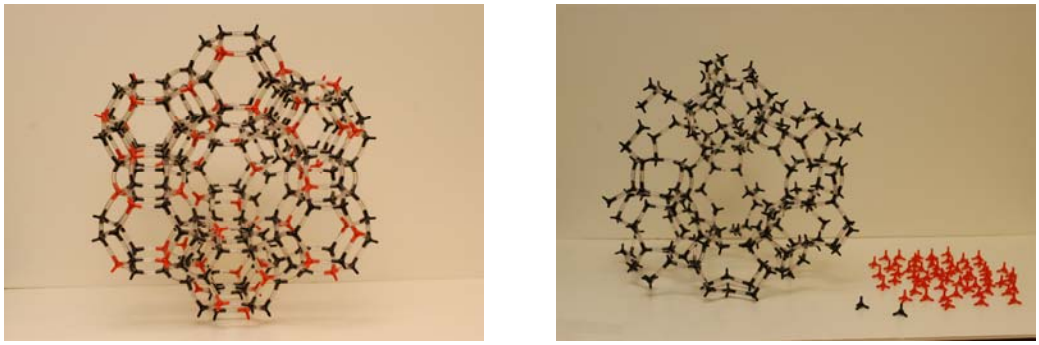

(c) Type Y

Figure 1.4: 3-dimensional models for dissolution of (a) analcime, Si:Al=2.0 (b) Type A zeolite, Si: Al ratio=1.0 (c) Type Y zeolite, Si:Al ratio=2.43. (From Hartman[15])

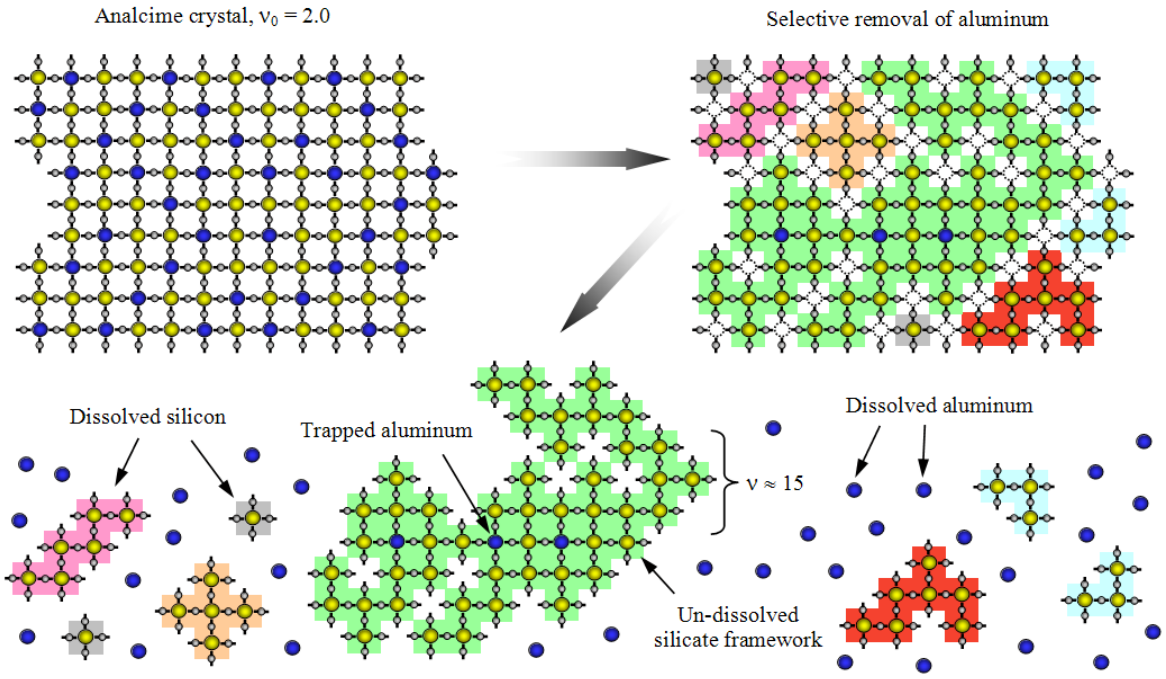

Figure 1.5: Cartoon of 2-dimensional repeating analcime units undergoing acid dissolution (From Hartman[14]).

After dissolution of analcime, Hartman observed a decline in silica concentration in solution, attributing it to polymerization and precipitation of dissolved silicate species[14].

Silica Nucleation, Precipitation, and Gelation

Most studies of silicate nucleation, precipitation, and gelation are between pH 2-11, and involve solutions of monosilicic acid or silica sols. Silicate precipitation after zeolite dissolution has been briefly studied by Hartman and Fogler[13], who concluded that precipitated silica does not affect dissolution of zeolites.

The nucleation of supersaturated solutions of monosilicic acid is generally considered to be homogenous (see Appendix C). Iler[11] states "Unless colloidal material is deliberately added, a supersaturated solution of silica undergoes spontaneous homogeneous nucleation that seems to be unaffected by small amounts of foreign matter." However, heterogeneous nucleation may take place if a suitable surface is present. Whitsitt and Barron[16] investigated the nucleation of monosilicic acid in the presence of fullerenol, and found formation of spherical silicate particles with fullerenol seeds at the particle centers. They concluded the –OH functional groups of the fullerenol surface reacted by condensation with monosilicic acid, with subsequent molecular deposition of monosilicic acid onto the particles.

Many studies of silicate nucleation exist, but the rate laws reported for nucleation are contradictory and the kinetics of monosilicic acid condensation are not completely understood. Contradictory silicate nucleation reaction orders of 1-5 have been reported[17]. The nuclei are thought to form by condensation of monosilicic acid, which is considered the monomer in nucleation/polymerization reactions. It is hypothesized that nuclei formation begins with monosilicic acid reacting to form disilicic acid, which reacts with monosilicic acid to form trisilicic acid, etc[11]. When the number of silicon atoms in the nuclei exceeds 3, the silanol –Si-O-H groups of the nuclei condense to siloxane –Si-O-Si-

bonds, forming ring structures. Once the nucleus reaches a critical size, monomer and dimer preferentially react with the nuclei and particle growth occurs[17].

After formation of the critical nuclei, particle growth occurs by condensation polymerization. The rate of condensation is controlled by an ionic mechanism[18]. Above pH 2, the rate of condensation is proportional to OH^-. Below pH 2, the rate of condensation is proportional[11] to H^+. The silica particles will undergo further *internal* condensation of internal silanol –Si-OH groups, becoming more compact structures as time progresses.

Icopini et al.[17] investigated silica nucleation in dilute solutions from pH 3-11. They found experimental evidence of a fourth order nucleation reaction and hypothesized the following reactions for nuclei formation:

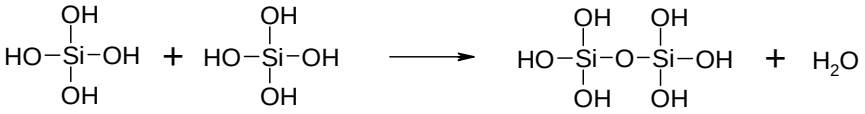
(1)

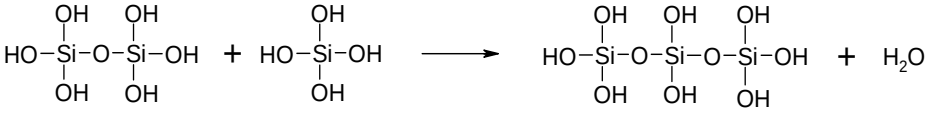
(2)

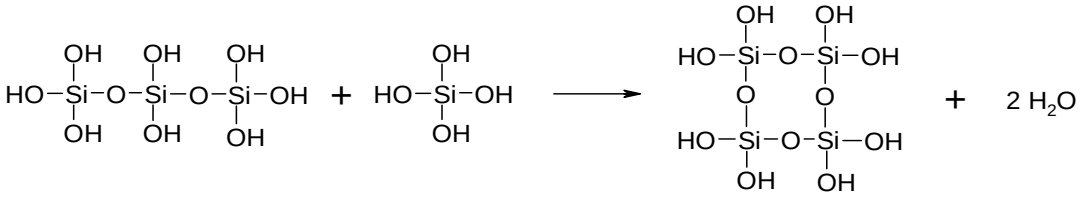
(3)

where the critical nucleus is a cyclic tetramer. The rate equation for this nucleation mechanism is $R = k_4[H_4SiO_4]^4$.

Rothbaum and Rohde[19] investigated silicate polymerization and deposition in dilute solutions at a pH value of 7.5. A rate equation was proposed to fit their

experimental data. The equation described monosilicic acid disappearance by two mechanisms: nucleation and polymerization.

$$-\frac{dx}{dt} = k_1 x^2 + k_2 \frac{x^n (x_0 - x)}{N}$$

where x is concentration of monomer, x_0 is initial degree of supersaturation of monomer, N is the average number of SiO_2 groups per polymer, and n is the average number of active sites per polymer. Rothbaum and Rohde assumed that the rate-limiting step for nucleation was the formation of dimer (the critical nucleus being disilicic acid), which results in the second-order rate law for the nucleation term. The second term describes monomer disappearance via reaction with polymer. Rothbaum and Rohde experimentally determined the value of n to be 3; thus, monomer disappearance by polymerization in their model was a 4^{th} order reaction. A drawback of the equation is that it requires knowledge of the average number of monomers in a particle and the average number of reactive sites per polymer.

The rate-determining step in polymerization of monosilicic acid is currently unknown. But some progress in unraveling polymerization kinetics was made by investigation of silicate speciation in near-neutral, dilute solutions using Si-29 NMR[20]. The study concluded that dimeric and monomeric species are in equilibrium, and furthermore, the formation of dimer is fast with a forward rate constant > 10^{-3} dm^3/mol/s.

Silicate Precipitation Inhibition

Precipitation of detrimental compounds during acidization may be inhibited by dissolution in alternative stimulation fluids, which prevent precipitation either by weaker acid strength or by chelation of metals. For example, Fredd and Fogler found that ethylenediaminetetraacetic acid (EDTA) and acetic acid chelate iron during carbonate acidization, preventing asphaltic sludge precipitation[21]. Precipitation of detrimental compounds during acidization may also be inhibited by addition of chelating agents or inhibitors to the acid formulation. For example, Tantayakom et al.[22] showed that presence of phosphonate scale inhibitors caused formation of smaller and more spherical barium sulfate particles.

Precipitation of silicate may be prevented by addition of chelating agents to solution. However, studies of silica chelation thus far are at circum-neutral pH, and not under the acidic conditions that occur during acidization. Lambert et al.[23] studied complexation of monosilicic acid with sugars at pH 11.7, and found that ribose formed a significant amount of a silicate-sugar complex. Sedah[24] studied complexation of monosilicic acid by substituted catechols, and found gallic acid to form the strongest monosilicic acid complex.

Formation Damage from Silicate Precipitation

Published studies on the mechanism of formation damage by silicate precipitation are rare. The most notable are by Gdanski[25], who conduted coreflood experiments of Berea sandstone cores. He found slower dissolution after silicon precipitation occurred, hypothesizing that dissolution was inhibited by a layer of precipitated silicon on the

formation surface. However, Gdanksi never confirmed this hypothesis. In fact, more recently, Hartman showed that precipitation of silica on analcime surface did not inhibit the dissolution of analcime[14].

Many questions remain about the mechanism of formation damage by silicate precipitation. For example, it is not known if dissolved silicon is carried further into the formation during acidization, where it then polymerizes. It is also not known if silicon causes damage by reducing the effective pore diameters in the formation or by forming bridges across pore throats, blocking off access to downstream pores. Ramachandran and Fogler[26,27] showed that colloidal particles may form multilayers on a pore wall or form hydrodynamic bridges (convective jamming) across pore throats at low Reynolds number. Futhermore, there is a possibility that silicate precipitation may actually reduce damage in formations. That is, precipitating silica may adhere potential damage-causing fines to the formation, preventing them from migrating and causing further formation damage[28].

Brief Overview of Chapters

Chapter 2, titled "Dissolution of Analcime and Subsequent Silica Precipitation in Various Acids" examines the analcime initial dissolution rates of silicon and aluminum in HCl, HBr, and HNO_3. Then, silica precipitation behavior in various strong acids is presented. It was then shown that silica precipitation and analcime dissolution are *decoupled*, that is, silica precipitation can be studied as a separate process by using monosilicic acid. Finally, it is shown by process of elimination that a condensation of silanol bonds within dissolving analcime particles occurs.

Chapter 3, titled "Silica Precipitation from Analcime Dissolution: Fundamental Mechanism and Effect of Acid Concentration" builds on Chapter 2 by examining the precipitation of silica from acidic solutions in more detail by using pure monosilicic acid solutions. Using UV-Vis, it was shown that the monomeric form of silica disappears from solution rapidly via a second-order reaction in HCl solutions. Then, using dynamic light scattering, it was shown that the monomer condenses very rapidly into ~5nm primary particles, which then flocculate to create silica flocs which grow exponentially in size. The flocculation was successfully modeling by a Smoluchowski equation modified for a geometric population balance. Finally, the rate of these processes is determined mainly by pH, with initial silicon concentration in solution having little effect on the rate.

Chapter 4, titled “Ionic Effects on Silica Precipitation in Acidic Solution” builds on Chapter 3 by conducting similar UV-Vis and dynamic light scattering experiments, but with salt added to the acidic solutions. From UV-Vis measurements, it was shown that the monomer disappearance is *third order* in the presence of salt. Dynamic light scattering showed an exponential increase in mean floc size with time. And, similarly to Chapter 3, the floc growth was modeled using a modified Smoluchowski equation. It was found that salt accelerated the monomer disappearance and floc growth. Both rates revealed the same ordering for rate acceleration by salts:

$$AlCl_3 > CaCl_2 > MgCl_2 > NaCl > CsCl > \text{No salt}$$

Chapter 5 summarizes the major findings of this research, and lastly, Chapter 6 contains suggestions for future research directions.

References

[1] Underdown, D. R.; Hickey, J. J.; Kalra, S. K. *Proceedings of 65th Annual SPE Technical Coference and Exhibition*, New Orleans, LA, 1990.
[2] Hartman, R. L. Ph.D. Dissertation, University of Michigan, Ann Arbor, MI, 2006, p.6.
[3] http://www.pttc.org/workshop_summaries/208.htm
[4] Nitters. G.; Roodhart, L.; Jongma, H.; Yeager, V.; Marten, B.; Fulton, D.; Dahl, J.; Jantz, E. SPE Annual Technical Conference and Exhibition, 1-4 October 2000, Dallas, Texas, 2000.
[5] Paccaloni, G.; Tambini, M. J. Petrol. Technol. **1993**, March, 256.
[6] Underdown, D. R.; Hickey, J. J.; Kalra, S. K. *Proceedings of 65th Annual SPE Technical Coference and Exhibition*, New Orleans, LA, 1990.
[7] Fredd, C.N. The Influence of Transport and Reaction on Wormhole Formation in Carbonate Porous Media, Ph.D thesis, University of Michigan-Ann Arbor, 1998, p.4.
[8] Breck, D. W. *Zeolite Molecular Sieves*; John Wiley and Sons: New York, 1974.
[9] http://www.iza-structure.org/databases/
[10] Hartman, R.L.; Jayasankar, A.; Jitapunhul, T.; Fogler, H. S. Industrial Affiliates Report 2003. 20th Annual Review.
[11] Iler, R. K. *The Chemistry of Silica: Solubility, Polymerization, Colloid and Surface Properties, and Biochemistry*; John Wiley & Sons: New York, 1979.
[12] Kline, W. E.; Fogler H. S. *J. Ind. Eng. Chem. Fund.* **1981**, *20*, 155.
[13] Hartman, R. L.; Fogler, H. S. *Ind. Eng. Chem. Res.* **2005**, 44, 7738.
[14] Hartman, R. L.; Fogler, H. S. *Langmuir* **2006**, *22*, 11163.
[15] Hartman, R. L.; Fogler, H. S. *Langmuir* **2007**, *23*, 5477.
[16] Whitsitt, E. A.; Barron, A. R *Chem. Commun.* **2003**, *9*, 1042.
[17] Icopini, G. A.; Brantley, S. L.; Heaney, P. J. *Geochim. Cosmochim. Acta*. **2005**, *69*, 293.
[18] Weres, O.; Yee, A.; Tsao, L. *J. Colloid Interf. Sci.* **1981**, *84*, 379.
[19] Rothbaum, H. P.; Rohde, A. G. *J. Colloid Interf. Sci.* **1979**, *71*, 533.
[20] Meinhold, R. H.; Rothbaum, H. P.; Newman, R. H. *J. Coll. Interf. Sci.* **1985**, *108*, 234.
[21] Fredd, C.N. The Influence of Transport and Reaction on Wormhole Formation in Carbonate Porous Media, Ph.D thesis, University of Michigan-Ann Arbor, 1998, p.33.
[22] Tantayakom, V.; Sreethawong, T.; Fogler, H. S.; deMoraes, F. F.; Chavaadej, S. *J. Colloid Interf. Sci.* **2005**, *284*, 57.
[23] Lambert, J. B.; Lu, G.; Singer, S. R.; Kolb, V. M. *J. Am. Chem. Soc.* **2004**, *126*, 9611.
[24] Sedah. I. F; Ohman, L.-O.; Sjöberg, S. *Acta Chem. Scand.* **1992**, *46*, 933.
[25] Gdanski, R.D. *SPE Prod. Facil.* **2000**, *15*, 279.
[26] Ramachandran, V.; Fogler, H. S. *Langmuir* **1998**, *14*, 4435.
[27] Ramachandran, V.; Fogler, H. S. *J. Fluid Mech.* **1999**, *385*, 129.
[28] Crowe, C. W. *J. Petrol. Technol.* **1986**, *39*, 233.

CHAPTER II

DISSOLUTION OF ANALCIME AND SUBSEQUENT SILICA PRECIPITATION IN VARIOUS ACIDS

Abstract

It is shown in this paper that initial dissolution rates of the zeolite analcime in the strong acids HCl, HBr, and HNO_3 are very similar and follow a Michaelis-Menten mechanism, analogous to the Langmuir-Hinselwood mechanism. The values of the Michaelis-Menten constants are calculated to be $V_{max,Si}$ equals $0.934*10^{-3}$, $0.972*10^{-3}$, $1.033*10^{-3}$ mol/g/min for HCl, HBr and HNO_3, respectively. The values of $K_{m,Si}$ are calculated to be 1.89, 2.30, and 2.35 mol/L for HCl, HBr and HNO_3, respectively. $V_{max,Al}$ values are calculated to equal $0.516*10^{-3}$, $0.522*10^{-3}$, $0.627*10^{-3}$ mol/g/min for HCl, HBr and HNO_3, respectively. The values of $K_{m,Al}$ are calculated to be 1.89, 2.44, and 2.66 mol/L for HCl, HBr and HNO_3, respectively. At proton concentrations less than 0.055M, analcime initial dissolution rate in citric acid was shown to be faster than initial dissolution rate in the strong acids studied.

Pure monosilicic acid solutions are shown to mimic the precipitation of silica dissolved from analcime in HCl. Thus, mineral dissolution and silica precipitation are *uncoupled* and pure monosilicic acid solutions may be used to study the precipitation of silicon dissolved from minerals.

Finally, it is shown that a recondensation of silanol groups within analcime occurs during acid dissolution. Furthermore, the recondensation is faster in different acids corresponding to the order $H_2SO_4 > HI > HBr > HCl > HNO_3$.

Introduction

Matrix acidization is a common technique for enhancing petroleum well productivity. Oil and/or natural gas production may increase to several times its former level after acidization. During matrix acidizing, mixtures of HCl/HF are injected into the near-wellbore region to dissolve formation minerals, to improve permeability and hence, output, of the well. The cementing minerals typically found in sandstone formations that dissolve are aluminosilicates such as feldspars, carbonates, and clays such as kaolinite, montmorillonite and illite. However, the sandstone in the Gulf of Mexico also includes the zeolite analcime. Zeolites are crystalline, microporous aluminosilicates. When analcime is present in a formation that undergoes acidization, analcime partially dissolves and then subsequently produces a powdery, white precipitate, which can block formation pores and decrease well productivity. A case study[1] revealed that analcime in Gulf of Mexico formations reacted with hydrochloric acid to form a precipitate, which was identified as a silica gel. Thus, we studied the dissolution of analcime in various acids as well as the subsequent silicate precipitation in various acids.

Previous researchers have studied dissolution of carbonates in hydrochloric acid[2,3] and aluminosilicates in hydrochloric and hydrofluoric acid mixtures[4,5,6,7,8]. In addition, the precipitations of silicates in mildly acid to alkaline solutions have been studied[9,10,11,12,13]. However, acidization typically involves high acid concentrations of 10 - 15wt% and at these low pH values, there is generally a lack of research on silicate dissolution and precipitation. Moreover, there is a shortage of research concerning zeolite dissolution *coupled* with silica precipitation. Only recently has Hartman and Fogler[6,7,8] studied the dissolution of various zeolites coupled with silicate precipitation.

Consequently, there is a need to further investigate the mechanisms and kinetics of these low pH systems. This study focuses on the dissolution of analcime in different acids, different acid concentrations and also on silicate precipitation from the analcime reaction products.

Background

The typical unit cell composition of hydrated analcime is $Na_2O \cdot Al_2O_3 \cdot 4SiO_2 \cdot 2H_2O$ (Si:Al = 2) Dissolution of analcime in hydrochloric acid is thought to follow the reaction:

$$Na_2O \cdot Al_2O_3 \cdot 4SiO_2 \cdot 2H_2O + 8HCl + 2H_2O \rightarrow$$

$$2AlCl_3 + 4Si(OH)_4 + 2NaCl + \text{larger undissolved silica particles,}$$

where the products are aluminum chloride, sodium chloride, monosilicic acid and larger undissolved silica particles[14]. It was previously established that the initial dissolution rate of analcime in hydrochloric acid follows a Langmuir-Hinshelwood mechanism, in which the proton from the acid strongly adsorbs to the analcime surface before decomposition into products[2]. Hartman also showed that the analcime dissolves in hydrochloric acid by removal of the framework aluminum, which then causes framework to break apart, releasing silica species into solution[3,4].

The monosilicic acid produced from reaction, $Si(OH)_4$, polymerizes in solution to form a sol, a precipitate, or a gel. The polymerization and subsequent gelation/precipitation of silica occurs in three steps[15]:

1) Formation of particle nuclei
2) Growth of particles: addition of monomer to particles and/or Ostwald ripening
3) Coagulation/Flocculation of particles to form a gel or precipitate, or formation of a stable silica sol.

Materials and Methods

Analcime particles from Mount St. Hilaire, Quebec (Ward Science) were pulverized with a mortar and pestle. The analcime was dry-sieved through a ASTM No.400 (38μm) sieve and the fraction <38 μm collected. This fraction was then wet-sieved through a 0.2μm filter. The particles were then dried in an oven at ~70° overnight. Thus, the particles used for this study have diameter 0.2μm<d<38μm. The acids used to dissolve analcime, hydrochloric, hydrobromic, sulfuric, and nitric acid, were all ACS grade and were obtained from Fisher Scientific. Hydroiodic acid, puriss p.a. grade, was obtained from Sigma-Aldrich. Citric Acid, ACS reagent grade, was also obtained from Sigma-Aldrich. Sodium metasilicate nonahydrate was obtained from Fisher Scientific, as were the silicon AAS/ICP standards.

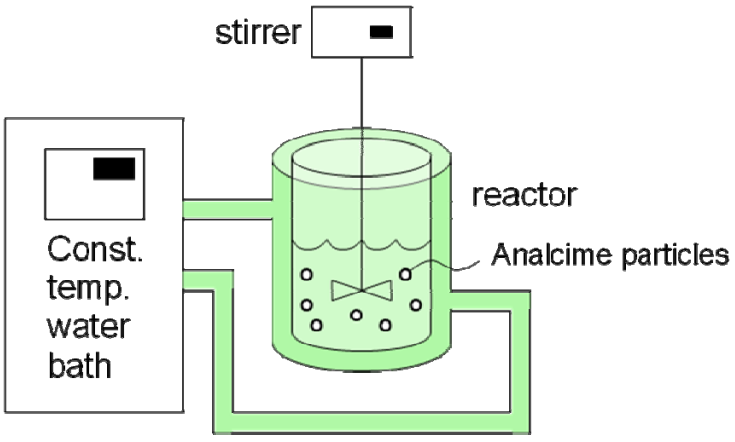

Figure 2.1: Reactor setup for analcime dissolution and pure monosilicic acid experiments.

Analcime was dissolved in acid in a 1000mL Pyrex, jacketed reactor. An overhead stirrer rotated a polyethylene impeller at 500 rpm and the circulating water bath was kept at 5.0°C during the reactions to ensure no diffusion limitations were present [6]. Samples of the reaction mixture were filtered through 0.2 micron Whatman polypropylene syringe filters and diluted before undergoing silicon and aluminum concentration analysis using either AAS (Perkin-Elmer 3100) or ICP-MS (Perkin-Elmer Elan 9000). The silicon concentrations in solution were then recorded and plotted as a function of time.

It is known that sodium metasilicate nonahydrate dissolves in water to form monosilicic acid (also known as orthosilicic acid).

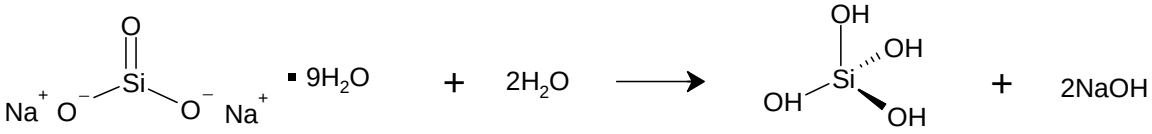

In the experiments with pure monosilicic acid, sodium metasilicate nonahydrate was pre-dissolved in deionized water in the chilled reactor. An appropriate amount of pre-cooled acid was then added to the reactor to initiate reaction. The procedure was otherwise the same as the analcime experiments.

The growing silica particle sizes were measured during reaction using dynamic light scattering (DLS) on a Malvern Zetasizer Nano ZS equipped with a 633nm red laser.

Results

Initial Dissolution Rate in Different Acids

The initial dissolution rate (IDR) method for solid-liquid reaction is based on taking data points at very short times after initiation of reaction[16]. This method ensures (1)the concentration of reactants, in this case hydrochloric acid and zeolite surface area, are virtually constant for these measured rates and (2)products are at low concentration so any reverse reaction (if any) may be neglected. The initial dissolution rate of analcime in various acids was measured using AAS or ICP-MS.

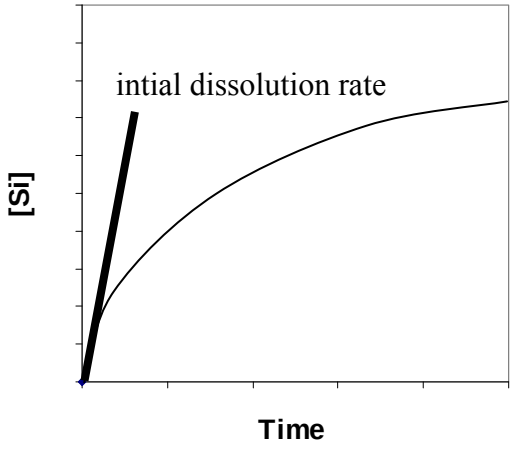

Figure 2.2: Illustration of initial dissolution rate.

As stated previously, Hartman and Fogler showed that the dissolution of analcime in hydrochloric acid follows a Langmuir-Hinshelwood mechanism[6] (analogous to the Michaelis-Menten mechanism for enzymatic reactions). For our studies, we used the Michalis-Menten equation because the Michalis-Menten constants have physical meaning:

$$-r_{i,0} = \frac{V_{MAX}[H^+]}{K_M + [H^+]}$$

,

where V_{MAX} is the theoretical maximum dissolution rate, and K_M is the $[H^+]$ concentration for half the theoretical maximum dissolution rate.

Analcime was dissolved separately in HCl, HBr, and HNO_3 to investigate the dependence of initial dissolution rate on acid anion. Figure 2.3 shows the dissolution of analcime in HCl, HBr, and HNO_3. For analcime dissolution in all three acids, the initial dissolution rate of analcime reaches a plateau at higher acid concentrations as the analcime surface becomes saturated with H^+, reaching a maximum dissolution rate. This result is consistent with a Langmuir-Hinshelwood dissolution mechanism for all three acids in which the proton reversibly absorbs onto the analcime surface, and then irreversibly dissociates into reaction products. Furthermore, the initial dissolution rates of silicon and aluminum from analcime does not vary with change of acid anion.

The initial dissolution rate of silicon is approximately twice that of aluminum in all three acids (see Table 2.1). That is, the initial silicon and aluminum dissolution rates are stoichiometric for analcime. Note that this observation shows up the in Michael-Menten constants: the value of $V_{max,Si}$ is approximately twice that of $V_{max,\ Al}$ and furthermore, the $K_{m,Si}$ and $K_{m,Al}$ are approximately equal. Thus, $-r_{Si,0} \approx 2*-r_{Al,0}$ at a given proton concentration .

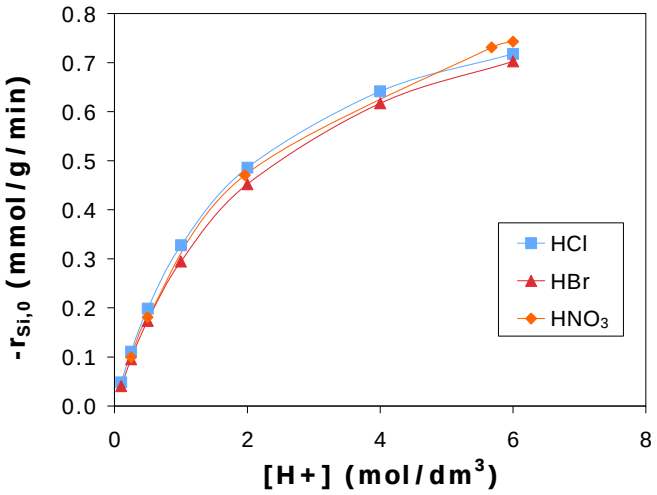

(a) silicon

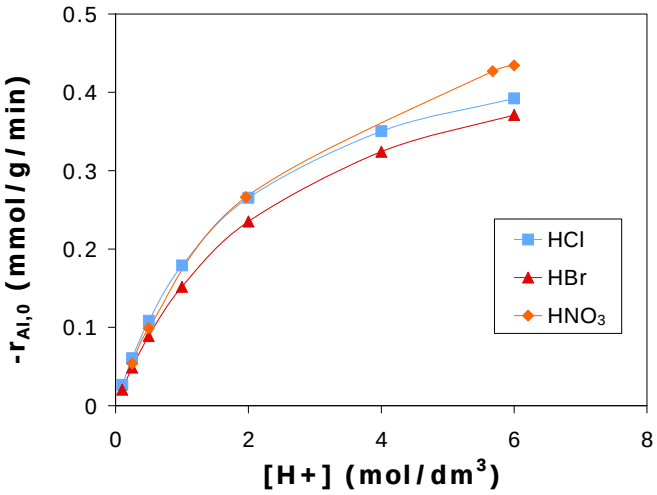

(b) aluminum

Figure 2.3: Initial dissolution rates of analcime in HCl, HBr, and HNO_3 (a) initial dissolution rates of silicon (b) intial dissolution rates of aluminum. *1 g analcime, 300 mL fluid, 5.0°C, 500RPM, d_p<38μ*m.

The Michaelis-Menten constants for the data in this study are given in Table 2.1.

Table 2.1: Michaelis-Menten constants for analcime dissolution in HCl, HBr, and HNO_3.

Acid	$V_{MAX, Si}*10^3$ (mol/g•min)	$K_{M, Si}$ (mol/L)	$V_{MAX, Al}*10^3$ (mol/g•min)	$K_{M, Al}$ (mol/L)
HCl	0.934	1.883	0.516	1.885
HBr	0.972	2.300	0.522	2.440
HNO_3	1.033	2.345	0.627	2.659
HCl (From Hartman thesis)	1.06	1.31	0.62	1.75
Citric Acid†	0.326	0.441	0.201	0.377

†These values are calculated for the equation $-r_{i,0} = \frac{V_{MAX}[\text{Citric Acid}]}{K_M + [\text{Citric Acid}]}$

All other values in the table calculate for the equation $-r_{i,0} = \frac{V_{MAX}[H^+]}{K_M + [H^+]}$

However, the initial dissolution rate of analcime in citric acid differs from the rate in HCl, HBr, and HNO_3. As seen in Table 2.1, the maximum dissolution rate in HCl, HBr, and HNO_3 is approximately $1*10^{-3}$ mol/g/min, while in citric acid the maximum dissolution rate is only $0.33*10^{-3}$ mol/g/min. Figures 2.4a and 2.4b show the initial dissolution rates in citric acid with the citric acid concentration converted to proton concentration. Comparing the initial dissolution rate of analcime versus $[H^+]$ in the different acids, it is seen that for $[H^+] < 1M$, the initial dissolution rate in citric acid is faster than that in the monoprotic strong acids. And conversely, for $[H^+] > 1M$, the initial dissolution rate in the strong acids is faster than that in citric acid, an organic triprotic acid. However, the maximum concentration of citric acid in aqueous solution at 5°C is approximately 3M, equivalent to $[H^+]=0.055M$. Thus, for $[H^+]<0.055M$ the initial dissolution rate in citric acid is faster than that in the strong acids; $0.055M<[H^+]<1M$ the

initial dissolution rate in citric acid would be faster, but these solutions are not physically possible; $[H^+]$>1M the initial dissolution rate in the strong acids are faster.

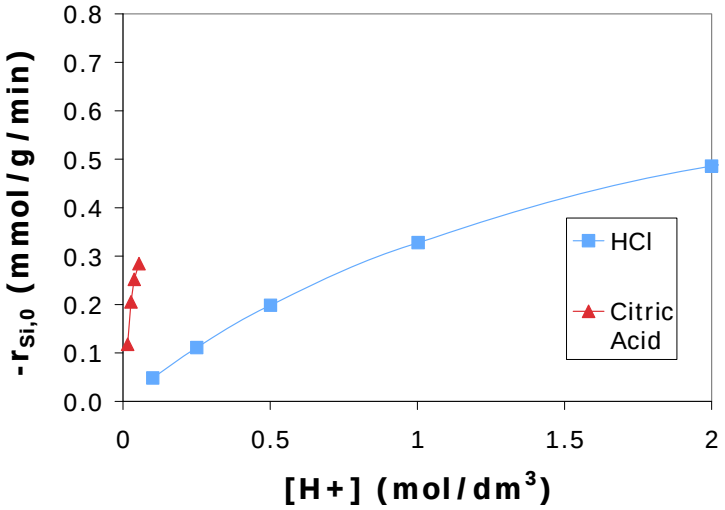

(a) silicon

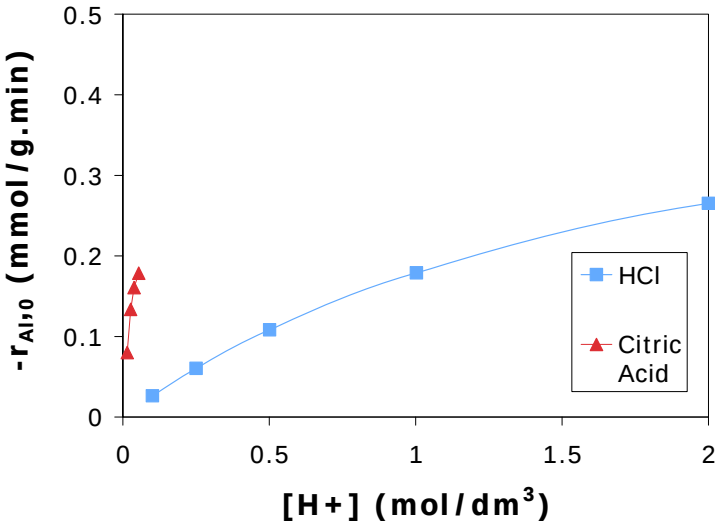

(b) aluminum

Figure 2.4: Initial dissolution rate of analcime in citric acid (a) initial dissolution rate of silicon in strong acid and citric acid (b) initial dissolution rate of aluminum in strong acid and citric acid. *0.5 g analcime, 300 mL fluid, 5.0°C, 500RPM, d_p<38μ*m.

Silicon Concentration Trajectories in Different Acids

Analcime was dissolved in HCl, HBr, HI, HNO_3, and H_2SO_4 while keeping the proton concentration constant at 8M between all five experiments. As can be seen in Figure 2.5, different acids affect the plateau height and the subsequent silicon precipitation. The varying plateau heights in different acids is shown to be a result of a recondensation of silanol groups (-Si-OH) within the analcime (see Chapter 3). That is, a lower plateau height implies that the recondensation reaction within dissolving analcime occurs faster. Thus, we can conclude that the recondensation reaction occurs faster in the acid order H_2SO_4 > HI > HBr > HCl > HNO_3. On the other hand, the different silica precipitation behaviour will be examined in more detail in the next section.

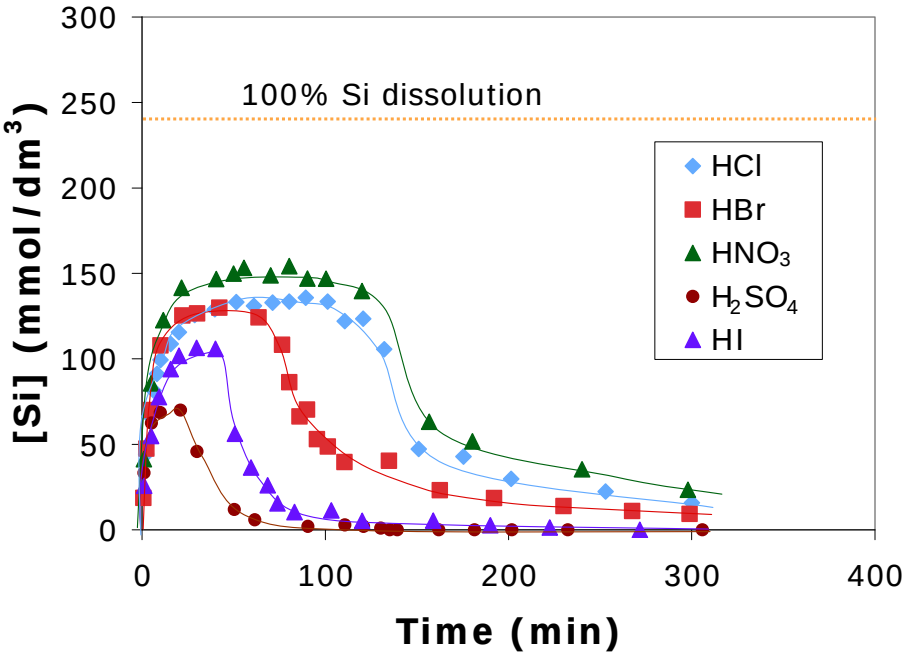

Figure 2.5: Silicon concentration profiles in HCl, HBr, HI, HNO_3, and H_2SO_4 with $[H^+]$=8M in all acids. *8 g analcime, 300 mL fluid, 5.0°C, 500RPM, d_p<38μm.*

Table 2.2: Silicon precipitation onset time and Silicon Plateau Height in Different Acids ($[H^+]$=8M for each acid).

Acid	τ_{onset} **(min)**	**Plateau Height (mmol/L)**
HCl	135	135
HBr	75	130
HNO_3	140	150
H_2SO_4	25	70
HI	40	105

We examine the silicon profile in HCl in more detail here. As the analcime dissolves, one observes three distinct regions in the silicon profile, as shown in Figure 2.6. In region 1, the silicon concentration in solution increases as the acid attacks the analcime, reaching a concentration plateau, which is less than 100% dissolved. In region 2, the silicon concentration measure by AAS stays virtually constant. Finally, in region 3, the silicon concentration in solution decreases, as silicon precipitates from solution.

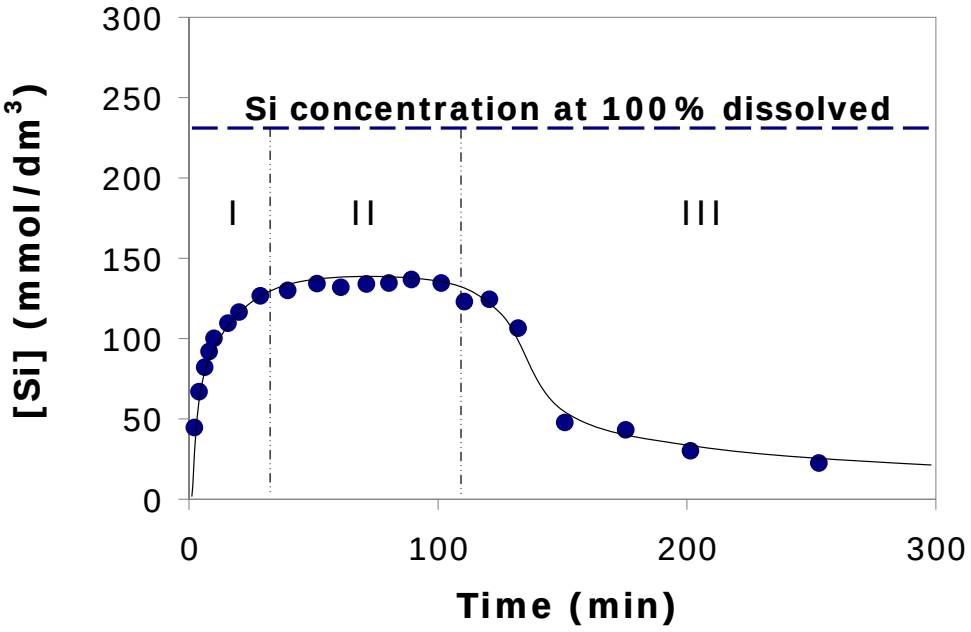

Figure 2.6: Silicon concentration during dissolution of 8g analcime in 300mL of 8M HCl. *Region 1*: Dissolution of analcime. *Region 2*: Silica particle growth. *Region 3*: Silica particles grow large enough to be filtered from solution.

We hypothesized that the silica precipitation happens independently of analcime dissolution. Thus, we examined the behaviour of pure monosilicic acid in solution. The initial concentration of monosilicic acid in solutions was the same as the silicon concentration at the analcime plateau height.

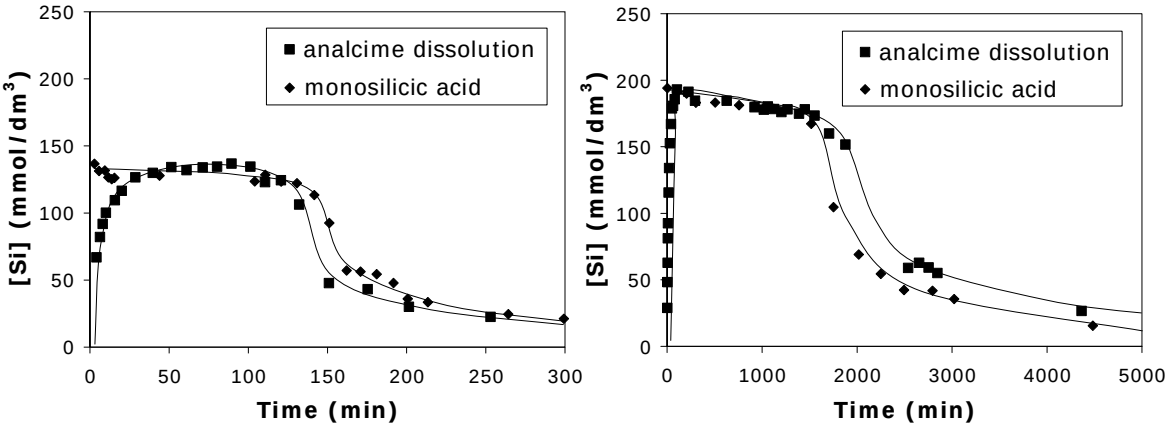

(a) 8M HCl (b) 4M HCl

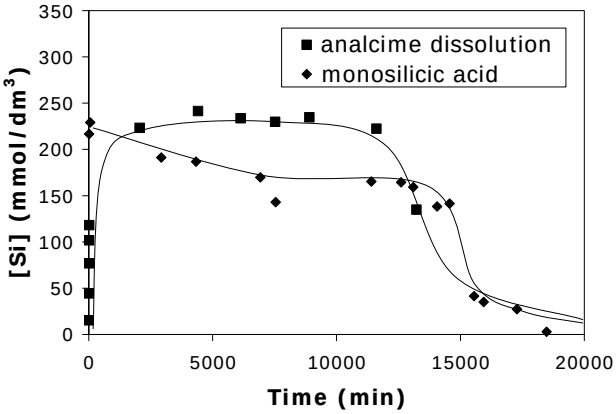

(c) 2M HCl

Figure 2.7: Comparison of silicon concentration profiles during analcime dissolution and monosilicic acid polymerization in 8, 4 and 2M HCl. *300 mL fluid, 5.0°C, 500RPM.*

We observed from Figure 2.7 that pure monosilicic acid precipitates in the same manner as the silicon dissolved from analcime. Thus, we conclude that analcime dissolution and silicon precipitation are *uncoupled*; that is the two processes do not affect each other. Using pure monosilicic acid to study the precipitation of silicon has the advantage of not containing undissolvable siliceous particles which remain the analcime systems.

Conclusions

- Analcime initial dissolution rate in the strong acids HCl, HBr, and HNO_3 follows a Langmuir-Hinselwood mechanism.
- At very low proton concentrations, analcime initial dissolution rate is faster in citric acid than in strong acids. However, at proton concentration greater than 1M, the analcime initial dissolution rate is faster in strong acids than in citric acid.
- Recondensation of silanol groups within analcime occurs faster in different acids corresponding to the order H_2SO_4 > HI > HBr > HCl > HNO_3.
- Pure monosilicic acid solutions may be used to study the precipitation of silicon dissolved from minerals because mineral dissolution and silica precipitation are *uncoupled*.

References

[1] Underdown, D. R.; Hickey, J. J.; Kalra, S. K. *Proceedings of 65th Annual SPE Technical Coference and Exhibition*, New Orleans, LA, 1990
[2] Lund, K.; Fogler H. S.; McCune, C.C. *Chem. Eng. Sci.*, **1973**, *28*, 691.
[3] Lund, K.; Fogler H. S.; McCune, C.C. *Chem. Eng. Sci.*, **1975**, *30*, 825.
[4] Kline, W. E.; Fogler H.S. *J. Colloid Interface Sci.*, **1981**, *82*, 93.
[5] Kline, W. E.; Fogler H.S. J. *Ind. Eng. Chem. Fund.* **1981**, *20*, 155.
[6] Hartman, R. L.; Fogler, H. S. *Ind. Eng. Chem. Res.* **2005**, 44, 7738
[7] Hartman, R. L.; Fogler, H. S. *Langmuir* **2006**, *22,* 11163.
[8] Hartman, R. L.; Fogler, H. S. *Langmuir* **2007**, *23,* 5477.
[9] Icopini, G. A.; Brantley, S. L.; Heaney, P. J. *Geochim. Cosmochim. Acta.* **2005**, *69*, 293.
[10] Crerar, D. A.; Axtmann, E. V.; Axtmann, R. C. *Geochim. Cosmochim. Acta* **1981**, *45*, 1259.
[11] Rothbaum, H. P.; Rohde, A. G. *J. Colloid Interf. Sci.* **1979**, *71*, 533.
[12] Makrides, A. C.; Turner, M.; Slaughter, J. *J. Colloid Interf. Sci.* **1980**, *73*, 345.
[13] Alexander, G.B.; Heston, W.M.; Iler, R.K., *J. Phys. Chem.* **1954,** *58*, 453.
[14] Hartman, R.L.; Jayasankar, A.; Jitapunhul, T.; Fogler, H. S. Industrial Affiliates Report 2003. 20th Annual Review.
[15] Iler, R. K. *The Chemistry of Silica: Solubility, Polymerization, Colloid and Surface Properties, and Biochemistry*; John Wiley & Sons: New York, 1979.
[16] Fogler, H. S. Chemical Reaction Engineering; Prentice Hall PRT: Upper Saddle River, NJ, 2005.

CHAPTER III

SILICA PRECIPITATION FROM ANALCIME DISSOLUTION: FUNDAMENTAL MECHANISM AND EFFECT OF ACID CONCENTRATION

Abstract

Silicon dissolved from zeolite analcime particles was shown to precipitate from solution under very acidic conditions ([HCl]=2 to 8M). Reaction rate studies were carried out in a batch reactor by monitoring the product concentrations using AAS or ICP-MS. Pure monosilicic acid solutions (prepared from sodium metasilicate nonahydrate) were shown to exhibit similar precipitation behavior as silicon dissolved from analcime. Thus, the precipitation of silicon from analcime dissolution was found to be is decoupled from the dissolution behavior, so that these processes may be studied separately.

Monosilicic acid solutions were used to study silicon precipitation behavior using UV-Vis and DLS techniques. It was shown by UV-Vis that monosilicic acid disappears rapidly from solution via a second order reaction under very acidic conditions. Within the first few minutes, the monosilicic acid has virtually all condensed and polymerized to form primary particles of ~5nm in diameter. These primary particles then flocculate, with the mean floc diameter increasing exponentially in size, as measured by DLS. Both the monomer disappearance rate and the flocculation rate were shown to

increase by orders of magnitude when the HCl concentration was increased from 2M to 8M

Introduction

Matrix acidization is a common technique for enhancing petroleum well productivity. Oil and/or natural gas production may increase to several times its former level after acidization. During matrix acidizing, HCl or mixtures of HCl/HF are injected into the near-wellbore region to dissolve formation minerals, increasing formation permeability and thus the output of the well. For example, in sandstone formations, the cementing minerals such as feldspars, carbonates, and clays such as kaolinite, montmorillonite and illite will dissolve, but bulk silica particles will not dissolve. However, up to 30% of matrix acidization treatments are not successful, in that the formation permeability may stay the same or even decrease after acidization. A case study revealed that when the zeolite analcime in Gulf of Mexico formations was dissolved with hydrochloric acid it produced a silica gel precipitate that blocked the pore space thereby restricting the flow of oil out of the reservoir[1]. Consequently, the widespread geological presence of analcime is an obstacle to the use of matrix acidization. Thus, in this study, we examined the reaction of hydrochloric acid with analcime.

Previous researchers have studied dissolution of carbonates in hydrochloric acid[2,3]and aluminosilicates in hydrochloric and hydrofluoric acid mixtures[4,5,6,7,8]. In addition, the precipitation of silicate in mildly acid to alkaline solutions has been studied[9, 10, 11, 12, 13, 14, 15, 16, 17, 18, 19]. However, acidization typically involves acid concentrations of 10 - 15wt%. At these low pH values, there are a lack of predictive

models and mechanisms to describe silicate precipitation. Moreover, there are insufficient studies concerning the dissolution of analcime coupled with precipitation. Only recently, studies on the dissolution of various zeolites coupled with silicate precipitation[6,7,8] have been carried out. Consequently, there is a need to further investigate the reaction mechanisms and kinetics of these low pH, dissolution-precipitation systems. This study focuses on the dissolution of analcime in solutions of different hydrochloric acid concentrations and the subsequent silicate precipitation from the analcime reaction products. The silicate precipitation was further studied using pure monosilicic acid.

Background

The typical unit cell composition of hydrated analcime is $Na_2O \cdot Al_2O_3 \cdot 4SiO_2 \cdot 2H_2O$ (Si:Al = 2). Dissolution of analcime in hydrochloric acid follows the reaction:

$$Na_2O \cdot Al_2O_3 \cdot 4SiO_2 \cdot 2H_2O + 8HCl + 2H_2O \rightarrow$$

$$2AlCl_3 + 4Si(OH)_4 + 2NaCl + \text{larger undissolved silica particles,} \qquad (3.1)$$

where the products are aluminum chloride, sodium chloride, monosilicic acid and larger undissolved silica particles[20]. It has been previously shown[7,8] that the analcime dissolves in hydrochloric acid by removal of framework aluminum, which then causes framework to break apart, releasing silica species into solution.

The monosilicic acid produced from reaction, $Si(OH)_4$, polymerizes in solution to form a sol, a precipitate, or a gel. The polymerization and subsequent gelation/precipitation of silica occurs in three steps[21]:

1) Formation of particle nuclei
2) Growth of nuclei: addition of monomer to nuclei
3) Coagulation/Flocculation of particles to form a gel or precipitate, or formation of a stable silica sol.

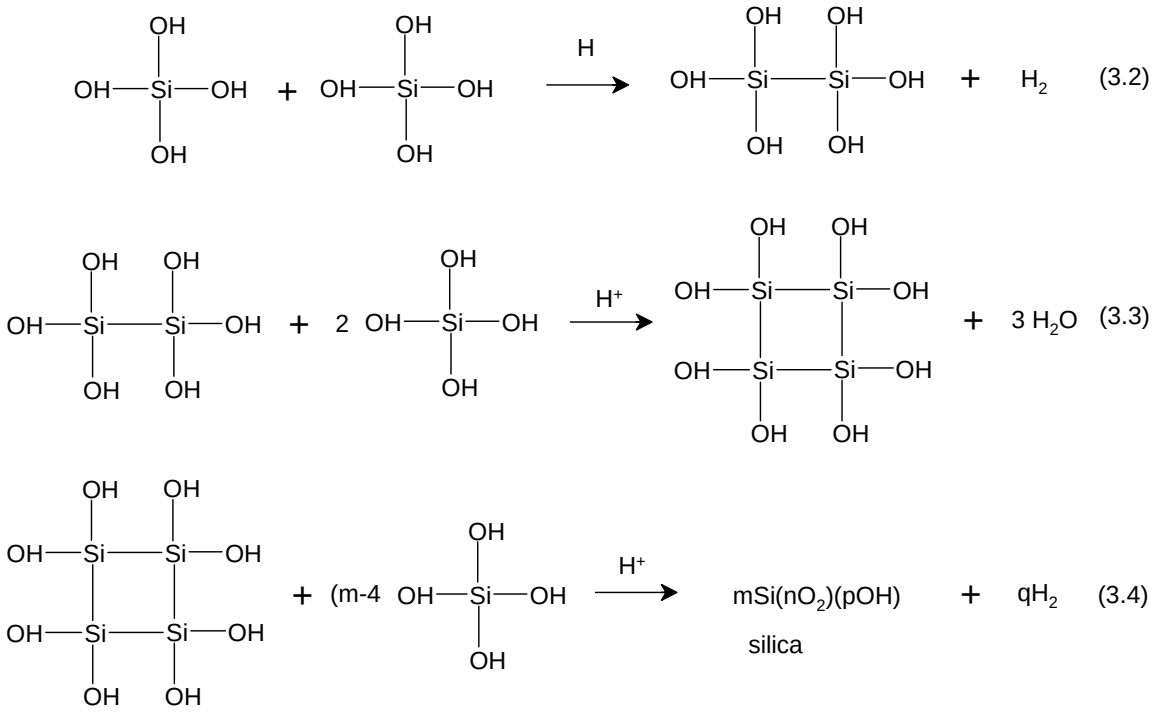

Figure 3.1: Polymerization of silica for critical nucleus.

In the above reaction schematic, the tetramer may be thought of as the silica nucleus[22]. As monosilicic acid adds to a nucleus, the silica particle tends to cyclize, forming a sphere. In other words, the silanol –Si-OH groups within a particle tend to undergo intraparticle condensation, forming a more compact particle[21]. The variable n in Figure 3.1 is a measure of the degree of condensation of the formed silica particle. n=1 indicates

that all the silanol (-Si-OH) groups within the silica particle have condensed to siloxane (-O-Si-O-) groups. n=0 indicates that there is no condensation of silanol (-Si-OH) groups within the particle

The primary factors affecting the polymerization/precipitation/gelation of silica are pH, temperature, and supersaturation ratio[21]. Particles formed at pH values less than 7 are generally smaller than particles formed at pH values between 7 and 10. At low pH values, the surfaces of silica particles are mostly –Si-OH groups. At *higher pH*, charged –Si-O $^{-}$ groups are present at the silica particle surface, which prevent coagulation and flocculation by double-layer electrostatic repulsion[21]. Thus, particles formed at *high pH* values are able to grow to large sizes by monomer addition and Ostwald ripening. The presence of salt at high pH values facilitates coagulation and flocculation by weakening the electrostatic repulsion between particles.

Materials and Methods

Analcime particles from Mount St. Hilaire, Quebec (Ward Science) were pulverized with a mortar and pestle. The analcime was dry-sieved through an ASTM No.400 (38μm) sieve and the fraction <38 μm collected. This fraction was then wet-sieved through a 0.2μm filter and then dried overnight in an oven at ~70°. Thus, the particles used for this study have diameter 0.2μm<d<38μm. The hydrochloric acid used to dissolve analcime was ACS grade obtained from Fisher Scientific. Sodium metasilicate nonahydrate was obtained from Fisher Scientific, as were the silicon AAS/ICP standards.

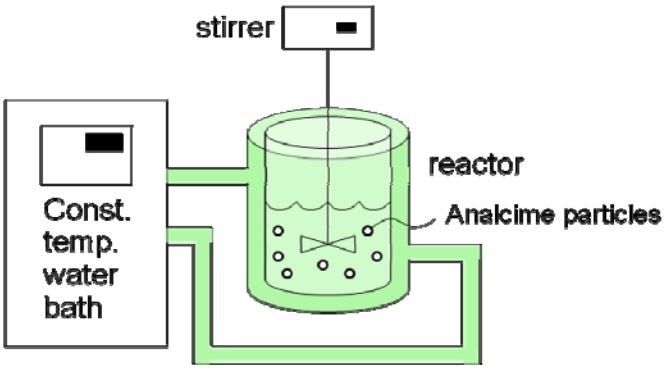

Figure 3.2: Reactor setup for analcime dissolution and pure monosilicic acid experiments.

Analcime was dissolved in acid in a 1000mL Pyrex, jacketed reactor shown schematically in Figure 3.2. An overhead stirrer rotated a polyethylene impeller at 500 rpm and the circulating water bath was kept at 5.0°C during the reactions; under these conditions analcime dissolution is reaction-limited[23]. Samples of the reaction mixture were filtered through 0.2 micron polypropylene syringe filters (Whatman) and diluted before undergoing analysis for silicon using AAS (Perkin-Elmer 3100) or ICP-MS (Perkin-Elmer Elan 9000). The silicon concentration in solution was then plotted as a function of time.

It is known that sodium metasilicate nonahydrate dissolves in water to form monosilicic acid (also known as orthosilicic acid).

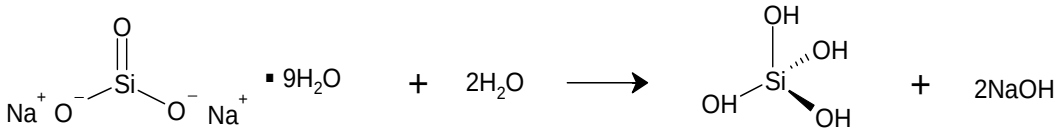

(3.5)

In the experiments with pure monosilicic acid, sodium metasilicate nonahydrate was pre-dissolved in deionized water in the chilled reactor. An appropriate amount of pre-cooled acid was then added to the reactor to initiate reaction. The procedure was otherwise the same as the analcime experiments.

The monosilicic acid ($Si(OH)_4$) concentration was followed during the reaction using a colorimetric method (ASTM D859-05). In this procedure, monosilicic acid reacts with a ammonium molybdate ((NH4)6Mo7-O 24·4H2 O) to produce yellow silicomolybdate compound which is then reduced to a blue silicomolybdate compound. The concentration of the blue silicomolybdate compound is then measured by the absorbance of light at 640 nm. This absorbance was measure via a UV-VIS spectrophotometer (model Cary Varian Bio 100).

It is known that the monomer form of silica, monosilicic acid forms silicomolybdate compound. However, higher order compounds such as dimeric silica and trimeric silica may and also react quickly with the molybdate. Because of this ambiguity, the silica that reacts with ammonium molybdate is given the general terminology "molybdate-reactive silica". However, the majority of "molybdate-reactive silica" is known to be monosilicic acid, with dimeric and trimeric silica possibly contributing to the measured concentration[16,18,24,25]. Thus, in this paper, we equate concentration of "molybdate-reactive silica" to concentration of monosilicic acid.

The growing silica particle sizes were measured during reaction using dynamic light scattering (DLS) on a Malvern Zetasizer Nano ZS equipped with a 633nm red laser.

Results

Analcime Dissolution in Hydrochloric Acid

The dissolution of analcime in 8M hydrochloric acid at 5°C will be referred to as the base case and compared with other HCl concentrations and acids. As the analcime dissolves, one observes three distinct regions in the silicon profile as shown in Figure 3.3. In region 1, the silicon concentration in solution increases as the acid attacks the analcime, reaching a concentration plateau. The silica in the analcime is less than 100% dissolved. In region 2, the silicon concentration in solution measured by AAS stays virtually constant. Finally, in region 3, the silicon concentration in solution decreases, as silicon precipitates from solution. Previous work showed that framework aluminum in zeolites always dissolves virtually 100% in HCl[6,7].

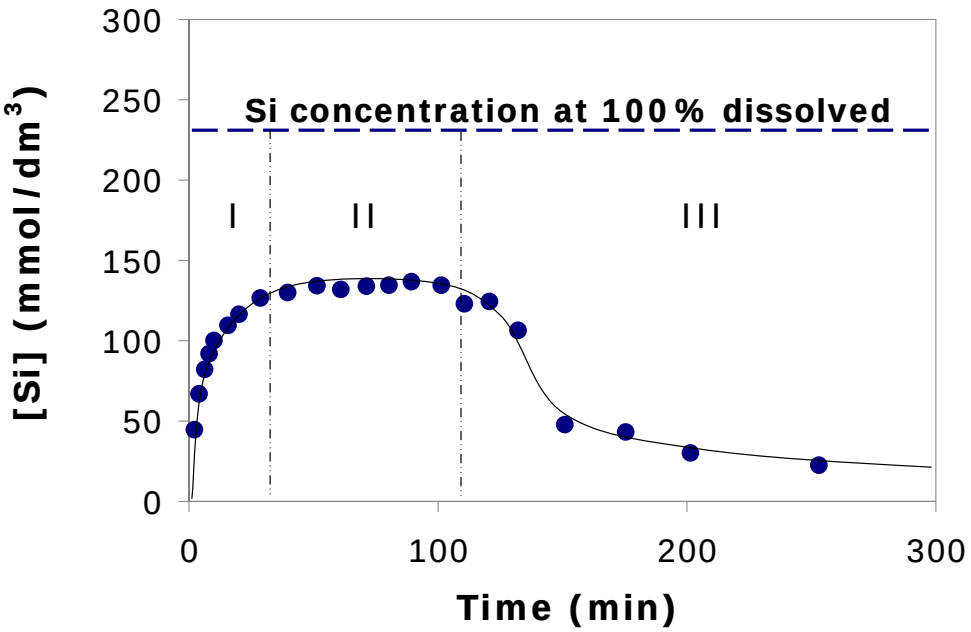

Figure 3.3: Silicon concentration during dissolution of 8g analcime in 300mL 8M HCl. *Region 1*: Dissolution of analcime. *Region 2*: Silica particle growth. *Region 3*: Silica particles grow large enough to be filtered from solution.

Analcime was dissolved in 2M, 4M, 8M, and 12M HCl. The entire silicon concentration profiles for these experiments are given in Figure 3.4. From the AAS measurements, one observes that a higher percentage of silicon dissolves from analcime at lower hydrochloric acid molarities.

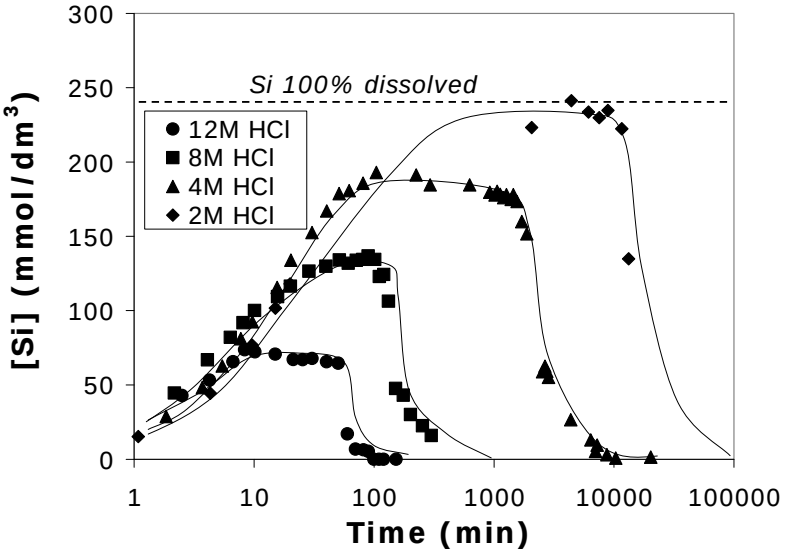

Figure 3.4: Silicon concentration in solution versus time in 12M, 8M, 4M, and 2M HCl. *8 g analcime, 300 mL fluid, 5.0°C, 500RPM, d_p<38μm.*

Furthermore, it has been shown that increasing the dissolution temperature does not change the silicon plateau height[13,26]. The temperature invariance of the plateau height suggests equilibrium between undissolved analcime and silicon in solution is determining the plateau height.

Our first hypothesis was that the undissolved silicious analcime particles were in equilibrium with dissolved silicon in solution. Thus, we tested if undissolved siliceous analcime particles from 8M HCl would dissolve further in 4M HCl. Undissolved silicious analcime particles 8M HCl were collected 30 minutes into reaction. At 30 minutes, the silicon is just reaching the plateau (Figure 3.3). The particles were collected

on a 0.2 micron filter and then dried. The particles were then immersed into a fresh 4M HCl solution, but the analcime particles exhibited little to no dissolution as measured by AAS (Figure 3.5). Therefore, the plateau height is not determined by undissolved siliceous analcime particles in equilibrium with solution.

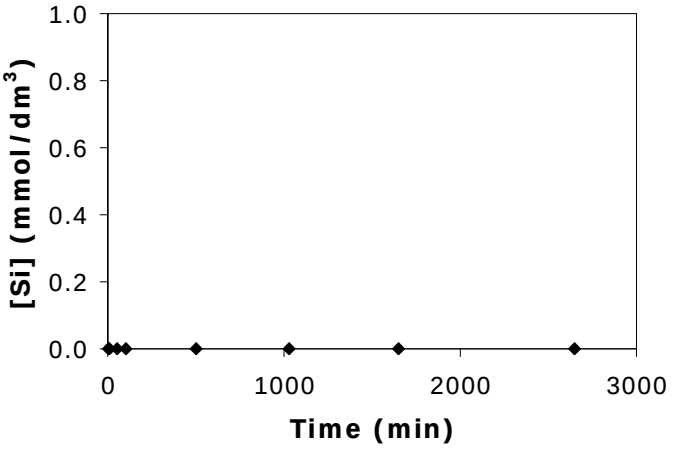

Figure 3.5: Analcime particles from 8M HCl solution, collected on 0.2 μm filters at 30 minutes into reaction immersed in 4M HCl. *300 mL fluid, 5.0°C, 500RPM.*

Our second hypothesis was that the silica was still dissolving from the analcime particles during the plateau and that the silicon already released from the analcime was polymerizing and forming silica particles with d>0.2μm at the same rate (recall that the measure AAS/ICP silicon concentration includes all particles less than 0.2μm). Consequently, it was hypothesized that if we were to polymerize pure monosilicic acid under the same reaction conditions, one should see the silicon concentration decreasing during the original plateau (30min≤t≤120min).

An aqueous solution of pure monosilicic acid was acidified to produce a solution of 8M HCl containing 135 mmol/L of silicon, which corresponds to the plateau height when analcime is dissolved in 8M HCl.

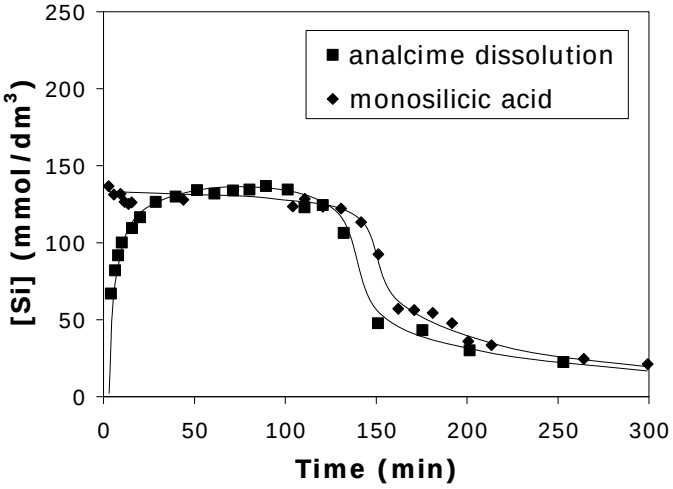

Figure 3.6: Comparison of silicon concentration profiles during analcime dissolution in 8M HCl and during monosilicic acid polymerization in 8M HCl. *300 mL fluid, 5.0°C, 500RPM.*

The concentration of silicon measured by AAS/ICP did not decrease during the original plateau. Furthermore, as can be seen in Figure 3.6, the silicon concentration-time trajectory matched that seen when analcime is dissolved under the same reaction conditions. Thus, it can be concluded that the precipitation of silica is independent of analcime dissolution. That is, the two processes of analcime dissolution and the subsequent silica precipitation are *uncoupled*.

Next, similar experiments with monosilicic acid in 4M and 2M HCl were carried out, with initial silicon concentrations of 190 mmol/L and 240 mmol/L, respectively. The silicon concentration-time trajectories of the pure monosilicic acid were similar to those from analcime dissolution were similar at all three acid concentrations, as can be seen in Figure 3.6 and 3.7. Therefore, it can also be concluded that two processes of analcime dissolution and the subsequent silica precipitation are *decoupled*, as we previously mentioned. Furthermore, we conclude the behavior of silica dissolved from minerals

does not depend on the identity of the minerals; the behaviour of dissolved silica is determined only by the concentration of dissolved silica in solution and reaction conditions.

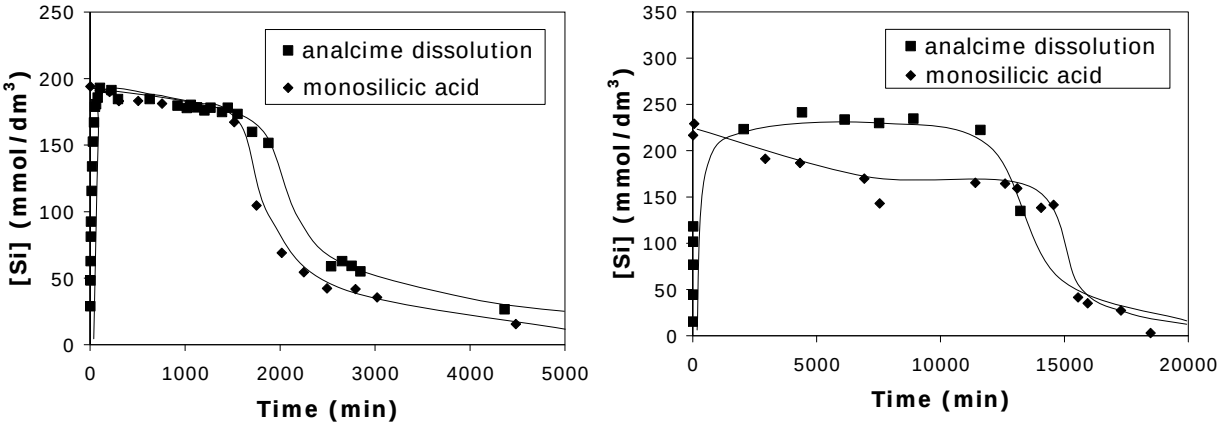

(a) 4M HCl (b) 2M HCl

Figure 3.7: Comparison of silicon concentration profiles during analcime dissolution and during monosilicic acid polymerization in (a) 4M and (b) 2M HCl. *300 mL fluid, 5.0°C, 500RPM.*

Silica Polymerization in Hydrochloric Acid

Because of the similarities to silicon precipitation from analcime, pure monosilicic acid solutions were used to further study the polymerization of silica under acidic conditions. The use of monosilicic acid has the advantage of not having undissolved silicious analcime particles in solution, thus allowing better characterization of the polymerization and growth of silica particles. The initial polymerization rates of pure monosilicic acid in 8, 4, 6 and 2M HCl were investigated at various initial concentrations of monosilicic acid using the silicomolybdate technique. The concentration-time data shows that the disappearance of pure monosilicic acid from

solution at very low pH is second order (Figure 8). That is, formation of a silicate dimer is the rate-limiting step in the initial polymerization process:

$$\frac{d[Si(OH)_4]}{dt} = -k_d[Si(OH)_4]^2 \tag{3.6}$$

Integrating,

$$\frac{[Si(OH)_4]_O}{[Si(OH)_4]} - 1 = [Si(OH)_4]_O k_d t \tag{3.7}$$

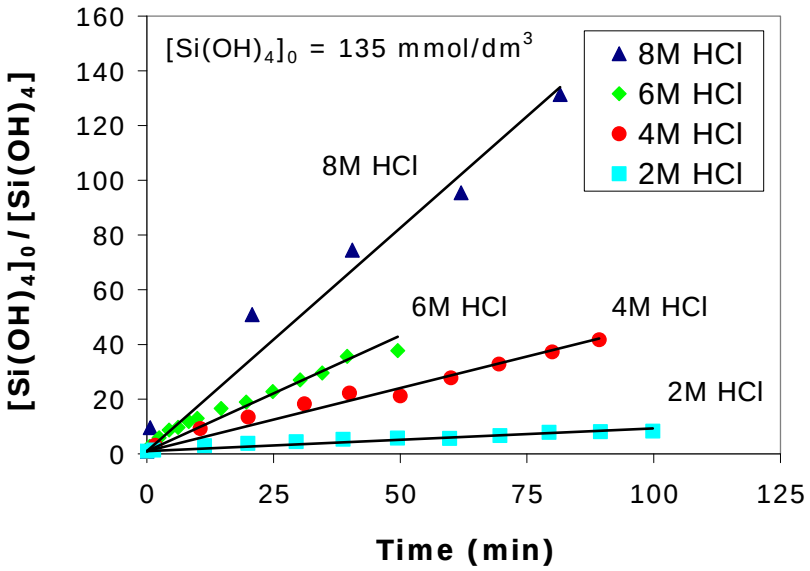

Figure 3.8: Normalized concentration of monosilicic acid vs time. Initial monosilicic acid concentration 135 mmol/L. *300 mL fluid, 5.0°C, 500RPM.*

Rothbaum and Rohde[18] have shown that a second bimolecular reaction as the first step of polymerization is consistent with their data. However, there are also many conflicting sets of data from other researchers. Reaction orders of 3 and 4 have also been reported[9,12,14]. This ambiguity may be because the reaction order of the initial polymerization may be different under different reaction conditions such as different pH or temperature.

The initial polymerization rate of monosilicic acid is a strong function of HCl concentration and a weak function of initial monosilicic acid concentration, as shown in Figure 3.9.

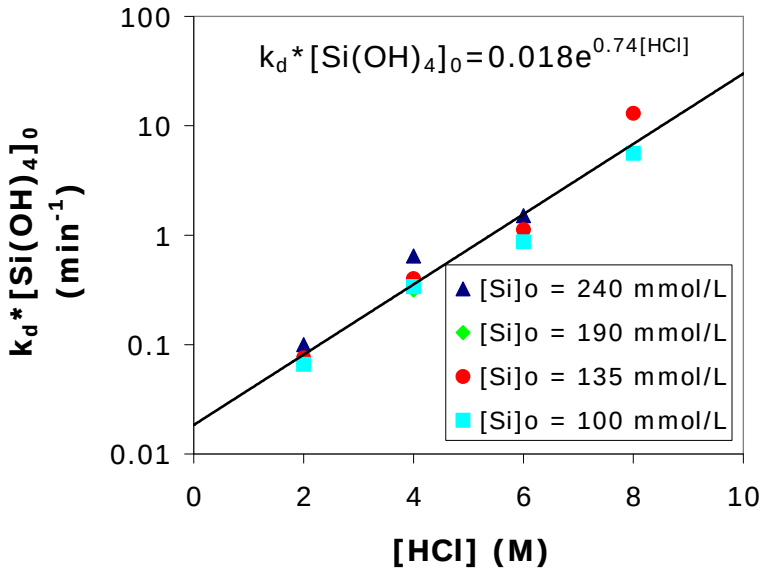

Figure 3.9: The initial polymerization rate constant multiplied by the initial monosilicic acid concentration at various HCl concentrations and initial silicon concentrations. *300 mL fluid, 5.0°C, 500RPM.*

The silica particles initially formed (c.a. 5nm in diameter) grow to larger sizes; this growth was studied by using dynamic light scattering measurements (DLS) on solutions of pure monosilicic acid in 2, 4, and 8M HCl. DLS data showed that the intensity distribution of the growing silica particles sizes follow a log-normal distribution (Figure 3.10).

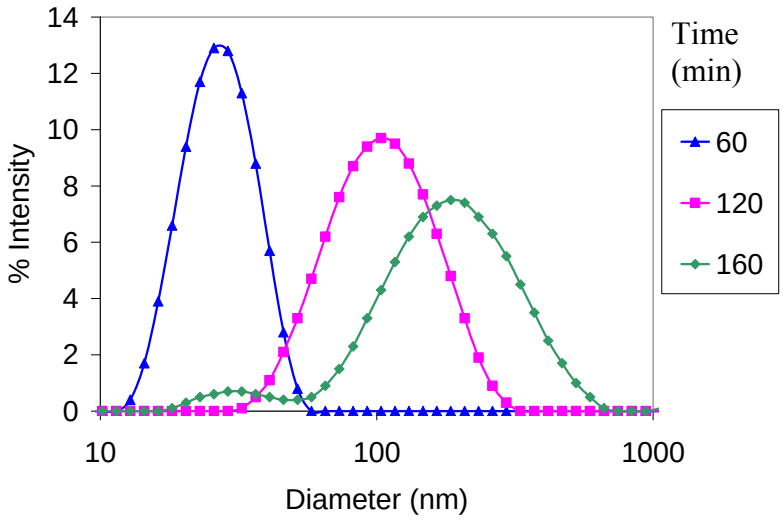

Figure 3.10: Distribution of silica particle by intensity 60, 120, and 160 minutes into reaction of pure monosilicic acid in 8M HCl. *300 mL fluid, 5.0°C, 500RPM.*

The mean particle diameter was calculated from this distribution and is show in Figure 3.11.

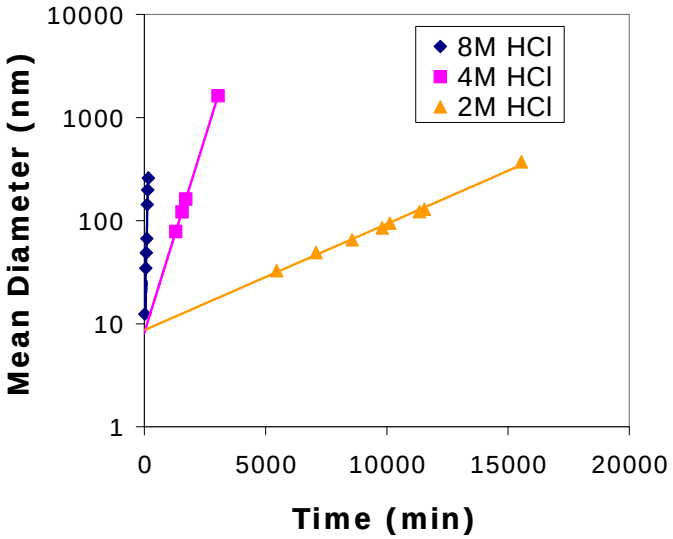

8M HCl: $5.37\exp(2.53*10^{-2}\,t)$

4M HCl: $5.20\exp(1.98*10^{-3}\,t)$

2M HCl: $5.57\exp(2.78*10^{-4}t)$

Figure 3.11: Mean particle diameter from intensity distribution.
$[Si(OH)]_0$ = 135 mmol/L for 8M HCl
$[Si(OH)]_0$ = 190 mmol/L for 4M HCl
$[Si(OH)]_0$ = 240 mmol/L for 2M HCl.
300 mL fluid, 5.0°C, 500RPM.

The growth of mean particle diameter can be fit to an exponential equation

$D = A\exp(k_p t)$.

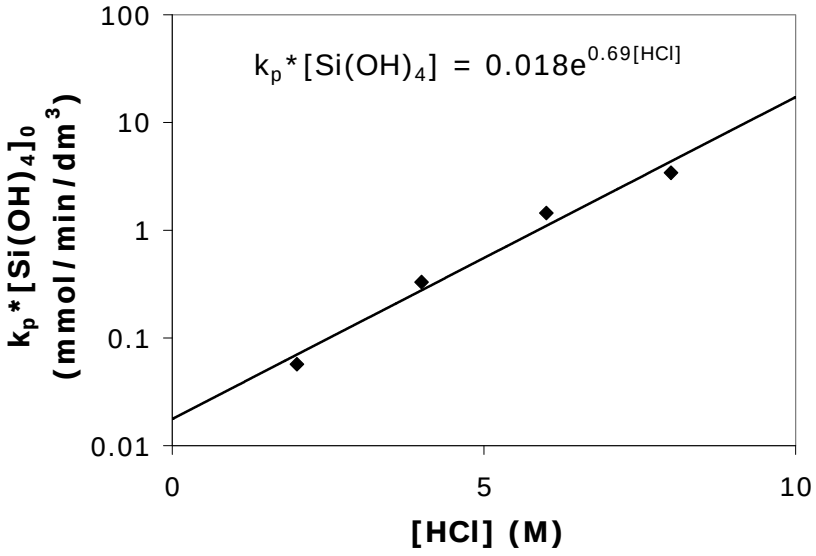

Figure 3.12: The particle growth rate constant multiplied by the initial monosilicic acid concentration at various HCl concentrations. Note: the point at 6M HCl was estimated from AAS data. *300 mL fluid, 5.0°C, 500RPM.*

Referring to Figure 3.11, one observes that extrapolation of the particle size back to t=0 gives an initial particle diameter of approximately 5nm. Using nucleation theory and assuming the 5nm particle is the "critical nucleus", one can calculate the supersaturation ration of silicon in the solution using the equations below:

$$n^* = \left(\frac{2}{3}\frac{\theta}{\ln S}\right)^3 \qquad \theta = \frac{\sigma \cdot s_1}{kT} \tag{3.8}$$

where n* is the number of monomers in the critical nucleus cluster, θ is the de-dimensionalized surface tension, S is supersaturation ratio, σ is surface tension, and s_1 is the surface area of the monomer.

For silica in solution, a value of 45 erg/cm^2 was used for the surface tension[27]. s_1 was calculated by using molecular weight of $Si(OH)_4$ (96 g/mol), dividing by Avogadro's number, and the dividing by silicon density of 2200 g/dm^3, to give a value of $7.2*10^{-29}$ m^3 for the v_1 (volume of monomer), which was then converted to monomer surface area assuming a spherical monomer.

The final step in the calculation is conversion of n* to nucleus diameter.

$$d = \left(\frac{6}{\pi} \left(\frac{v_1 \cdot n^*}{\varphi} \right) \right)^{\frac{1}{3}} \tag{3.9}$$

where φ is the solid volume fraction of a cluster. The value of φ is approximated to be 0.6366, which is the solid volume fraction in random close packing of spheres[28].

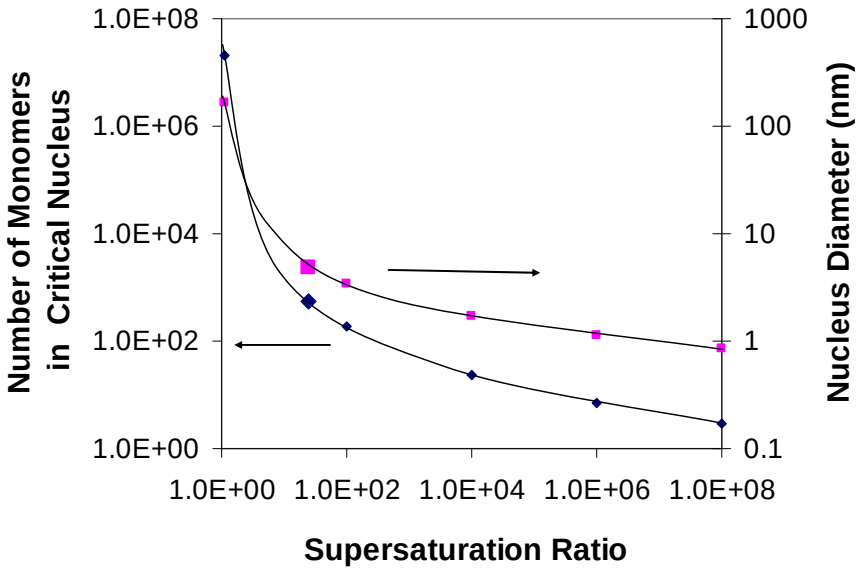

Figure 3.13: Number of silica monomers in a critical nucleus and diameter of critical nucleus versus supersaturation ratio for a spherical silica nucleus.

From the above equations, for a silica critical nucleus of 5nm, the number of monomers is estimated to be 580, and the supersaturation ratio is estimated to be 25 (comes from Figure 3.13).

The initial silica polymerization rate and the particle growth rate are both strong functions of HCl concentration and weak functions of initial monosilicic acid concentration. Furthermore, the values of $k_d*[SiOH_4]$ (min^{-1}) and $k_p*[SiOH_4]$ ($mmol/min/dm^3$) are very similar, as shown in Figure 3.14.

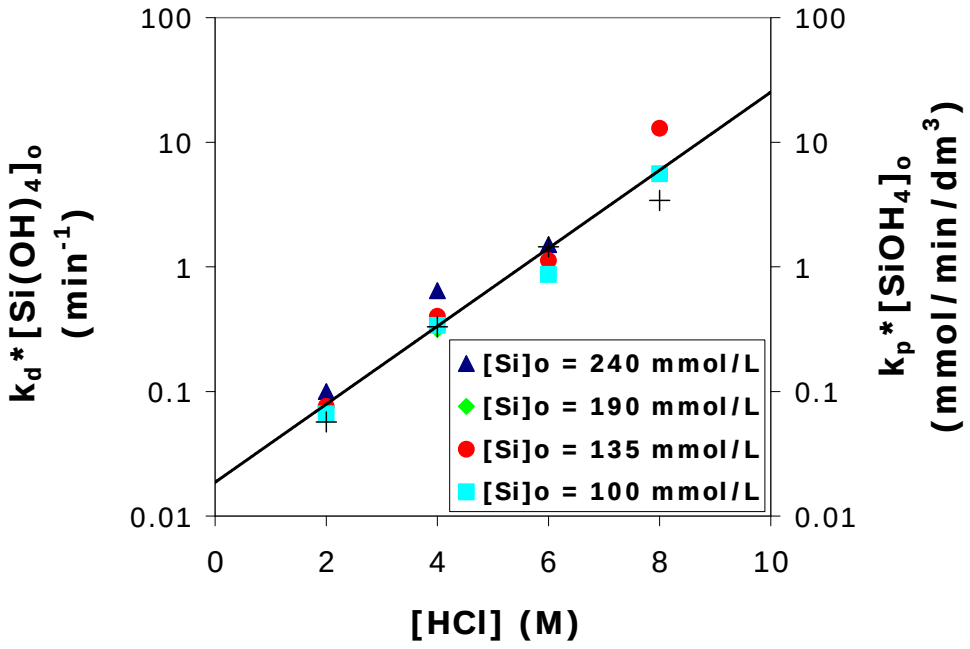

Figure 3.14: Comparison of initial polymerization rate constant and particle growth rate constant. *300 mL fluid, 5.0°C, 500RPM.*

It was previously shown that the analcime dissolution and silica precipitation are decoupled. Thus, it can be said that during the silica plateau measured by AAS/ICP, the silica particles have formed and are growing larger. Then, when the particles grow to 200 nm in diameter, they are filtered out of the solution by the 0.2µm filters. Consequently, the silicon concentration in the filtered solution shows a drop in the measured silica concentration. Referring to Figure 3.15, the DLS data for 8M HCl shows that the mean silica particle size reaches 200 nm at 142 minutes. We also see that the

drop in silicon concentration measured by AAS/ICP occurs around 140 minutes, showing that the DLS and AAS/ICP results are consistent.

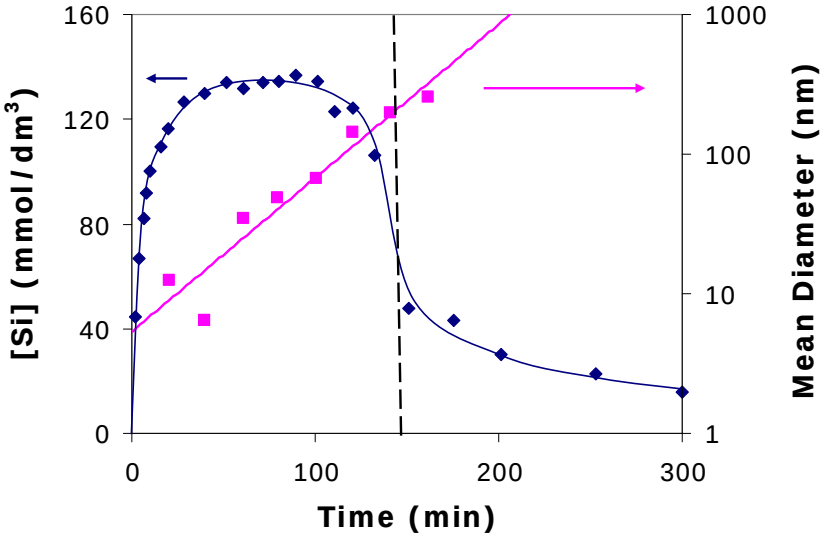

Figure 3.15: The mean silica particle size reaches 200 nm when precipitation occurs as measured by AAS/ICP. *8M HCl, 300 mL fluid, 5.0°C, 500RPM.*

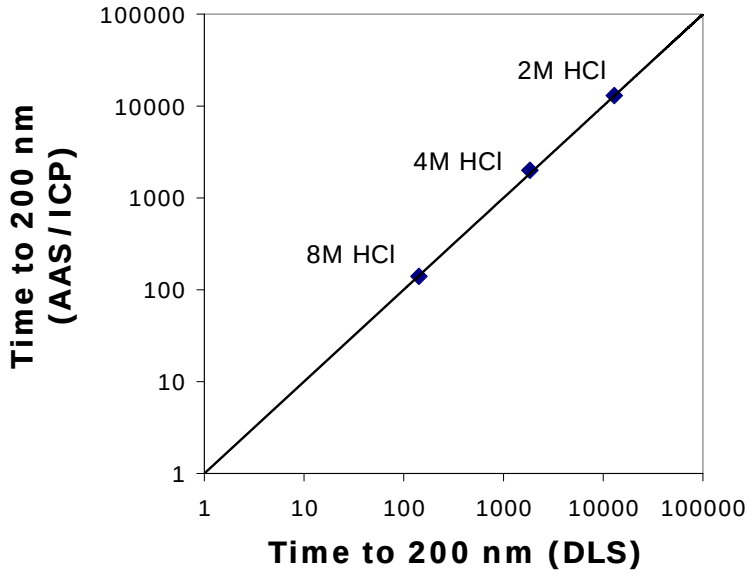

Figure 3.16: Time for growing silica particles to reach 200nm as measured by DLS and AAS/ICP. Solid line is y=x.

There is good agreement between DLS and AAS/ICP data over many, many orders of magnitude (Figure 3.16).

Modeling of Silica Particle Growth

The first question that needs to be answered is "what is mechanism of the silica particle growth?" Two mechanisms were proposed: (1) a core-shell mechanism in which monomers continuously add to growing silica particles to increase their size (2) a flocculation mechanism in which primary silica particles are initially formed and subsequent particle growth is through flocculation.

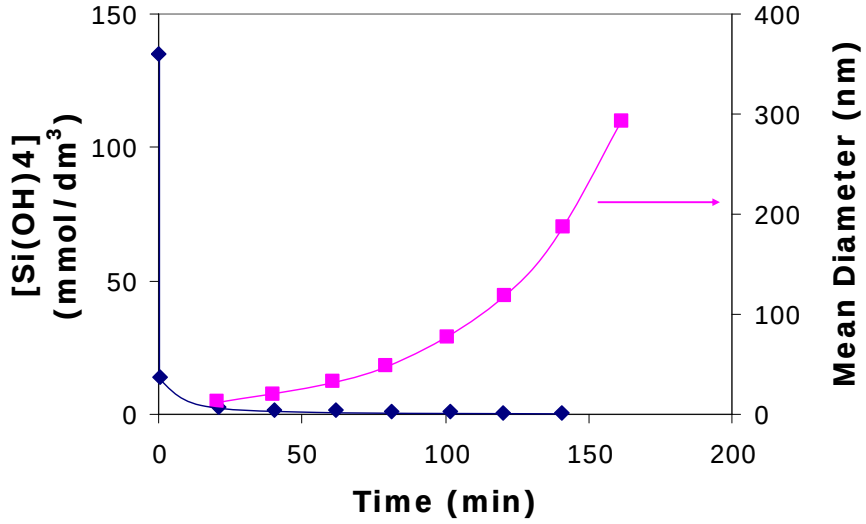

Figure 3.17: Comparison of silica monomer disappearance with silica particle growth. *8M HCl,$[Si]_0$=135 mmol/L, 300 mL fluid, 5.0°C, 500RPM.*

Referring to Figure 3.17, it is seen that monomer (monosilicic acid) disappears very rapidly within the first 20 minutes; however the silica particles continue to increase exponentially in size up to 160 minutes. Consequently, monomer addition cannot be the

mechanism for particle growth. Thus, particle growth by flocculation was chosen as the basis for our model.

The well-known Smoluchowski equation for colloid flocculation kinetics was proposed first. However, the system includes particles from 5-1000 nm in diameter, making application of the original Smoluchowski equation computationally expensive, if not virtually impossible. That is, for a final aggregate diameter of the order of 1μm, 10^8 ordinary differential equations must be solved simultaneously. Consequently, we decided to apply geometric scaling to the population balance differential equations for flocs with a geometric number of primary particles (e.g. for geometric scale R=2, the number of primary particles is 1, 2, 4, 8 etc. for i=1, 2, 3, 4 etc.) The geometric population balance reduces the number of ordinary differential equations from 10^8 to 28 when a value of R = 2 is used[29]. This geometric population balance technique has previously been applied to other systems, but unfortunately in these systems scaling of *volume* and not the number of primary particles was used[30,31]. Geometric scaling of the volume conserves volume but not mass in systems with fractal aggregates. Geometric scaling of the number of primary particles conserves number of primary particles and ensures conservation of mass, even with fractal aggregates.

The Smoluchowski equation was modified to take into account the geometric population balance on primary particles:

$$\frac{dC_i}{dt} = \frac{K_{i-1,i-1}}{R} C_{i-1}{}^2 + C_{i-1} \sum_{j=1}^{i-2} K_{i-1,j} \frac{R^{j-1}}{R^{i-1} - R^{i-2}} C_j - C_i \sum_{j=1}^{i-1} K_{i,j} \frac{R^{j-1}}{R^i - R^{i-1}} C_j - C_i \sum_{j=i}^{N-1} K_{i,j} C_j \tag{3.10}$$

$$K_{i.j} = c^* (d_i + d_j)^2 \tag{3.11}$$

where R is the geometric scale (R=2 in our model), $K_{i,j}$ is the collision kernel between the i^{th} and j^{th} aggregate, d_i is the diameter of the i^{th} aggregate, and c is a constant which is proportional to the collision efficiency. Note that the collision kernel here is for reaction-limited aggregation[32].

The system of modified Smoluchowski equations was solved in Matlab 2008a using ode23. Here, 30 equations in total were used, with the largest aggregate containing 2^{29} number of primary particles. The primary particle diameter used was 5 nm, estimated from the DLS data (see Figure 3.11). The collision efficiency parameter "c" was the only fitting parameter in our model. The fractal dimension was assumed to be 2.0, in accordance with other reaction-limited systems[33,34]. The particle size distributions that were output from the modeling were used to calculate the mean aggregate diameter at each time.

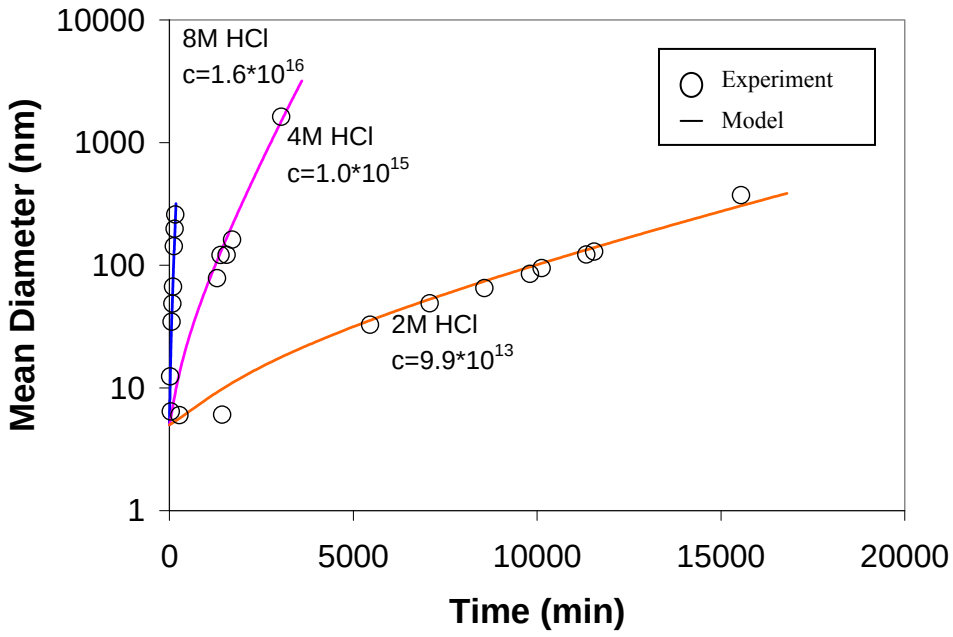

Figure 3.18: Smoluchowski equation modeling of DLS data.

Figure 3.18 shows that excellent agreement was achieved using the geometric population balance (GPB) to predict the observed mean particle diameter measured by DLS.

The GPB modeling gives the same qualitative PSD change with time that is observed with DLS. However, the DLS data shows a smaller standard deviation than the GPB model data, resulting in taller, sharper peaks for the DLS data as compared to the Smoluchowski model data (Figure 3.19).

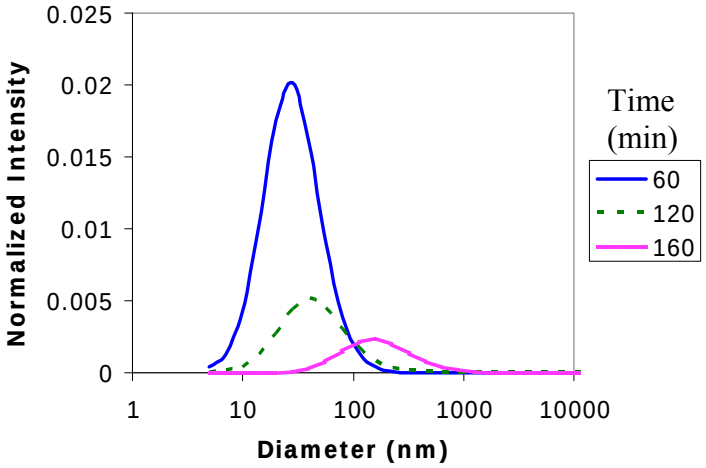

(a) PSD from modeling

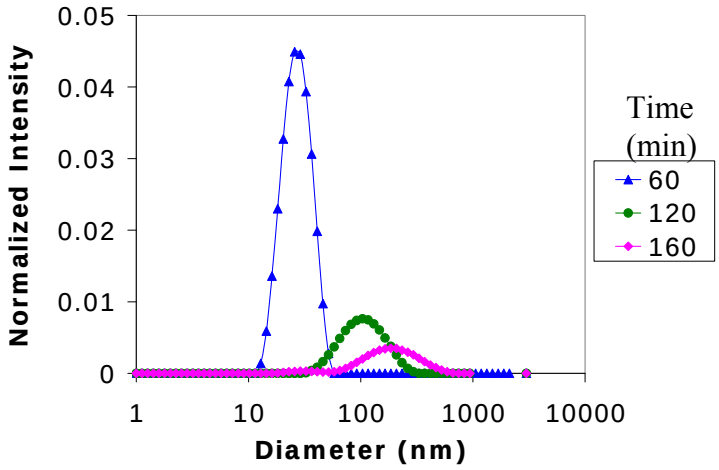

(b) PDS Evolution from DLS data

Figure 3.19: (a) Particle size distribution by intensity from Smoluchowski equation modeling (b) Particle size distribution by intensity from DLS. *8M HCl,$[Si]_0$=135 mmol/L, 300 mL fluid, 5.0°C, 500RPM.*

For more details about the modeling and conversion of intensity distributions to particle frequency distributions, see Appendix A. For the Matlab code, see Appendix B.

Analcime Dissolution in Hydrochloric Acid (Revisited)

It was previously established in the section "*Analcime Dissolution in Hydrochloric Acid"* that the varying plateau height in different HCl concentrations was not due to a solubility issue (analcime surface in equilibrium with solution) nor was it due to equilibrium between analcime dissolution and silica precipitation during the plateau. Since the plateau is not caused by equilibrium between analcime and solution, the only possibility left is that the plateau occurs because the analcime particles are becoming "undissolvable".

As previously mentioned, analcime dissolution occurs by the almost complete removal of framework aluminum, which then causes silica to be released into solution[7,8]:

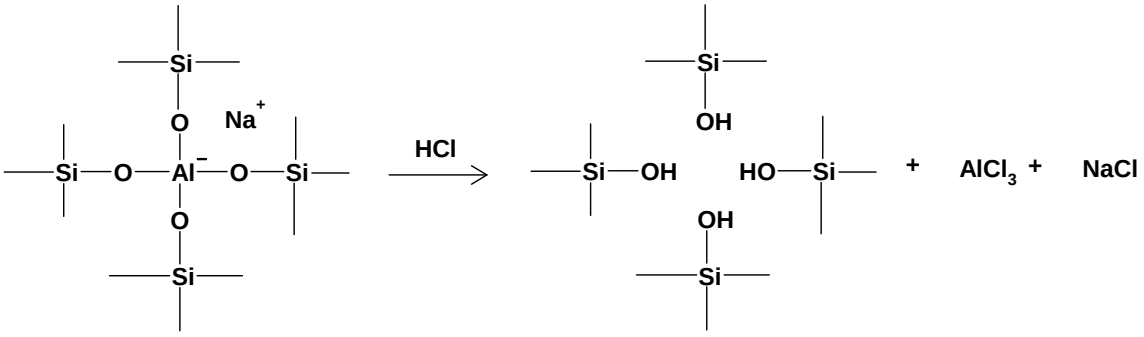

A recondensation reaction may then occur, where silanol groups within the dissolving analcime condense to form siloxane bonds (-O-Si-O-) bonds, which are undissolvable in HCl solutions:

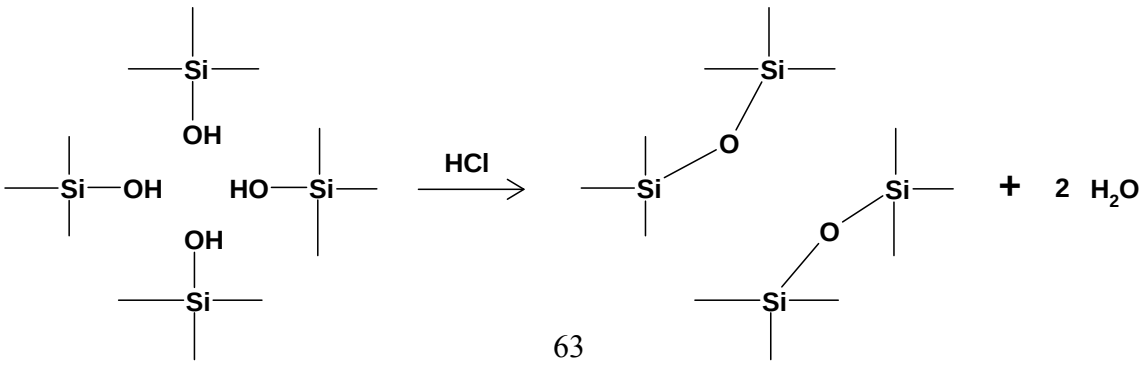

The process would occur faster in greater concentrations of HCl, explaining the lower plateau height at higher HCl concentrations. Furthermore, this process may be constrained by the spatial configuration of the formed silanol groups within the analcime, which explains the invariance of the plateau height with temperature.

Conclusions

1. The behaviour of silicon dissolved from analcime can be mimicked using pure monosilicic acid solutions.
2. The monosilicic acid disappears from solution via a second order reaction.
3. The monomers form primary particles of 5nm within the first few minutes of reaction. These particles then flocculate by reaction-limited aggregation to give an exponential increase in mean particle size.
4. Both the monosilicic acid disappearance and silica particle flocculation increase more in increasing concentrations of HCl.
5. The particle growth can be successfully modeled by using a geometric population balance.

Industrial Implications

Major industrial implications:

- 10-15 wt% hydrochloric acid is used either as a preflush or stand-alone fluid during acidization. However, a higher concentration of HCl does not always result in more dissolution, and may result in less dissolution for certain minerals like analcime.
- Before acidization, an analysis of structural integrity of the formation should be carried out to estimate the maximum amount of formation rock that can be dissolved without structural collapse. The amount of formation rock dissolved can then be controlled by varying the concentration of HCl.
- The behaviour of dissolved silica during acidization can be examined by simply knowing three pieces of information: silica concentration, temperature, and pH. The specific minerals from which the silicon was dissolved do not matter!
- Therefore, if a mineralogical analysis is done on the formation, and it is known to what extent silicon is dissolved from each mineral in HCl, the behaviour of the silicon in the formation can be reproduced in the lab by simply putting the appropriate concentration of monosilicic acid in the relevant concentration(s) of HCl.
- The most important industrial application of the work is that low concentration of HCl (2M) should be used to acid stimulate reservoirs containing the zeolite analcime. The two reasons are:
    1. More analcime is dissolved thereby increasing the pore space and permeability to a greater extent.

2. The time for silica precipitation in 2M HCl is sufficiently long (~10,000 minutes) that the spent acid can be withdrawn from the well before silica precipitation occurs.

References

[1] Underdown, D. R.; Hickey, J. J.; Kalra, S. K. *Proceedings of 65th Annual SPE Technical Coference and Exhibition*, New Orleans, LA, 1990.
[2] Lund, K.; Fogler H. S.; McCune, C.C. *Chem. Eng. Sci.*, **1973**, *28*, 691.
[3] Lund, K.; Fogler H. S.; McCune, C.C. *Chem. Eng. Sci.*, **1975**, *30*, 825.
[4] Kline, W. E.; Fogler H.S. *J. Colloid Interface Sci.*, **1981**, *82*, 93.
[5] Kline, W. E.; Fogler H.S. J. *Ind. Eng. Chem. Fund.* **1981**, *20*, 155.
[6] Hartman, R. L.; Fogler, H. S. *Ind. Eng. Chem. Res.* **2005**, 44, 7738.
[7] Hartman, R. L.; Fogler, H. S. *Langmuir* **2006**, *22,* 11163.
[8] Hartman, R. L.; Fogler, H. S. *Langmuir* **2007**, *23,* 5477.
[9] Alexander, G.B.; Heston, W.M.; Iler, R.K., *J. Phys. Chem.* **1954,** *58*, 453.
[10] Conrad, C.F.; Icopini, G. A.; Yasuhara, H.; Bandstra, J. Z.; Brantley, S. L.; Heaney, P.J. *Geochim. Cosmochim. Acta* **2007**, *71*, 531.
[11] Crerar, D. A.; Axtmann, E. V.; Axtmann, R. C. *Geochim. Cosmochim. Acta* **1981**, *45*, 1259.
[12] Goto, K. *J. Phys. Chem.* **1956**, *60*, 1007.
[13] Harris, R. K; Knight, C. T. G.; Smith, D. N. *J. Chem. Soc. Chem. Comm.* **1980**, *15*, 726.
[14] Icopini, G. A.; Brantley, S. L.; Heaney, P. J. *Geochim. Cosmochim. Acta.* **2005**, *69*, 293.
[15] Iler, R. K. *J. Colloid Interf. Sci.* **1980**, *75*, 138.
[16] Makrides, A. C.; Turner, M.; Slaughter, J. *J. Colloid Interf. Sci.* **1980**, *73*, 345.
[17] Okamoto, G.; Okura, T.; Goto, K. *Geochim. Cosmochim. Acta* **1957**, *12*, 123.
[18] Rothbaum, H. P.; Rohde, A. G. *J. Colloid Interf. Sci.* **1979**, *71*, 533.
[19] Sjoberg, S. *J. Non-Cryst. Solids* **1996**, *196*, 51.
[20] Hartman, R.L.; Jayasankar, A.; Jitapunhul, T.; Fogler, H. S. Industrial Affiliates Report 2003. 20th Annual Review.
[21] Iler, R. K. *The Chemistry of Silica: Solubility, Polymerization, Colloid and Surface Properties, and Biochemistry*; John Wiley & Sons: New York, 1979.
[22] Icopini, G. A.; Brantley, S. L.; Heaney, P.*J. Geochim. Cosmochim. Acta* **2005**, *69*, 293.
[23] Hartman, R. L. Ph.D. Dissertation, University of Michigan, Ann Arbor, MI, 2006.
[24] Perry, C. C.; Keeling-Tucker, T. *J. Biol. Inorg. Chem.* **2000**, *5*, 537.
[25] Iler, R. K. *J. Colloid Interf. Sci.* **1980**, *75*, 138.
[26] Unpublished citric acid data.
[27] Weres, O.; Yee, A.; Tsao, L. *J. Colloid Interf. Sci.* **1981**, *84*, 379.
[28] Scott, G.D.; Kilgour, D. M. *J. Phys. D App. Phys.* **1969**, *2*, 863.
[29] Maqbool, T., Raha, S., and Fogler, H.S. (2007). Kinetics of Asphaltene Precipitation and Flocculation Experiments and Modeling. The 8th International Conference on Petroleum Phase Behavior and Fouling, Pau, France.
[30] Batterham, R. J.;Hall, J. S.; Barton G., *International Symposium on Agglomeration (3rd)*, Nurnberg, 1981, p. A136–A150.
[31] Hounslow, M. J.; Ryall, R.L.; Marshall, V.R. *AIChE J.* **1988**, *34*, 1821.
[32] Ball, R. C.; Weitz, D. A.; Witten, T. A.; Leyvraz, F. *Phys. Rev. Lett.* **1987**, *58*, 274.
[33] Martin, J. E.; Wilcoxon, D. S.; Odinek, J. *Phys. Rev. A* **1990**, *41*, 4379.
[34] Burns, J. L.; Yan, Y.; Jameson, G. J.; Biggs, S. *Langmuir* **1997**, *13*, 6413.

CHAPTER IV

IONIC EFFECTS ON SILICA PRECIPITATION IN ACIDIC SOLUTIONS

Abstract

During matrix acidization of sandstone petroleum reservoirs in the Gulf of Mexico, silica precipitation has become a serious problem in the petroleum industry. Silica precipitation during acid treatments causes a pore blockage which dramatically reduces the permeability of reservoirs and oil productivity. Previous work by the authors studied the effect of acid concentrations on the rate of silica precipitation. However, native interstitial fluids in the reservoirs containing salts such as Na^+, Ca^{2+}, Mg^{2+} can mix with the injected acid. Consequently, we initiated a study on the influence of salts on precipitation behavior.

Five different chloride salts (NaCl, CsCl, $MgCl_2$, $CaCl_2$, and $AlCl_3$) were used to investigate silica particle growth and aggregation phenomena. The results indicate that the presence of different salts accelerate the particle growth rate in the following order:

$$AlCl_3 > CaCl_2 > MgCl_2 > NaCl > CsCl > \text{No salt}$$

Dynamic Light Scattering results showed that the silica particle size increases exponentially with time. These particle growth rates were simulated using the reaction-limited aggregation (RLA) model under the framework of geometric population balance. From UV-Vis experiments, it was found that the monosilicic acid disappears from solution very rapidly and the monosilicic acid disappearance kinetics obeys third-order rate law dependence. It was also found that disappearance rate constants, particle growth rate constants, and aggregation rate constant, regardless of salt types, increase exponentially as a function of ionic strength.

Introduction

Matrix acidization is the injection of HCl and/or HCl/HF acid mixtures into the porous media to disslove the mineral and increase the pore space, thereby increasing the oil production. During matrix acidization, the stimulating fluid injected into a geological formation dissolves clays and aluminosilicate minerals in the near-wellbore region that sometimes leads to silica precipitation. Silica precipitation during acidization causes a pore blockage, which dramatically reduces the permeability of formations and decreases, rather than increases, oil productivity[1,2]. Matrix acidization treatments of HCl alone are common and are used for carbonate reserviors and sandstone reserviors that contain certain minerals such as the zeolite analcime. The dissolution of analcime is followed by the precipitation of siliceous product which blocks the reservoir pore space. For example, it has been shown to be the cause of ineffectiveness of the acid stimulation treatments in the Gulf of Mexico[3]

Fundamental studies of zeolite dissolution/precipitation in very acidic conditions have been proposed to better understand the mechanism and kinetics of these processes. Basic parameters such as pH, temperature, and type of zeolite were studied to reveal the scientific principles of zeolite *dissolution* phenomena[4,5]. Nevertheless, fundamental knowledge of the subsequent *silica precipitation* in low pH conditions has not been well-established because silica precipitation is very complex. Silica in solution can be present in many different chemical and physical forms. Furthermore, silica precipitation is influenced by pH, temperature, water chemistry, and suspended solids, all of which play an important role in accelerating or retarding the precipitation.

Gorrepati and Fogler[6] investigated the gelation/precipitation of silica in highly acidic solutions. Pure monosilicic acid solutions were found to mimic the analcime dissolution products and thus were used to study the kinetics of silicic acid monomer disappearance and silica particle growth. It was found that monosilicic acid disappears from solution very rapidly and the disappearance rate is second order with respect to the molar concentration of monosilicic acid. Furthermore, dynamic light scattering (DLS) data showed that the silica particle size increases exponentially with time. However, interstitial water in petroleum reserviors contain a significant amount of salts and foreign metals (Na^+, Mg^{2+}, Ca^{2+}, SO_4^{2-} etc.) that can mingle with the injected acid and reaction products to influence silica precipitation[7]. Therefore, in this study, we investigate the effect of salts and ionic strength on silica precipitation. The basic principles of aggregation modeling and the role of salts in precipitation phenomenon are discussed. These ionic effects can eventually be taken into consideration when developing effective matrix acidization treatments.

Background

Analcime is a naturally occurring zeolite which can be found in geological formation worldwide including Scotland, Iceland, Russia, United States, Canada, Australia, and India[8]. The dissolution phenomena of analcime in acidic solutions has been recently investigated. The reaction for the dissolution of analcime in hydrochloric acid is:

$$Na_2O \cdot Al_2O_3 \cdot 4SiO_2 \cdot 2H_2O + 8HCl + 2H_2O \rightarrow 2AlCl_3 + 4Si(OH)_4 + 2NaCl, \qquad (4.1)$$

where the products are aluminum chloride, sodium chloride, and monosilicic acid.

The proposed dissolution mechanism consists of a reversible hydrogen-ion sorption and subsequent surface reaction[9]. Dissolution of analcime occurs when hydrogen ions attack oxygen-aluminum bonds in the analcime framework, resulting in aluminum removal and the release of silicon compounds from analcime. Once dissolved, silicon polymerizes and eventually forms a gel/precipitate[4,6].

Silica polymerization begins with the condensation of monosilicic acid to form cyclic oligomers which then form three-dimensional polymer particles that can function as nuclei with radii of the order of a few angstroms. These nuclei may remain dispersed for long periods of time until condensation reactions cause coalescence and precipitation from solution. The time depends on the pH values, temperature, degree of supersaturation, and salinity due to the presence of other substances[10,11,12,13,14,15,16]. These nuclei may also grow to larger sizes by addition and polymerization of silicic acid on their surfaces.

In the petroleum industry, silica precipitated as a result of acid treatments has been referred to as “hydrated silica”, “colloidal silica gel” or “amorphous silica”[3,17,18]. These terms all describe the gelatinous, hydrated silica gels or amorphous precipitates

that result from acidization treatment. Recent work by Gorrepati and Fogler[6] found that increasing HCl concentrations can promote the particle growth rate as well as the monomeric silicic acid disappearance rate and that exponential particle size growth was observed. They also showed that the possible mechanism of silica particle growth is coagulation/flocculation of silica particles; not monomer addition.

Ionic effects on silica systems in *circum-neutral pH* systems have been extensively studied in terms of ionic strength and the presence of salt. Recent studies have revealed that the rate of silica polymerization increases with increasing ionic strength[12,19,20]. In addition, the effect of counterion or salt in silicic acid solutions in mildly acidic to alkaline conditions has been studied. Makrides *et al.*[11] and Chan *et al.*[21] found that precipitation (polymerization) rate increases with increasing salt concentration. Marshall and Warakomski[22] reported that cations increase silica polymerization in *circum-neutral solutions* in the order of:

$$Mg^{2+} > Ca^{2+} > Sr^{2+} > Li^{+} > Na^{+} > K^{+}$$

and the order of anionic effect was found as

$$I^{-} > Br^{-} > Cl^{-}.$$

Their results are in contrast to our results which found that $CaCl_2 > MgCl_2$ in extremely acidic conditions. However, the basic mechanism by which salts accelarate silica precipitation is still in debate. In this study, we investigate salt effects on silica precipitation and also particle growth rate in acidic conditions.

Materials and Methods

The silica used in this study was supplied in a form of Sodium Metasilicate Nonahydrate (SMN); 44 – 47.5% total solids, $Na_2O_3Si \cdot 9H_2O$, M.W. 284.19, by Thermo Sci Acros Organics. The Si content in SMN determined using ICP/MS was found to be between 0.103 and 0.104 gSi/gSMN. Analytically pure 35 – 37% wt. trace metal grade HCl solution, NaCl, $MgCl_2 \cdot 6H_2O$, $CaCl_2 \cdot 2H_2O$, and $AlCl_3 \cdot 6H_2O$ were supplied by Fisher Chemical. CsCl was provided by Sigma-Aldrich. Ultrahigh-purity deionized water provided by a MilliQ system was used as a diluent in the preparation of all solutions.

First, 13.82 grams of SMN were dissolved in a cooling jacketed 3-pronged glass reactor containing a 70mL of 5°C deionized water (DI) for approximately 50 minutes. The solution was magnetically stirred at a stirring speed of 500 rpm and cooled by a circulation system with a constant coolant temperature of 5.0°C. Once dissolved, a hydrochloric acid solution and a solution of make-up DI water and salt (cooled down to 5.0°C prior to addition) were added into the reactor to initiate reaction. The final properties of this solution were 1M salt, 4M HCl, 170mM $Si(OH)_4$, and 300mL total of solution.

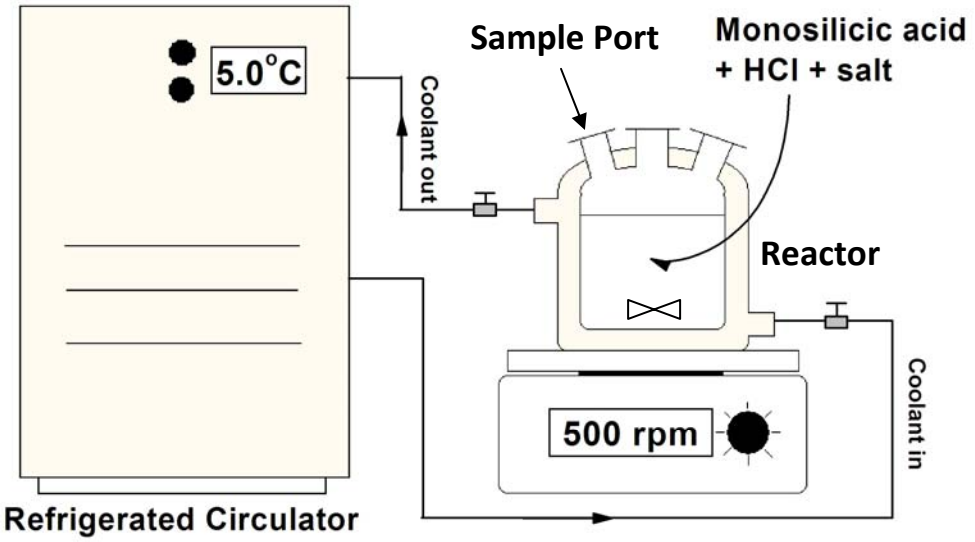

Figure 4.1: Experimental setup.

Sample Characterization

1. *Si Content in Solution Using Inductively-Coupled Plasma Mass Spectroscopy (ICP-MS)*

   Samples were manually obtained using micropipettes and drawn through polypropylene-membrane filters (d_{pore} = 0.2μm) at short interval times and placed into 50mL sample tubes. Filtrate solutions were diluted twice with a dilution ratio of 2 to 50 to reach the appropriate concentration for compositional analysis using ICP/MS (ELAN9000, Perkin Elmer).

2. *Silica Particle Growth Using Dynamic Light Scattering (DLS)*

   Samples were withdrawn from the reactor at particular times and immediately placed into sample vials for silica particle size measurement using DLS (Nano ZS, Malvern) at a constant temperature of 5.0°C. Intensity-mode particle diameter

DLS measurements were used to calculate the mean particle size. The particle size data were compared with ICP/MS data and with results from reaction-limited aggregation model (RLA model) recently developed and modified by Gorrepati and Fogler[6].

3. *Monosilicic Acid Concentration in Solution Using Molybdate-Blue Method and Ultraviolet-Visible Light Spectroscopy (UV-Vis)*

   Samples were withdrawn at short reaction times and transferred to 50mL sample tubes. The solutions were diluted twice using dilution ratios of 2 to 50 and 2 to 45, respectively. Molybdate solution was then added, causing the color of solutions to change from clear to blue. The UV-Visible spectroscopy (Cary100, Varian) was used to determine the concentration of silicic acid remaining, which was quantified in terms of "molybdate reactive silica" according to ASTM D859-05 (Molybdenum-blue method for silica-in-water analysis).

Results

For the analcime precipitation studies, Gorrepati and Fogler[6] showed a similarity in silicon concentration-time profiles of both analcime and pure monosilicic acid ($Si(OH)_4$) solutions. This similarity is due to the fact that dissolving sodium metasilicate nonahydrate (SMN) in water will produce monosilicic acids which can mimic the silica precipitation after analcime dissolution. Therefore, we used SMN as the Si source instead of analcime throughout the course of research.

Base Case Experiment

The base case in our investigation was a 300-mL solution of 170mmol/L $Si(OH)_4$ and 4M hydrochloric acid at 5.0°C and 500rpm. Samples were withdrawn at different time, filtered through a 0.2μm PP filter, and characterized using ICP/MS technique. Figure 2 shows the concentration of Si in filtered samples as a function of time. One notes the end of a plateau region at 1950 minutes where measured Si concentration decreased drastically. At 1,950 minutes particles greater than 0.2μm had formed in the solution and were not able to permeate through the 0.2μm filters. Consequently Si could not be seen with the ICP and the concentration of Si in the withdrawn samples decreased drastically. The time to reach 0.2μm matches the result obtained by dynamic light scattering (see Figure 4.3).

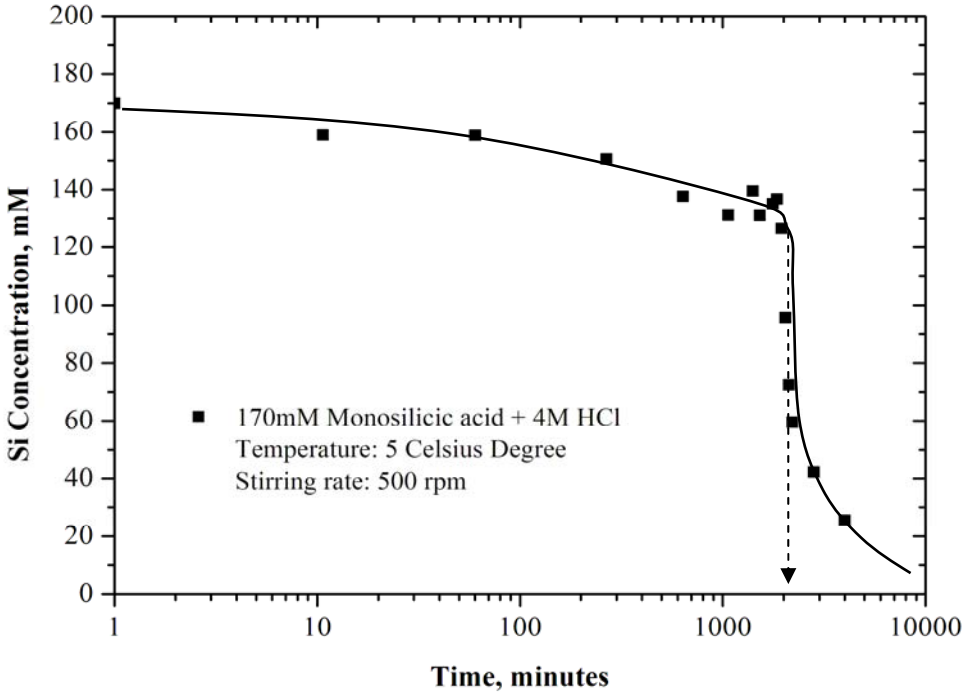

Figure 4.2: Concentration – time trajectory in 170mmol/L monosilicic acid + 4M HCl solution (base case) measured by ICP/MS.

Silica particle sizes were also monitored at different times using Dynamic Light Scattering (DLS) and are shown in Figure 4.2. The measurement relied on the fact that silica particles are assumed to be spherical[12]. The mean silica particle size determined from the intensity as a function of particle diameter distribution was found to grow exponentially with time as according to the relationship (Note that k_G in this chapter was denoted k_P in Chapter 3):

$$D(t) = D_o \cdot \exp(k_G t) \qquad (4.2)$$

where D(t) is the particle diameter with respect to time (nm)

D_o is an extrapolated initial particle size (nm) (~5nm for all experiments)

k_G is the particle growth rate constant (min^{-1}).

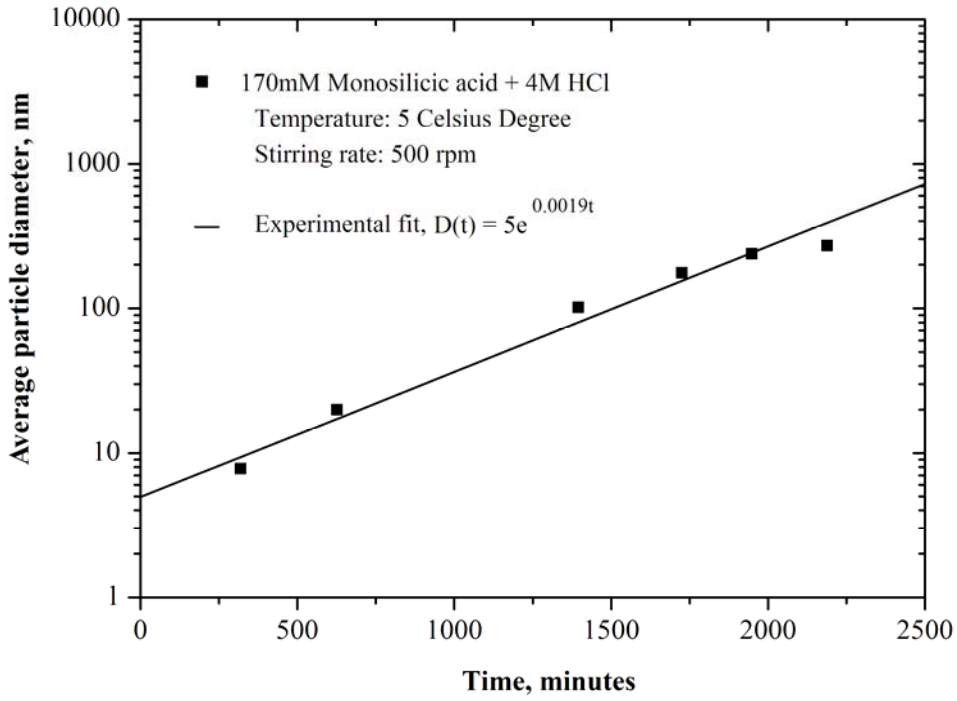

Figure 4.3: Mean silica particle diameter versus time in our base case solution measured using dynamic light scattering.

Salt Experiments: Precipitation Investigated Using ICP/MS and DLS Techniques

A number of experiments were carried out where different salts were added to a solution of [$Si(OH)_4$ + 4M HCl]. The salt studies used NaCl, CsCl, $MgCl_2$, $CaCl_2$, and $AlCl_3$ to investigate their influence on particle growth and aggregation phenomena of silica suspensions. Figure 4 shows the Si concentration in the filtered samples as a function of time. The times to reach a particle diameter of 0.2μm increase in the order of:

Pure HCl (base case) > CsCl > NaCl > $MgCl_2$ > $CaCl_2$ > $AlCl_3$.

The shorter the time to reach 0.2 μm, the fater the silica particle growth rate.

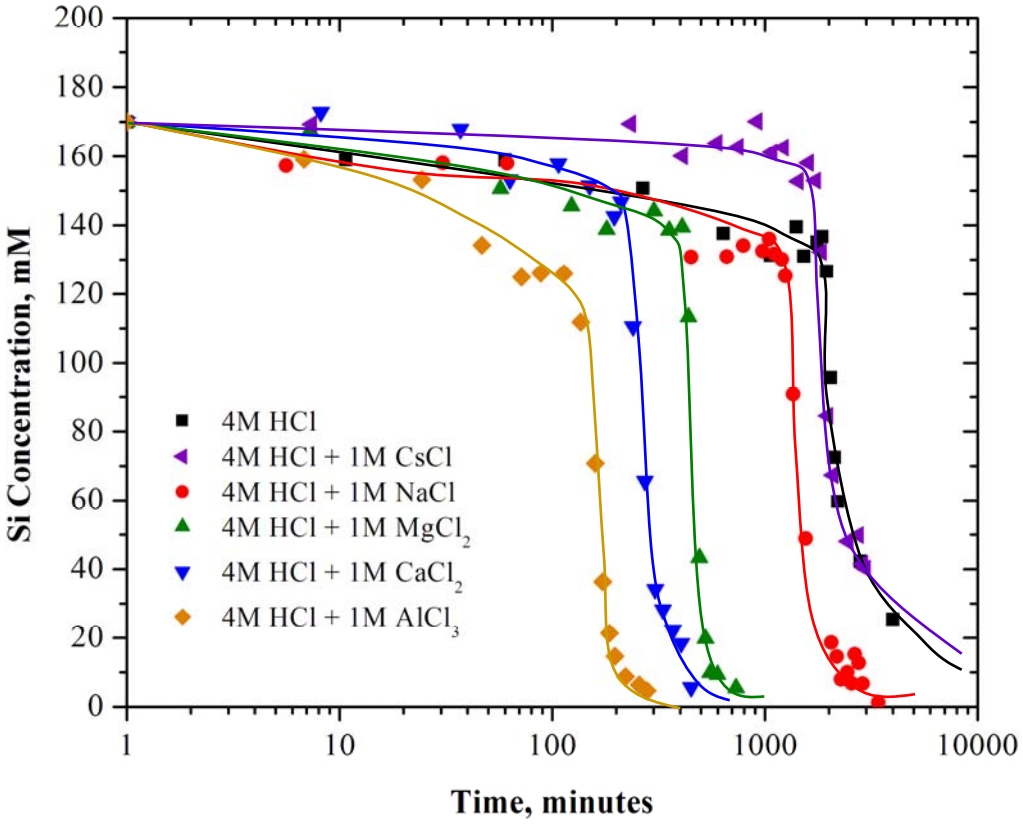

Figure 4.4: Si concentration profiles as a function of time obtained from different salt solutions measured by ICP/MS.

DLS data in Figure 4.5 show the exponentially increasing growth of silica particles can be expressed mathematically expressed in the form given by Equation 4.2. Among different salts, the trivalent inorganic salt $AlCl_3$ at 1 M is more effective at promoting particle growth than the divalent and monovalent salts at the same concentration[15], which follows the same order of salts obtained by ICP. Table 4.1 shows an excellent agreement between the ICP/MS and DLS data.

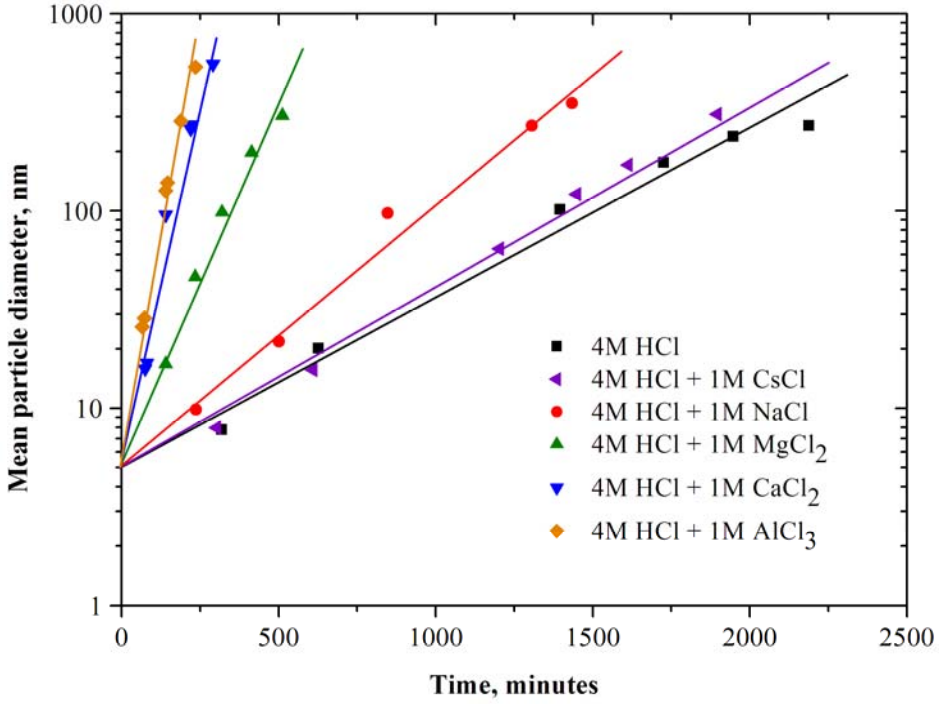

Figure 4.5: Mean silica particle diameter versus time obtained from dynamic light scattering.

Table 4.1: Comparison of times to reach 0.2µm analyzed using ICP/MS and DLS.

Solution	Time to reach 0.2µm observed from ICP/MS (minutes)	Time to reach 0.2µm measured from DLS (minutes)
170mM + 4M HCl (Base case)	1,964	1,822
170mM + 4M HCl + 1M CsCl	1,695	1,715
170mM + 4M HCl + 1M NaCl	1,125	1,210
170mM + 4M HCl + 1M $MgCl_2$	447	434
170mM + 4M HCl + 1M $CaCl_2$	210	211
170mM + 4M HCl + 1M $AlCl_3$	133	172

Particle Growth Predictions Using Geometric Population Balance

Previous work by Gorrepati and Fogler[6] showed that the particle growth measured by DLS is due to aggregation of primary silica particles. In this section modified Smoluchowski equation for colloidal aggregation under the framework of geometric population balance (GPB) was used to study the mechanism of silica particle growth.

In general, the aggregation of particles was first described by von Smoluchowski in 1917. A fundamental assumption of the Smoluchowski approach is that aggregation is a second-order rate process, in which the rate of collision is proportional to the product of concentration of two colliding species, simply refer to 'i-th' and 'j-th' aggregates[23]. Assuming effective collisions in forming aggregate, the Smoluchowski coalgulation equation for the k-th aggregates, where k = i + j, is given as:

$$\frac{dn_k}{dt} = \frac{1}{2}\sum_{\substack{i+j\to k \\ i=1}}^{i=k-1} K_{ij} c_i c_j - c_k \sum_{k=1}^{\infty} K_{ik} c_i \qquad (4.3)$$

where k = the number of aggregate units (k = 1, 2, 3, …, N),

c_i = molar concentration of i-th aggregates (M), and

K_{ij} = collision kernel describing the rate at which i- aggregate coagulate with j-th aggregate (l/M/min).

The former term represents the rate of formation of k-th aggregates through binary collision of small aggregates. The latter accounts for the loss of k-th aggregates according to collision with any other aggregates. The aggregation phenomena can be usually catagorized into 2 different types: Diffusion-Limited Aggregation (DLA) and Reaction-Limited Aggregation (RLA). DLA occurs when the collision efficiency of two aggregates achieves unity and particle growth follows power-law kinetics, whereas RLA

happens in cases of very low collison efficiency and follows an exponential particle growth law[24].

In order to solve the population balance equation (4.3) for each species, the Smoluchowski equation is computationally very expensive. For a final aggregate diameter of the order of 1μm 10^8 ordinary differential eqautions must be solved simultanously. Therefore, a geometric population balance (GPB) which assumes a geometric spacing between two subsequent aggregates, R, was used. That is, the i-th aggregate contains R^{i-1} number of primary particles. For instance, a geometric population balance reduces[25] the number of ordinary differential equations from 10^8 to 28 when R = 2 The generation and depletion terms in equation (4.3) have been modified to take the form;

$$\frac{dn_i}{dt} = \frac{K_{i-1,i-1}}{R} c_{i-1}^2 + c_{i-1} \sum_{j=1}^{i-2} \frac{R^{j-1}}{R^{i-1} - R^{i-2}} K_{i-1,j} c_j - c_i \sum_{j=1}^{i-1} \frac{R^{j-1}}{R^i - R^{i-1}} K_{i,j} c_j - c_i \sum_{j=1}^{N-1} K_{i,j} c_j \qquad (4.4)$$

Term I **Term II** **Term III** **Term IV**

Term I: R number of (i-1)-th aggregates to form one i-th aggregate (Generation 1).

Term II: An i-th aggregate to be created by the collision between one (i-1)-th aggregate and $\frac{R^{i-1} - R^{i-2}}{R^{j-1}}$ number of j-th aggregates (j<i-1) (Generation 2).

Term III: An i-th aggregate reacting with $\frac{R^i - R^{i-1}}{R^{j-1}}$ j-th aggregates to form the (i+1)-th aggregate (j<i) (Depletion 1).

Term IV: The formation of one (j+1)-th aggregate by one j-th aggregate (j≥i) and $\frac{R^j - R^{j-1}}{R^{i-1}}$ i-th aggregates (Depletion 2).

For silica particle growth studies by Gorrepati and Fogler[6] the aggregation process was modeled with a geometric spacing (R) of 2, the fractal dimension of 2 was used regarding the reaction-limited system, and a total number of 30 differential equations (for aggregates containing 1, 2, 4, …, $2^{(30-1)}$ primary particles) which were simultaneously solved. A geometric spacing of 2 was used to calculate the aggregate size, meaning that the x-th aggregate has 2^{x-1} numbers of primary units. For example, the forth aggregate has 2^3 (or 8) primary units.

The important parameters that need to be identified for modeling were collision kernel and the size of primary unit. The reaction-limited collision kernel proposed by Ball et al.[26] and the primary silica particle size of 5nm were used in the model (Gorrepati and Fogler[6]). The expression of reaction-limited collision kernel is given below:

$$K_{ij} = C(d_i + d_j)^2 \tag{4.5}$$

where C = aggregation rate constant ($1/M/min/m^2$),

d_i, d_j = particle diameter of i-th and j-th aggregate, repectively (m).

The simulated particle size profiles based on the reaction-limited aggregation (RLA) kernel are shown in Figure 4.6. One observes that the development of silica aggregate size perfectly matches with the mean particle size data gained from DLS for all salts studies and that the reaction-limited aggregation model (RLA model) well describes the evolution of silica particle size.

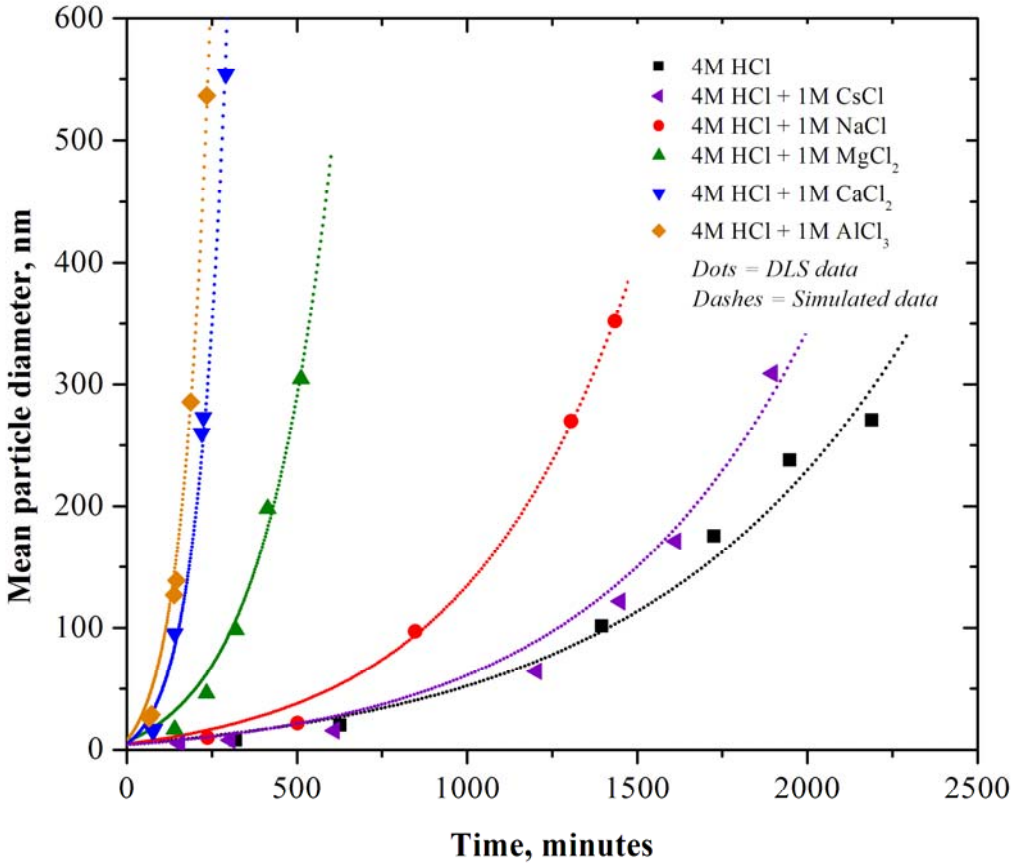

Figure 4.6: Comparison of experimental and simulated evolution of silica particles using RLA model.

The evolution of particle size distribution in time simulated within the framework of geometric population balance provided the systematic approach for estimating the size of silica aggregate. Taking advantage of this RLA model, we could compare the times to reach 0.2μm obtained from ICP/MS and DLS with one from the geometric population balance model.

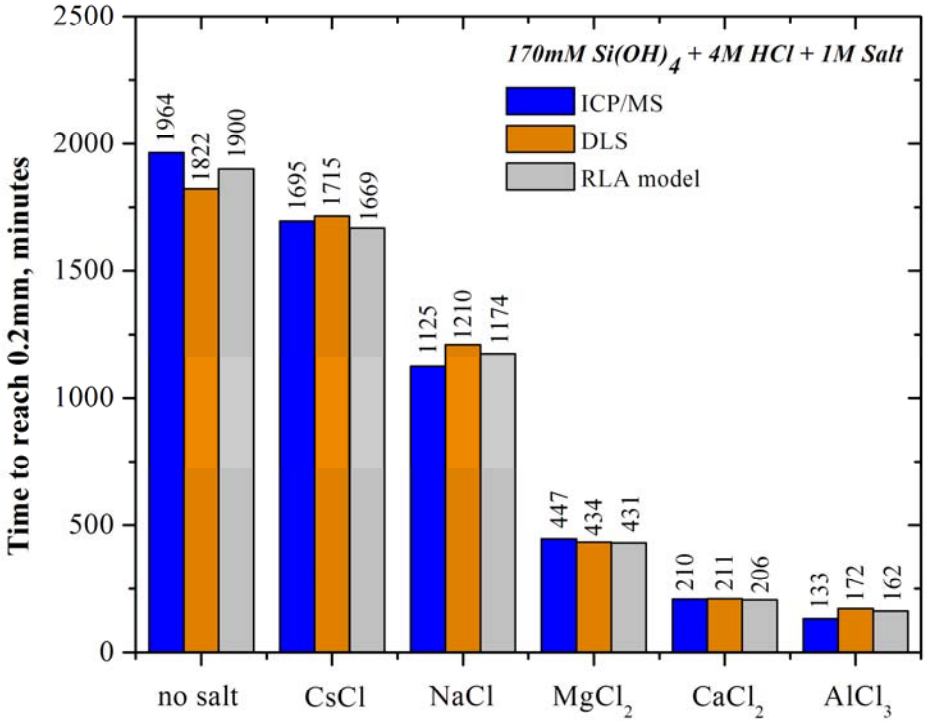

Figure 4.7: Precipitation times (time to reach 0.2µm) obtained from different salts and different techniques.

Figure 4.7 presents the comparison on precipitation times (the time for the silica particles to reach 200 nm) observed from 3 different approaches, and shows the good agreement between ICP/MS, DLS data and simulated data from RLA model. One concluds that the presence of salt shortens the precipitation times and hastens the particle growth in order of 1M salt addition to 4M HCl by:

$$AlCl_3 > CaCl_2 > MgCl_2 > NaCl > CsCl > \text{pure 4M HCl}.$$

Analysis of Monosilicic Acid Disappearance Kinetics

The data show that aggregation of silica primary particles is governed by a reaction-limited mechanism and the presence of salt can accelerate silica particle flocculation. To study the entire process, the kinetics of the disappearance of silicic acid monomer was investigated by the Molybdenum-blue method (ASTM D859-05) where UV-Vis spectroscopy was used to analyze the monosilicic acid disappearance kinetics.

Figure 4.8 shows that the kinetic of monosilicic disappearance at analogous conditions obey a third-order rate law dependence at short times before reaching its equilibrium stage. The rate equation of monosilicic acid disappearance could be written as;

$$\frac{d[Si(OH)_4]}{dt} = -k_D[Si(OH)_4]^3 \qquad (4.6)$$

where k_D denotes the disappearance rate constant. Direct integration of equation (4.6) yields the following relationship;

$$\frac{1}{2}\left[\frac{1}{[Si(OH)_4]^2} - \frac{1}{[Si(OH)_4]_o^2}\right] = k_D t \qquad (4.7)$$

The plot of rate function, as refered to $\left\{\frac{1}{2}\left[\frac{1}{[Si(OH)_4]^2} - \frac{1}{[Si(OH)_4]_o^2}\right]\right\}$, versus time and disappearance rate constants at different salt systems are given in Figure 4.8 and Table 4.2, respectively. The disappearance rate constant k_D can be obtained from the slope of the linear relationship between the rate function and time. It was found that rate constants increase when salt was introducted into the acid solution. The different salts can accelerate the kinetics of monosilicic acid disappearance in the order of

$$AlCl_3 > CaCl_2 > MgCl_2 > NaCl > CsCl > \text{Pure 4M HCl.}$$

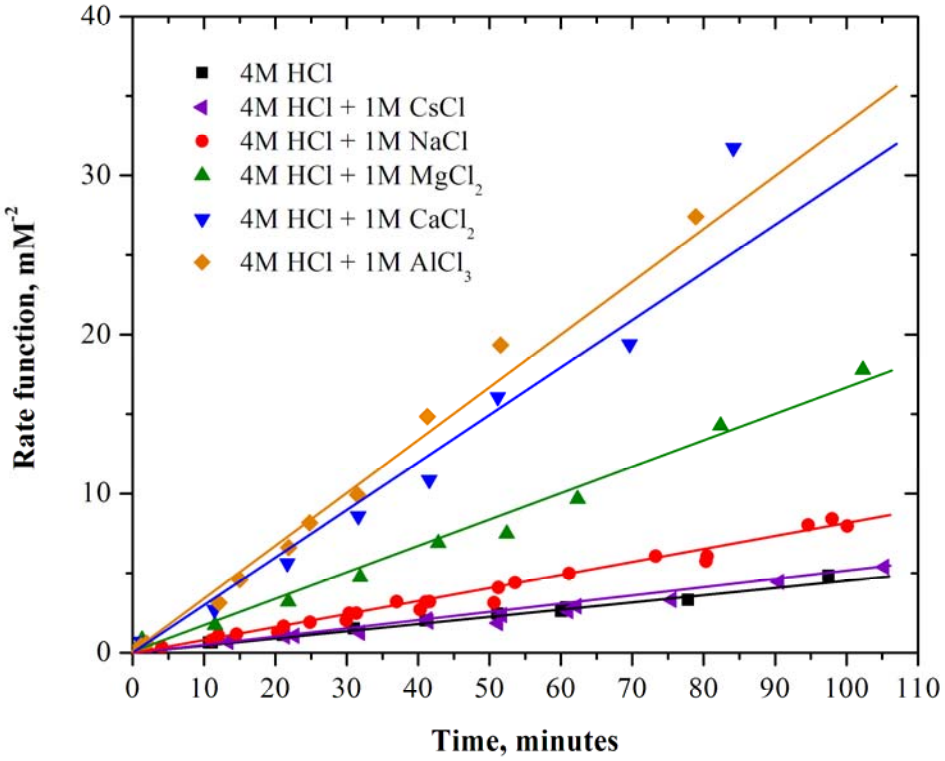

Figure 4.8: The rate function plotted vs.time for the molydate-reactive silica data: Initial $Si(OH)_4$ concentration of 170mM, 5.0°C and 500rpm.

Recall that the exponential fit to the DLS data was based on an assumption that the formation of primary particle takes place virtually instantly at t = 0. From previous work by Gorrepati and Fogler[6], it is observed that monosilicic acid disappears very rapidly in acid solutions to form primary silica particles. Thus, the assumpation that the primary particles are formed at t = 0 is acceptable. It has been noticed that total silica concentration, as measured by ICP/MS, was found to be much higher than the molybdate reactive silica concentration. The molybdate reactive silica test will expose monomers, possibly dimers, of silicic acid in the solution whereas ICP/MS will detect the total amount of silica species less than 200μm permeating through polypropylene filters.

Table 4.2: Comparison of particle growth rate constants (k_G), aggregation rate constants (C), and disappearance rate constants (k_D) obtained from salts experiments. The rate constant values for the basecase (4M HCl, no salt) were used for kg_o, C_o, and k_{Do}.

Solution	Ionic strength (M)	k_G (Eqn 4.2) (min^{-1})	C (Eqn 4.5) ($M^{-1}.min^{-1}.m^{-2}$)	k_D (Eqn 4.7) ($M^{-2}.min^{-1}$)	kg/kg_o	C/C_o	k_D/k_{Do}
170mM + 4M HCl **(Base case)**	4	0.0019	5.897×10^{16}	4.60×10^{4}	1.00	1.00	1.00
170mM + 4M HCl + 1M CsCl	5	0.0024	6.726×10^{16}	4.90×10^{4}	1.26	1.14	1.07
170mM + 4M HCl + 1M NaCl	5	0.0030	9.546×10^{16}	7.90×10^{4}	1.58	1.62	1.72
170mM + 4M HCl + 1M $MgCl_2$	7	0.0078	2.574×10^{17}	1.66×10^{5}	4.11	4.36	3.61
170mM + 4M HCl + 1M $CaCl_2$	7	0.0170	5.448×10^{17}	3.43×10^{5}	8.95	9.24	7.46
170mM + 4M HCl + 1M $AlCl_3$	10	0.0184	6.648×10^{17}	3.47×10^{5}	9.68	11.27	7.54

Effect of Ionic Strength on Silica Aggregation and Monosilicic Acid Disappearance

A relationship between ionic strength and polymerization rate constant for silica systems in *mildly acid to alkaline* circumstances has been proposed by Fleming[19]. The relationship is emprical, but is similar to the Bronsted-Guggenheim approach for activity coefficients and is shown below:

$$\ln k_p = A\frac{\sqrt{I}}{1+\sqrt{I}} + B \ , \tag{4.8}$$

where $I = \frac{1}{2}\sum_{i=1}^{n} Z_i^2 C_{i,\infty}$ = ionic strength,

Z_i = charge of ion *i*,

$C_{i,\infty}$ = concentration of ion *i* in bulk solution (M),

k_p =silica polymerization rate constant (units vary, see Table 4.2)

and A, B = empirical constants.

Equation 4.8 was applied to the silica system in *very low pH* conditions. Figure 4.9 shows the ionic strength dependence of particle growth rate, aggregation rate, and disappearance rate. They indicate that particle growth rate constant (k_G, Eqn 4.2), aggregation rate constant (C, Eqn 4.5), and disappearance rate constant (k_D, Eqn 4.7), for the different salts, increase exponentially with respect to the ionic strength function.

From Figure 4.9, one observes that aggregation of silica particles and disappearance kinetics are promoted as the ionic strength of the solution increases, regardless of salt types. A higher ionic strength results in a faster silica aggregation/particle growth and monosilicic acid disappearance.

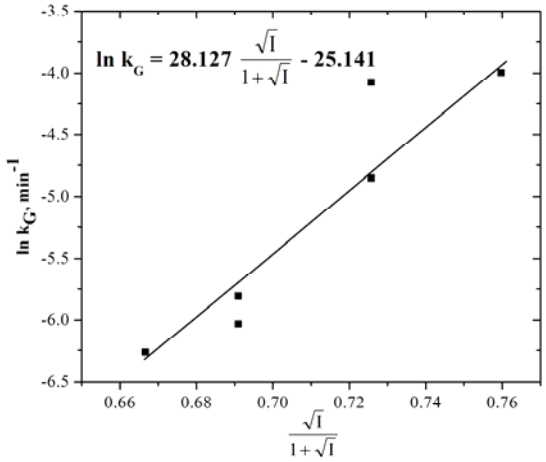

(a)

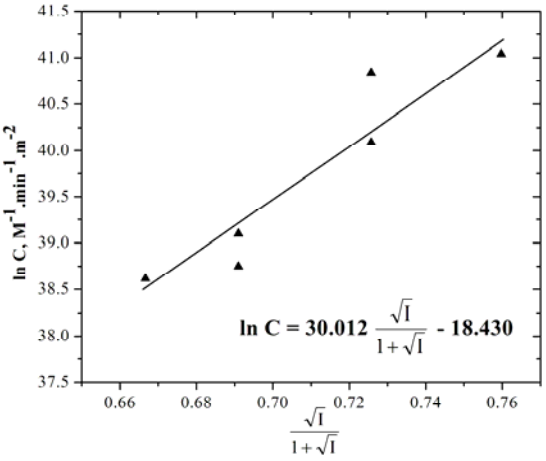

(b)

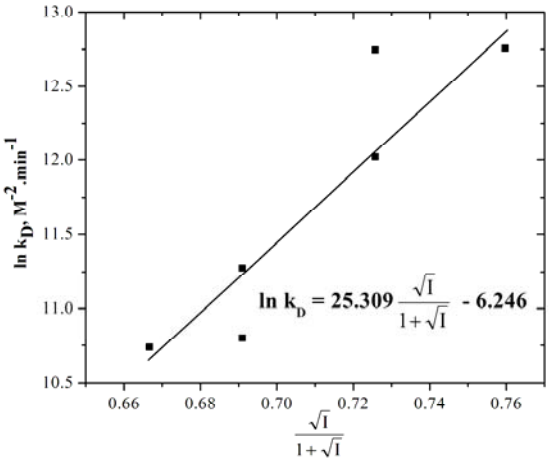

(c)

Figure 4.9: Dependence of the natural logarithm of (a) particle growth rate constant (b) aggregation rate constant and (c) disappearance rate constant, on the ionic strength function.

The plots in Figure 4.9 were normalized by normalizing all values to the basecase, which was 4M HCl and no salt. All rate constants were normalized to the basecase. The ionic strength function was also normalized to the basecase, which had a ionic strength value of 0.667 (see Figure 4.10).

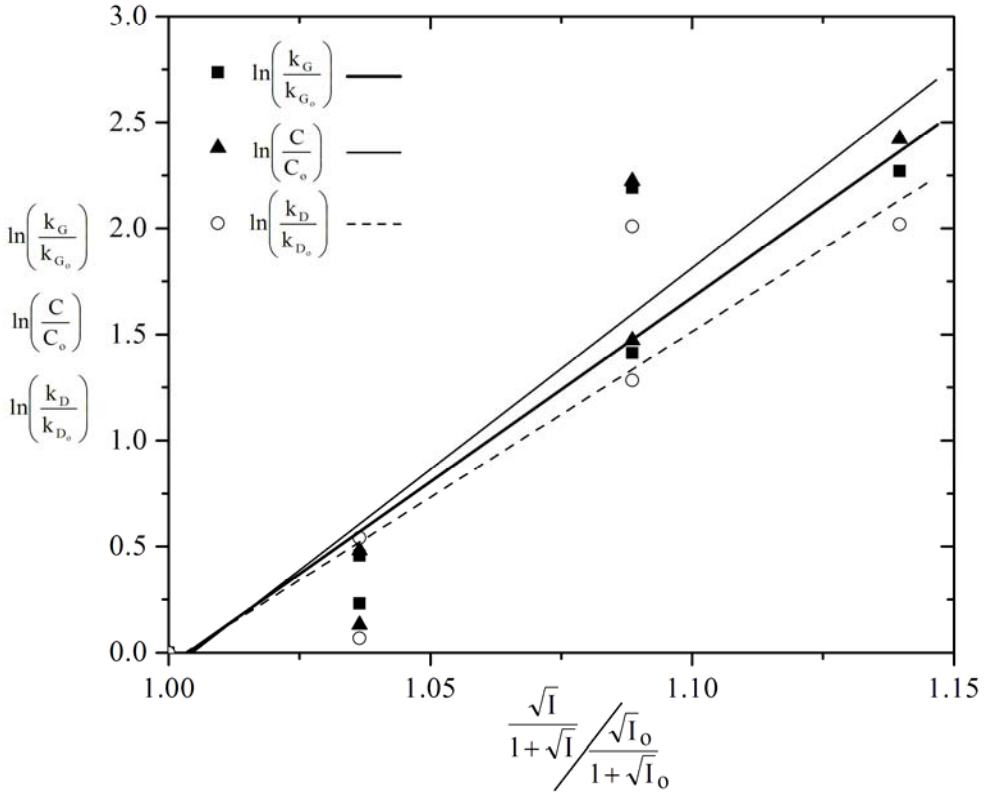

Figure 4.10: Dependence of the natural logarithm of particle growth rate constant aggregation rate constant and disappearance rate constant, on the ionic strength function.

In the colloidal science literature, the interaction between charged colloidal particles in a liquid medium has been explained in terms of classical DLVO forces, i.e. attractive van der Waals force and repulsive electrical double layer force. The sum of DLVO forces can determine the stability of colloidal particles in a solution. The colloidal stability decreases when the repulsive force is larger than the attractive force. The stability of suspended particles decreases as the ionic strength of the medium increases because the increase in ionic strength reduces the electrical double layer thickness and thus weakens the repulsive force. The weakened repulsive force enables two colloidal particles to attract each other more easily, resulting in the coagulation of particles.

However, fast aggregation in the case of high ionic strength silica systems is not only the result of the fact that the repulsive force is weakened as the electrical double layer thickness decreases. In our high ionic strength systems, the double layer thickness was calculated to be around 0.5Å. Consequently, classical DLVO forces cannot completely describe the interaction of silica particles due to the occurrence of an additional short-range repulsive force. A number of researchers have been investigated the origin of this short-range repulsive force. Several workers believe that the silica colloidal particle itself is strongly bound to water molecules in nature, and this additional force may arise from surrounding water molecules, preventing two suspended particles to approach each other and form the aggregate. This force is called a "hydration force"[27,28]. Other researchers hypothesize that this repulsive force may arise from the existence of "silica hairs", which are silanol groups (Si-OH) and silicilic acid ($Si\text{-}O^-$) groups protruding from the surface of silica particles[29,30]. These protruding groups may contribute to a steric force to prevent two particles coming into contact. These hairs may lie down at higher ionic strength offering less steric resistance[31]. Further studies are needed to investigate the origin of that additional force. This short-range repulsive force needs to be incorperated into the classical DLVO thoery in order to allow us to better understand the overall interaction of silica suspended particles.

Conclusions

The effects of salts and ionic strength on silica aggregation and kinetics of monosilicic acid disappearance were investigated at low temperature and highly acidic conditions. Experiments on mixtures of pure monosilicic acid, HCl, and chloride salt were carried out under the analogous conditions previously described from HCl. It was found that silica particle size increases exponentially with respect to time and the monosilicic acid disappearance kinetics assume to be second-order rate law dependence. In salts experiment, it was shown that the presence of salt promotes the silica particle growth, aggregation, and disappearance kinetics. Among different salts at the same molar concentration, salts accelarate the particle growth in the following order:

$$AlCl_3 > CaCl_2 > MgCl_2 > NaCl > CsCl.$$

The evolution of the silica aggregate size have been successfully simulated using the modified Smoluchoski equation coupled with the geometric population balance (GPB). In addition, the results indicate that aggregation and disappearance rate constants increase exponentially as a function of ionic strength.

References

[1] Lund, K.; Fogler H. S.; McCune, C.C. *Chem. Eng. Sci.*, **1973**, *28*, 691.
[2] Crowe, C.; Masmonteil, J.; Touboul, E.;Thomas, R. *Oilfield Rev.*, **1992**, *4*, 24.
[3] Underdown, D. R.; Hickey, J. J.; Kalra, S. K. *Proceedings of 65th Annual SPE Technical Coference and Exhibition*, New Orleans, LA, 1990.
[4] Hartman, R. L.; Fogler, H. S. *Langmuir* **2006**, *22*, 11163.
[5] Hartman, R. L.; Fogler, H. S. *Langmuir* **2007**, *23*, 5477.
[6] Gorrepati, E., and Fogler, H.S. *Industrial Affiliates Report*, University of Michigan, 2008.
[7] Schechter, R. S. *Oil Well Stimulation*; Prentice Hall: New Jersey, 1992.
[8] King, R. J. *Geol. Today*, **2001**, *17*, 236.
[9] Hartman, R. L.; Fogler, H. S. *Ind. Eng. Chem. Res.* **2005**, 44, 7738.
[10] Iler, R. K. *The Chemistry of Silica: Solubility, Polymerization, Colloid and Surface Properties, and Biochemistry*; John Wiley & Sons: New York, 1979.
[11] Makrides, A. C.; Turner, M.; Slaughter, J. *J. Colloid Interf. Sci.* **1980**, *73*, 345.
[12] Icopini, G. A.; Brantley, S. L.; Heaney, P. J. *Geochim. Cosmochim. Acta.* **2005**, *69*, 293.
[13] Goto, K. *J. Phys. Chem.* **1956**, *60*, 1007.
[14] Weres, O.; Yee, A.; Tsao, L. *J. Colloid Interf. Sci.* **1981**, *84*, 379.
[15] Crerar, D. A.; Axtmann, E. V.; Axtmann, R. C. *Geochim. Cosmochim. Acta* **1981**, *45*, 1259.
[16] Suttle, C. A.; Price, N. M.; Harrison, P. J.; Thompson, P. A. *J. Phycol.* **1986**, *22*, 234.
[17] Gdanski, R. D. *SPE Prod. Facil.* **1998**, *13*, 75.
[18] Thomas, R. L.; Nasr-El-Din, H. A.; Lynn, J. D.; Mehta, S. *Proceedings – Society of Petroleum Engineers Annual Technical Conference and Exhibition*, New Orleans, LA, 2001.
[19] Fleming, B. A. *J. Colloid Interf. Sci.* **1986**, *110*, 40.
[20] Potapov, V. V.; Serdan, A. A.; Kashpura, V. N.; Gorbach, V. A.; Tyurina, N. A.; Zubakha, S. V. *Glass Phys. Chem.*+ **2007**, *33*, 44.
[21] Chan, S. H.; Neusen, K. F.; Chang, C. T. *Proceedings of the ASME-JSME Thermal Engineering Joint Conference*, 1987.
[22] Marshall, W. L.; Warakomski, J. M. *Geochim. Cosmochim. Acta* **1980**, *44*, 915.
[23] Elimelech, M.; Gregory, J.; Jia, X.; Williams, R. *Particle Deposition & Aggregation: Measurement, Modeling, and Simulation*; Butterworth-Heinemann: Oxford, 1995.
[24] Rungkana, V.; Somasundaran, P.; Kapur, P. C. *AIChE J.* **2004**, *51*, 1233.
[25] Maqbool, T.; Raha, S.; Fogler, H. S. *The 8th International Conference on Petroleum Phase Behavior and Fouling*, Pau, France, 2007.
[26] Ball, R. C.; Weitz, D. A.; Witten, T. A.; Leyvraz, F. *Phys. Rev. Lett.* **1987**, *58*, 274.
[27] Yotsumoto, H.; Yoon, R. H. J. *Colloid Interf. Sci.* **1993**, *157*, 434.
[28] Horn, R. G.; Smith, D. T.; Haller, W. *Chem. Phys. Lett.* **1989**, *162*, 404.
[29] Vigil, G.; Xu, Z. H.; Steinberg, S.; Israelachvili, J. *J. Colloid Interf. Sci.* **1994**, *165*, 367.
[30] Israelachvili, J. N.; Wennerström, H. *Nature* **1996**, *379*, 219.
[31] Yokoyama, A.; Srinivasan, K. R.; Fogler, H. S. *Langmuir* **1989**, *5*, 534.

CHAPTER V

CONCLUSIONS

Dissolution of the Zeolite Analcime and Subsequent Silica Precipitation in Various Acids

Analcime initial dissolution rate in the strong acids HCl, HBr, and HNO_3 was shown to follow a Langmuir-Hinshelwood mechanism and can be expressed by a Michaelis-Menten rate law. This is in partial agreement with Hartman and Fogler (2005) who showed that analcime dissolution rate in HCl follows a Langmuir-Hinshelwood mechanism. Dissolution of analcime in different acids results in different silicon plateau heights. It is shown that the different plateau heights are due to recondensation of silanol groups within analcime; that is, a lower plateau height indicates that the silanol –Si-OH groups within the dissolving mineral recondense, forming siloxane –O-Si-O- bonds faster. This recondensation reaction occurs faster in different acids corresponding to the order

$$H_2SO_4 > HI > HBr > HCl > HNO_3.$$

At very low proton concentrations, analcime initial dissolution rate is faster in citric acid than in strong acids. However, at proton concentration greater than 0.055M, the analcime initial dissolution rate is faster in strong acids than in citric acid.

Pure monosilicic acid solutions may be used to study the precipitation of silicon dissolved from minerals because mineral dissolution and silica precipitation are *decoupled*.

Silica Precipitation from Analcime Dissolution: Fundamental Mechanisms and Effect of Acid Concentration

As was shown in the previous chapter, the behaviour of silicon dissolved from analcime can be mimicked using pure monosilicic acid solutions. That is, silicon concentration in solution, as measured by AAS or ICP-MS, is similar for silicon dissolved from analcime and silicon from commercially available sodium metasilicate nonahydrate. This is assuming, of course, similar reaction conditions and same "plateau height".

Using pure monosilicic acid solutions, it was found that monosilicic acid disappears very rapidly from acidic solution via a second order reaction, as measured by UV-VIS. During this time, the monomers are rapidly forming nuclei, which then grow to form particles 5 nm in diameter within the first few minutes of reaction. These 5 nm particles then flocculate by reaction-limited aggregation to give an exponential increase in mean particle size. This flocculation is successfully modeled by a modified Smoluchowski equation with a reaction-limited kernel.

The whole monomer disappearance, nucleation, and aggregation process is more rapid in increasing concentrations of HCl. Furthermore, during analcime dissolution plateau height is lower in lower HCl concentrations, indicating that the recondensation reaction discussed in Chapter 2 is more rapid at higher concentrations of HCl

Ionic Effects on Silica Precipitation in Acidic Solutions

The effects of salts and ionic strength on silica aggregation and kinetics of monosilicic acid disappearance were investigated under very low temperature and highly acidic condition. A set of experiments of the mixture of pure monosilicic acid, HCl, and chloride salt were carried out under the analogous condition described previously. It was found that silica particle size increases exponentially with respect to time and the monosilicic acid disappearance kinetics assume to be second-order rate law dependence. In these salt experiments, it was shown that the presence of salt promotes the silica particle growth, aggregation, and disappearance kinetics. Among different salts at the same molar concentration, salts accelerate the particle growth in the following order: $AlCl_3 > CaCl_2 > MgCl_2 > NaCl > CsCl$. The evolution of the silica aggregate size has been successfully simulated using the modified Smoluchowski equation coupled with the geometric population balance. In addition, the results indicate that aggregation and disappearance rate constants increase exponentially as a function of ionic strength.

Overall Industrial Implications

- The most important industrial application of the work is that low concentration of HCl (2M) should be used to acid stimulate reservoirs containing the zeolite analcime. The two reasons are:
    1. More analcime is dissolved thereby increasing the pore space and permeability to a greater extent
    2. The time for silica precipitation in 2M HCl is sufficiently long (~10,000 minutes) that the spent acid can be withdrawn from the well before silica precipitation.

CHAPTER VI

FUTURE WORK

Four significant avenues for extending this research are identified in this chapter:

1. Imaging of Silica Aggregates and Fractal Dimension Studies
2. Salt Effect Mechanism on Silica Polymerization and Aggregation
3. Formation Deposition Studies by Coreflood Experiments
4. Silica Precipitation Inhibition

Imaging of Silica Aggregates and Fractal Dimension Studies

Direct imaging of the silica particle would confirm what we have indirectly proven in this research: that silica particles in acidic conditions rapidly form primary particles of ~5 nm in diameter, then flocculate to form fractal aggregates that grow exponentially in size. Unfortunately, imaging of silica particles is extremely difficult because hydrated silica particles are easily deformed, and tend to stick to each other. Thus, during the course of any type of evaporation of solvent, silica particles become more concentrated and stick together, forming a precipitate or gel. SEM and TEM, *ex situ* techniques were attempted for direct imaging of silica particles. Liquid-phase AFM an *in situ* technique, was attempted for direct imaging of silica particles. SAXS, also an *in situ* technique, was attempted for indirect particle size distribution measurements and aggregate fractal dimension measurements.

SEM imaging of silica particles was attempted. As a first attempt, a drop of reaction solution was placed on sticky carbon tape mounted on an aluminum SEM stub.The solution was allowed to air dry, but in SEM images, silica particles appeared as a dried, cracked gel. This was true whether the silica source was analcime or sodium metasilicate nonahydrate. The same was true when the drop of solution was dried with a heat gun. Another route we explored was freeze-drying the reaction solutions, then imaging the dried silica particles. Unfortunately, freeze-drying the reaction solutions did not preserve the silica particles, and upon SEM imaging, we only saw large clumps of dried silica gel.

TEM imaging of silica particle was also attempted. In this technique, a carbon grid (300 mesh, Ted Pella) coated with lacey formvar was dipped into a pure monsilicic acid solution during reaction. The grid was dragged through the solution quickly in an attempt to catch some of the silica particles on the grid. The grid was then allowed to air-dry at room temperature and then TEM imaging was attempted. This technique allowed us to image the silica particles for a short time, but within a few seconds of the electron beam hitting the silica particles, we saw movement of the silica particles, and it appeared as if water in the particle was evaporating, distorting and destroying the particle. However, TEM has been used to previously image silica particles[1]. In addition, there have been studies where cryo-TEM successfully imaged silica particles[2]

Another technique we considered for imaging was AFM. Icopini *et al.* was able to use AFM to estimate the size of primary silica particles in solutions with pH 7; the particles were estimated to be ~3 nm in diameter[3]. Unfortunately, our attempt at using

liquid AFM to image silica particles *in situ* was unsuccessful and we did not observe any particles.

Finally, we attempted to use small-angle x-ray scattering (SAXS) to obtain particle size distributions and fractal dimension during the course of aggregation. SAXS has been previously used to investigate fractal dimension of silica sols[45]. However, the scattering intensities that were measured during our experiments were extremely low; thus, useable data was not obtained.

Although we did not obtain successful data with the above techniques, this is not to say that useful data can not be obtained with these techniques. On the contrary, previous researchers have used these techniques on silica sols. Thus, any continuing research should look into using these techniques and work out any details that would hinder the use of these technique on our low-temperature, acidic silica solutions. These techniques above could be used to 1) confirm the fractal silica aggregates that we indirectly postulated from the data in this thesis 2) obtain a better grasp of the processes that occur during silica polymerization and flocculation in acidic solutions.

Salt Effect Mechanism on Silica Polymerization and Aggregation

The fundamental mechanism by which salts influence precipitation and aggregation of silica is still unknown. In colloidal science, the interaction between charged colloidal particles in a liquid medium has been explained in terms of classical DLVO forces, i.e. attractive van der Waals force and repulsive electrical double layer force. The sum of DLVO forces can determine the stability of colloidal particle in the solution. The colloidal stability decreases when the repulsive force is larger than the attractive one. From a practical point of view, the stability of suspended particles

decreases as the ionic strength of the medium increases because the increase in ionic strength not only reduces the electrical double layer thickness but also weakens the repulsive force. The weakened repulsive force enables two colloidal particles to attract each other more easily, resulting in the coagulation of particles.

However, the fast aggregation, in case of silica system, is not only the result of the fact that the repulsive force is weakened as the electrical double layer thickness decreases. That is, classical DLVO forces cannot completely describe the interaction of silica particles due to the occurrence of the additional short-range repulsive force. A number of researchers have been investigated the origin of this short-range repulsive force. Several workers believe that the silica colloidal particle itself is strongly bound to water molecules in nature, and this additional force may arise from surrounding water molecules, preventing two suspended particles to approach each other and form the aggregate. This force is called a “hydration force”.

Some researchers hypothesize that this addition repulsive force may instead arise from the existence of “silica hairs”, which are silanol groups (Si-OH) and silicilic acid ($Si\text{-}O^-$) groups protruding from the surface of silica particles. These protruding groups may contribute to the steric force to prevent two particles coming into contact. Further studies are needed to investigate the origin of that additional force. This short-range repulsive force needs to be incorperated into the classical DLVO thoery in order to allow us to better understand the overall interaction of silica suspended particles.

Formation Deposition Studies by Coreflood Experiments

To move this research into the realm of practical application, an applied example is shown below. Say, for instance, a well is drilled and a core of the sandstone formation rock is obtained. It is desired to carry out a matrix acidization of 8M HCl on the formation. A mineralogical analysis is conducted on the core, and it is found to contain 5 wt% analcime, 5 wt% calcite, 15 wt% feldspar, and 75 wt% quartz. From the known chemical composition of these minerals, the molecular weight of their unit cell is known. In addition, the (mol Si)/(mol unit cell) is known. Then, if one knows the percent of silicon that dissolves from each mineral, we can calculate the concentration of silica in the acidizing fluid.

Table 6.1: Calculation of amount of silica in acidizing fluid for a representative sandstone core.

Mineral	Wt% in core	Unit cell molecular weight	Mol Si/ Mol Unit Cell	%Si that dissolves in 8M HCl
Quartz	75	60 g/mol	1	0
Feldspar	15	x†	y†	z‡
Calcite	5	100 g/mol	0	-
Analcime	5	440 g/mol[6]	2	55

†Depends on specific type of feldspar.

‡Will need to be determined by batch experiment.

With the information in Table A.1, we can then calculate the moles of silicon that will dissolve from the core minerals per gram of core:

$$\underbrace{0.75\frac{1}{60}*0}_{\text{Quartz}}+\underbrace{0.15\frac{y}{x}*\frac{z}{100}}_{\text{Feldspar}}+\underbrace{0.05*\frac{0}{100}*0}_{\text{Calcite}}+\underbrace{0.05*\frac{2}{440}0.55}_{\text{Analcime}} \quad \frac{\text{mol Si that will dissolve}}{\text{g core}}$$

Then, we can convert this value into concentration of Si released into the acidizing fluid by multiplying by overall core density and dividing by porosity:

$$\frac{\text{mol Si that will dissolve}}{\text{g core}} \cdot \frac{\text{g core}}{\text{volume core}} \cdot \frac{\text{volume core}}{\text{pore volume}} = \frac{\text{Mol Si}}{\text{Pore Volume}} .$$

Then, we can predict how fast the silica released into the acidizing fluid will polymerize and flocculate using the data or techniques in this thesis. For example, say that the amount of silicon that will dissolve per gram of core was calculated to be $1.8*10^{-5}$ (mol Si)/(g core). Then, converting to concentration of acidizing fluid:

$$1.8*10^{-5}\frac{\text{mol Si}}{\text{g core}}*\frac{2200\text{ g core}}{\text{L core}}*\frac{\text{L core}}{0.3\text{ L pore}}=\frac{0.132\text{ mol Si}}{\text{L pore}}=132\frac{\text{mmol}}{\text{L}}$$

It is now known from this research how 132 mmol/L of Si will behave in 8M HCl. We can predict that the silica particles growing inside the formation will grow to 200 nm in about 140 min, and silica particles will grow to 1000 nm in about 200 minutes (see Chapter 3). The silica particle flocculation rate can be controlled by using different concentrations of HCl, as previously shown in this research. If a lower flocculation rate is desired, a lower concentration of HCl should be utilized.

Of course, these silica particle diameters are a rough estimate because the concentration of silicon in solution is assumed to be uniform and the silica particle growth rates are for 5 degrees Celcius. However, the temperature effect on polymerization/flocculation issue can be overcome by studying solutions of pure monosilicic acid at the appropriate silicon concentration and temperature. (Also recall that temperature does not affect the percent of silicon dissolved from a mineral). A larger

obstacle is that these precipitation and flocculation rate calculations are for a batch reactor, and not for an acid flowing through a core.

A future researcher could model the fluid mechanics of HCl acidization in a core, modeling the core as a packed bed reactor and taking into account the silicon dissolution and flocculation occurring in the core. A lumped-parameter model could be developed, similar to that developed by Lund and Fogler[7].

Silica Precipitation Inhibition

The inhibition of silica precipitation has been investigated only briefly. Previous researchers in the Fogler group have attempted to dissolve analcime in the chelating agents EDTA and citric acid. It was found that analcime barely dissolves in EDTA. It was also found that dissolution in citric acid may proceed at a faster or slower rate than HCl, depending on concentration and reaction conditions. That is, the results for citric acid were ambiguous.

In addition, the silica precipitation inhibitor Versaflex Si made by Alco Chemical did not influence silica precipitation, even at concentrations of inhibitor of 10,000ppm. There is some research suggesting that polymers containing side-carboxyl groups may inhibit silica precipitation, but again, there has not been a systematic study of the effect of these polymers on precipitation.

Ribose was also added to a acidic solution containing silica, with, again, no effect on silica precipitation.

As mentioned in the introduction, a study by Sedah suggests that gallic acid will chelate silicon in solution. Gallic acid is a derivative of catechol, a well known chelator

of silica. Gallic acid and catechol have not been investigated for silica complexation in acidic solutions as of yet.

References

[1] Whitsitt, E. A ; Barron, A. R. *J Colloid Interf. Sci.* **2005**, *287*, 318.
[2] Snyder, M. A.; Lee, J. A.; Davis, T. M.; Scriven, L. E.; Tsapatsis, M. *Langmuir* **2007**, *23*, 9924.
[3] Icopini, G. A.; Brantley, S. L.; Heaney, P.*J. Geochim. Cosmochim. Acta* **2005**, *69*, 293.
[4] Ågren, P.; Counter, J.; Laggner, P. *J. Non-Cryst. Solids* **2000**, *261*, 195.
[5] Knoblich, B.; Gerber, T. *J. Non-Cryst. Solids* **2001**, *283*, 109.
[6] Breck, D. W. *Zeolite Molecular Sieves*; John Wiley & Sons: New York, 1974.
[7] Lund, K; Fogler, H. S. *Chem. Eng. Sci.* **1976**, *31*, 381

APPENDICES

APPENDIX A

SILICA PARTICLE GROWTH MODELING AND DYNAMIC LIGHT SCATTERING DATA CONVERSION DETAILS

Details of Modeling and Conversion of Particle Size Distributions

The original Smoluchowski equation for generation and depletion of a k^{th} aggregate *containing k number of primary particles* is(Elimelech, 1995):

$$\frac{dC_k}{dt} = \frac{1}{2}\sum_{\substack{i+j=k \\ 1\le i\le k-1}} K_{i,j}C_iC_j - C_k\sum_{j=1}^{\infty} K_{k,j}C_j \qquad \text{(A.1)}$$

C_i is the concentration of flocs with i number of primary particles,

$K_{i,j}$ is the collision kernel for flocs with i and j number of primary particles.

In our modified Smoluchowski equation, there are two terms for the generation of an i^{th} aggregate and two terms for the depletion of the i^{th} aggregate. Again, R is the geometric scaling factor (e.g. if R=2 the 1^{st}, 2^{nd}, 3^{rd}, and 4^{th} aggregates would consist of 1, 2, 4, and 8 primary particles, respectively).

$$\frac{dC_i}{dt} = \boxed{\frac{K_{i-1,i-1}}{R}C_{i-1}^{\,2}} + \boxed{C_{i-1}\sum_{j=1}^{i-2}K_{i-1,j}\frac{R^{j-1}}{R^{i-1}-R^{i-2}}C_j} - \boxed{C_i\sum_{j=1}^{i-1}K_{i,j}\frac{R^{j-1}}{R^{i}-R^{i-1}}C_j} - \boxed{C_i\sum_{j=i}^{N-1}K_{i,j}C_j} \qquad \text{(A.2)}$$

Generation 1 | Generation 2 | Depletion 1 | Depletion 2

Note: in the modified equation, the "i^{th} aggregate" contains R^{i-1} primary particles, *not* i primary particles.

Table A.1: Reactions used in the geometric Smoluchowski equation.

Mechanism	**Reaction**		
Generation 1	$RA_{i-1} \rightarrow A_i$		
Generation 2	$A_{i-1} + mA_j \rightarrow A_i$	$j < (i-1)$	$m = \frac{R^{i-1} - R^{i-2}}{R^{j-1}}$
Depletion 1	$A_i + mA_j \rightarrow A_{i+1}$	$j < i$	$m = \frac{R^{i} - R^{i-1}}{R^{j-1}}$
Depletion 2	$mA_i + A_j \rightarrow A_{j+1}$	$j \geq i$	$m = \frac{R^{j} - R^{j-1}}{R^{i-1}}$

In our geometric population balance, the flocculations that occur are always between m smaller aggregates and 1 aggregate one size less than the product aggregate, to give the product aggregate. Using this framework, we can then derive the two types of generation of ith aggregate and two types of depletion of ith aggregate.

In generation 1, the $(i-1)^{th}$ aggregate may react with another $(i-1)^{th}$ aggregate to form the i^{th} aggregate.

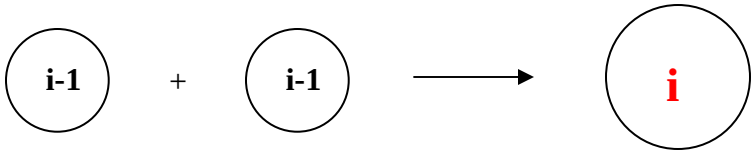

Figure A.1: Generation 1 mechanism.

In generation 2, the $(i-1)^{th}$ aggregate may react with smaller aggregates to form the i^{th} aggregate.

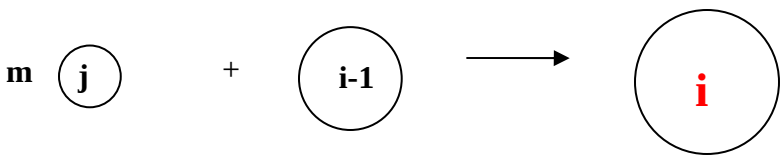

Figure A.2: Generation 2 mechanism.

In depletion 1, the i^{th} aggregate may flocculate with aggregates smaller than itself to give the $(i+1)^{th}$ aggregate.

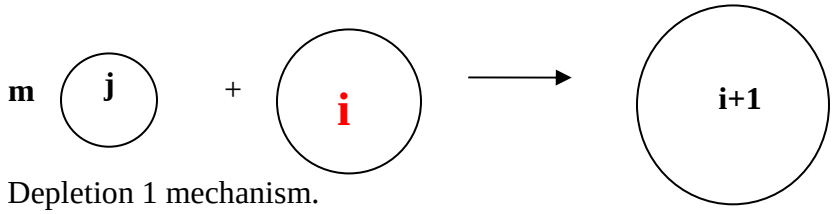

Figure A.3: Depletion 1 mechanism.

In depletion 2, the i^{th} aggregate may flocculate with a j^{th} aggregate larger than or equal to itself to give the $(j+1)^{th}$ aggregate.

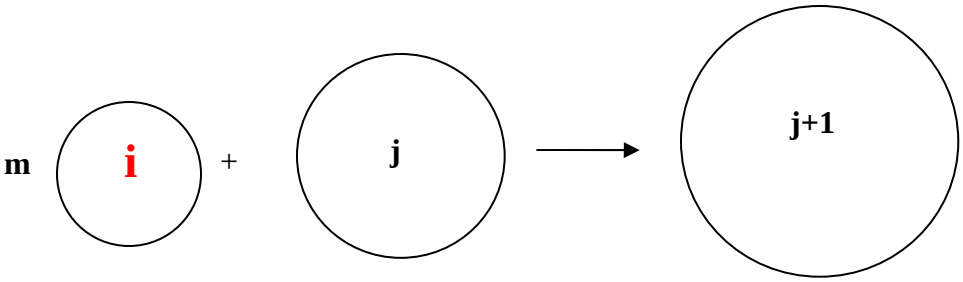

Figure A.4: Depletion 2 mechanism.

In our model for silica flocculation, the geometric population balance equation was written for 30 species (i.e. the largest species had 2^{29} number of primary units). Again, the collision kernel used was for reaction-limited aggregation (Ball):

$$K_{i.j} = c*(d_i + d_j)^2 \qquad \text{(A.3)}$$

To calculation d_i and d_j for the kernels, the diameter of the i^{th} (or j^{th}) aggregate can be calculated assuming that the aggregate is a fractal aggregate and that the fractal dimension is 2.0:

$$n_i = \left(\frac{d_i}{d_1} \right)^{D_f} \qquad \text{where} \qquad n_i = R^{i-1} \tag{A.4}$$

Where n_i is the number of primary particles in the ith aggregate, d_i is the diameter of the ith aggregate, d_1 is the diameter of the primary particles (set equal to 5nm because it is the value of particle diameter from the DLS data extrapolated to t=0), and D_f is the fractal dimension.

The 30 coupled differential equations were solved in Matlab 2008a using ode23. The only fitting parameter in the equations was the single value of "c" (a measure of the collision efficiency) in the collision kernels. The output of the differential equation solver was the concentration of each i^{th} aggregate versus time.

The next step was to convert the concentration of each i^{th} aggregate to the mean diameter for comparison with DLS data. The procedure is described below.

At a *given time*:

1) Convert concentration of each particle to intensity. That is,

$$\frac{I}{I_o} = \left(\frac{D}{D_o} \right)^6 \frac{C}{C_o} \tag{A.5}$$

where I_o, D_o, and C_o are reference values. For our conversion, we used reference values for the smallest particle, i.e. D=5nm. Thus, we set D_o equal to 5nm, C_o equal to the concentration of 5nm primary particles at the given time, and I_o to an arbitrary value of 1.

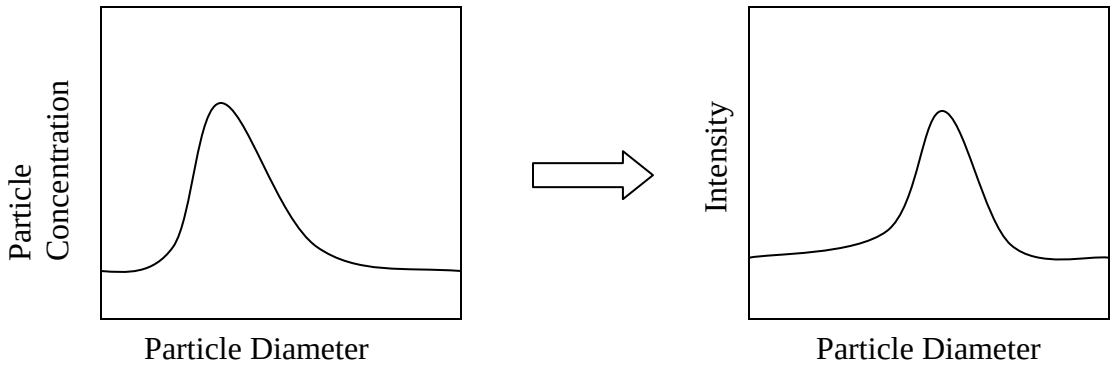

Figure A.5: Particle size number distributions from the Matlab simulation are converted to particle intensity distributions.

2) Calculate mean diameter from the intensity distributions:

$$\bar{d} = \frac{\sum_i d_i * I_i}{\sum_i I_i} \tag{A.6}$$

This gives the mean diameter from the intensity distribution for a certain time t.

3) Normalize the intensity vs. particle diameter distribution. That is, the area under the intensity vs. particle diameter distribution should be equal to 1. To do this, approximate the area under the intensity vs. diameter curve. Then, divide the intensity values by the area under the curve. This normalization procedure will allow comparison between the Matlab output and the DLS data.

4) Repeat steps 1-3 for the particle concentration vs. diameter data at each time t from the Matlab output.

Zetasizer Data Analysis

The Zetasizer Nano ZS outputs can output size distribution data in three ways: it can give the intensity distribution, which is the most accurate because it is the raw data (Zetasizer manual), it can give volume distribution, which it calculates internally by converting intensity to volume, and it can give particle frequency distribution, which is also calculated internally by converting intensity to particle number frequency.

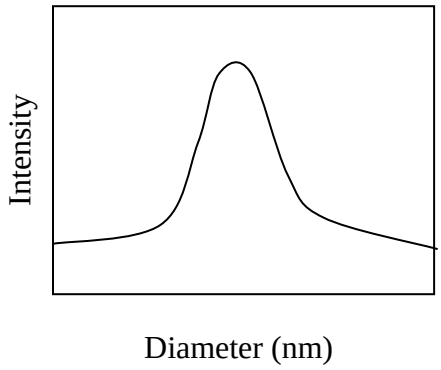

Figure A.6: Particle intensity distributions are the raw data output from the Zetasizer dynamic light scattering measurents.

The three distributions are related as such: intensity of a particle is proportional to the diameter of that particle to the 6^{th} power, volume of a particle is proportional to the diameter of that particle to the 3^{rd} power.

As stated above, we only use the intensity distribution from the Zetasizer. This distribution data is compared with the intensity distribution output from the Matlab model.

APPENDIX B

MATLAB R2008a CODE FOR SILICA PARTICLE FLOCCULATION MODELING

In file “ODE_Generation.m”:

```
function out = ODE_Generation(t,y,junk,Kernel)

%----------global variables that are used in this .m file--------
global N_s;
global R;
%-----------------------------------------------------------------


for k=1:N_s;
    sum=0;
    % NOTE:Kernel values are calculated in Si_particle_growth_acid.m

        %-------------------Generation 2 Mechanism-----------------
        if (k>2)
            for j=1:k-2
                sum=sum+Kernel(j,k-1)*((R^(j-k+1))/(R-1))*y(j)*y(k-1);
            end
        end
        %-------------------Generation 2 Mechanism-----------------


        %-------------------Generation 1 mechanism-----------------
        if (k>1)
            sum=sum+Kernel(k-1,k-1)*(1/R)*(y(k-1)*y(k-1));
        end
        %-------------------Generation 1 mechanism-----------------


        if (k<N_s)
        %-------------------Depletion 2 mechanism------------------
             for j=k:N_s-1
                sum=sum-Kernel(j,k)*y(j)*y(k);
             end
        %-------------------Depletion 2 mechanism------------------
```

```
        %-------------------Depletion 1 mechanism-----------------
        if (k>1)
             for j=1:k-1
                 sum=sum-Kernel(j,k)*((R^(j-k))/(R-1))*y(j)*y(k);
             end
        end
        %-------------------Depletion 1 mechanism-----------------
        end

   x(k)=sum;

end

%-----the output of this .m file is "out", which is a column vector
%whose elements are differential equations for each species.  For
%example, out(1)is the differential equation for d[y(1)]/dt, the change
%of species 1 (flocs with one primary particle) vs. time.  Similarly,
%out(3) is the change of species 3 (flocs with 2^(3-1)=4 primary
%particles) vs. time.-------------------------------------------------

out=x';
```

In file “Si_particle_growth_acid.m”:

```
%--------------global variables mean the value of these varibles are
%accessible to all functions declaring them global.  For example, if
%thevalue of "R" is changed in this .m file, then the value of "R" for
%the Si_particle_growth_acid.m file is changed because that file
%declared "R" a global variable---------------------------------------
global N_s;
global d_p;
global lamda;
global c;
global R;
%-----------------global variables-------------------------------------


%-----------------values of constants used in this code---------------
R=2; % geometric spacing for number of primary particles in each floc
lamda=2; % parameter for kernel calculations
N_s=30 % number of total species, equal to ODEs solved simultaneously
N_t=200; %number of "time points" for the code
Mw_monomer=96; %molecular weight of Si(OH)4 in g/mol
rho=2200; % density of amorphous silica is ~2200 g/L
M_v=Mw_monomer/((6.023*(10^26))*rho); % molecular vol of Si(OH)4 in m^3
dia_monomer=(6*M_v*7/22)^(1/3); % in meters, assuming spherical monomer
epsi=0.6366; % solid volume fraction in random close packing
%-----------------values of constants used in this code----------------


%--------------------initial concentration vector---------------------
y0=linspace(0,0,N_s);
tspan=linspace(0,tf,N_t);
%--------------------initial concentration vector---------------------


%-------------------------8 molar HCL---------------------------------
c=2.0*10^16; % a measure of the collision efficiency
Df=2.0; % fractal dimension
py=[12.4 6.42 34.6 48.71 66.92 143 198.2 258.6]; %DLS diam data in nm
tx=[20.36 39.93 61.02 79.50 100.62 120.63 141.37 161.77]; %DLS time
data in minutes
tf=3600*3; % final time in seconds
d_p(1)=5*(10^(-9)); % primary particle diameter in meters
no_molecule_primary=epsi*(d_p(1)/dia_monomer)^3 %number of molecules in
the primary particle
y0(1)=0.13/no_molecule_primary; %initial primary particle concentration
in kmol/m^3 or equivalently mol/L
%-------------------------8 molar HCL---------------------------------


%-------------------------4 molar HCL---------------------------------
%c=1*10^15;
%Df=2.0;
%py=[6.0 78.5 121.3 121.5 161.7 1624];
%tx=[270.9 1296.2 1391.0 1555.3 1708.9 3039.4];
```

```
%tf=3600*60;
%d_p(1)=5*(10^(-9));
%no_molecule_primary=epsi*(d_p(1)/dia_monomer)^3
%y0(1)=0.19/no_molecule_primary;
%-----------------------4 molar HCL---------------------------------


%-------------------------2 molar HCL---------------------------------
%c=9.9*10^13;
%Df=2.0;
%py=[6.1 32.7 49.0 65.1 85.0 94.6 122.3 129.2 372.3];
%tx=[1434 5459 7079 8566 9807 10125 11342 11552 15548 ];
%tf=3600*280;
%d_p(1)=5*(10^(-9));
%no_molecule_primary=epsi*(d_p(1)/dia_monomer)^3
%y0(1)=0.24/no_molecule_primary;
%-------------------------2 molar HCL---------------------------------


%---------------Calculation of diameter of each species--------------
p_size_lo=d_p(1);
n_m = zeros(1,N_s);
n_m(1)=1;
for j=2:N_s
   n_m(j)=R^(j-1);
        d_p(j)=p_size_lo*((n_m(j))^(1.0/Df));
end
%---------------Calculation of diameter of each species--------------


%------------------Calcuation of Kernel values-----------------------
Kernel=zeros(N_s);
 for j=1:N_s
    for k=1:N_s
Kernel(j,k)=c*(d_p(j)+d_p(k))^lamda;
    end
 end
%------------------Calcuation of Kernel values-----------------------


%--Simultaneously solve ODEs in "ODE Generation.m" using solver ode23--
  options = odeset('NonNegative',[1:30],'RelTol', 1e-15,'AbsTol',1e-
  15,'InitialStep',0.00000001);
  [T,Y]=ode23('ODE_Generation',tspan,y0,options,Kernel);
  %tpan is time vector, y0 is initial concentration vector, options is
  %the ode solver options, and Kernel contains the value of the kernels

  %output is matrix [T,Y], the first column of this matrix is the
  %tspan vector, the second column of this matrix is the concentration
  %of y(1) (the primary particles) corresponding to each time in tspan.
  %The third column of this matrix is the concentration of y(2), the
  %floc with 2 primary particles corresponding to each time in tspan,
  %etc.
%--Simultaneously solve ODEs in "ODE Generation.m" using solver ode23--
```

```
%------------------------Check mole conservation-----------------------
s=zeros(1, N_t);
for j=1:N_t
    total_monomers=0;
    for i=1:N_s;
    total_monomers=total_monomers+Y(j,i)*(R^(i-1));
    end
    s(j)=total_monomers; % number of total monomers at each time
end
%------------------------Check mole conservation-----------------------


%--------Convert solver-output concentration data to intensity data----
   intensity=zeros(N_t, N_s);
   for j=1:N_t
       for i=1:N_s
           intensity(j,i)=Y(j,i)/Y(j,1)*(d_p(i)/d_p(1))^6;
       end
   end
%--------Convert solver-output concentration data to intensity data----


%---------Calculate mean diameter from the intensity distributions-----
  avg_diameter_intensity=zeros(1,N_t);
  for j=1:N_t
      intensity_sum=0;
      total_intensity=0;
      for i=1:N_s
          intensity_sum=intensity_sum+intensity(j,i)*d_p(i);
          total_intensity=total_intensity+intensity(j,i);
      end
      avg_diameter_intensity(j)=intensity_sum*10^9/total_intensity;
  end
%---------Calculate mean diameter from the intensity distributions-----


%---------Plot mean intensity diameter calculated from ODE solver
%output and plot DLS mean intensity diameter--------------------------
  semilogy(tx,py,'o',T/60,avg_diameter_intensity);
  xlabel ('Time, min'),ylabel ('mean aggregate diameter, nm')
%---------Plot mean intensity diameter calculated from ODE solver
%output and plot DLS mean intensity diameter--------------------------


xlswrite ('scratch',Y) % Print any matrix to the first sheet in
"scratch.xls" in the working directory
```

APPENDIX C

SILICA PRECIPITATION WITH ANALCIME FILTERED OUT OF SOLUTION

8 grams of analcime were dissolved in 300 mL of 8M hydrochloric acid. The reactor was kept at 5.0°C and the solution was stirred at 500 rpm. A second reactor was pre-cooled to 5.0°C. Thirty minutes into the reaction, when the silicon had reached its plateau height, 60 mL of the reaction solution was filtered with 0.2 micron filters into the second reactor. The filtered solution was then stirred at 500 rpm. The concentration of silicon in solution was followed in both solutions using AAS.

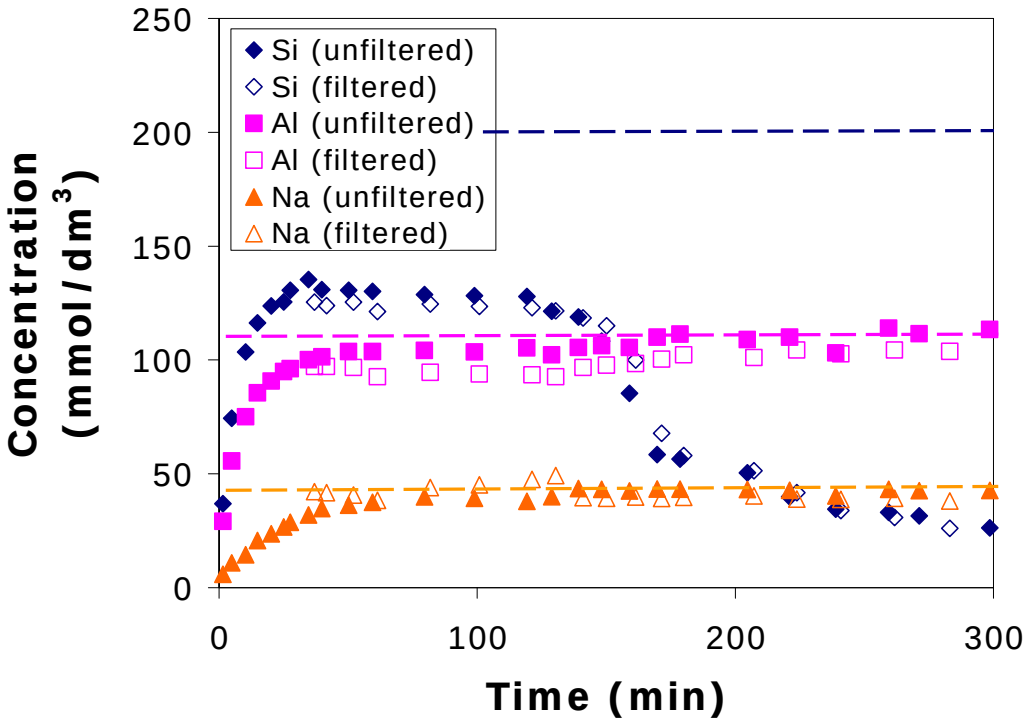

Figure C.1: Concentration of silicon, aluminum, and sodium after analcime dissolution in an unfiltered and a filtered solution. Analcime particles filtered out at 30 minutes for the filtered solution.

From Figure C.1, one observes that silica precipitates in the same manner whether analcime particles exist in the solution or do not. Thus, it is concluded that the presence of analcime particles do not influence silica precipitation behaviour in 8M hydrochloric acid. This supports our statement in the introduction that precipitation of silicon is generally homogenous. In addition, this experiment logically leads to using pure monosilicic acid solutions to study silicon precipitation after analcime dissolution.

APPENDIX D

EFFECT OF TEMPERATURE ON PLATEAU HEIGHT AND PRECIPTIATION AS MEASURED BY AAS OR ICP-MS

For this appendix, we will define the "precipitation time" in different solutions to be the approximate time the silicon concentration decreases as measured by AAS or ICP. For example, the precipitation time of the base-case would be 130 minutes.

As shown in figures D.1 and D.2 below, temperature affects the precipitation time, i.e the rate of silica particle growth, but it does not affect the silicon plateau height.

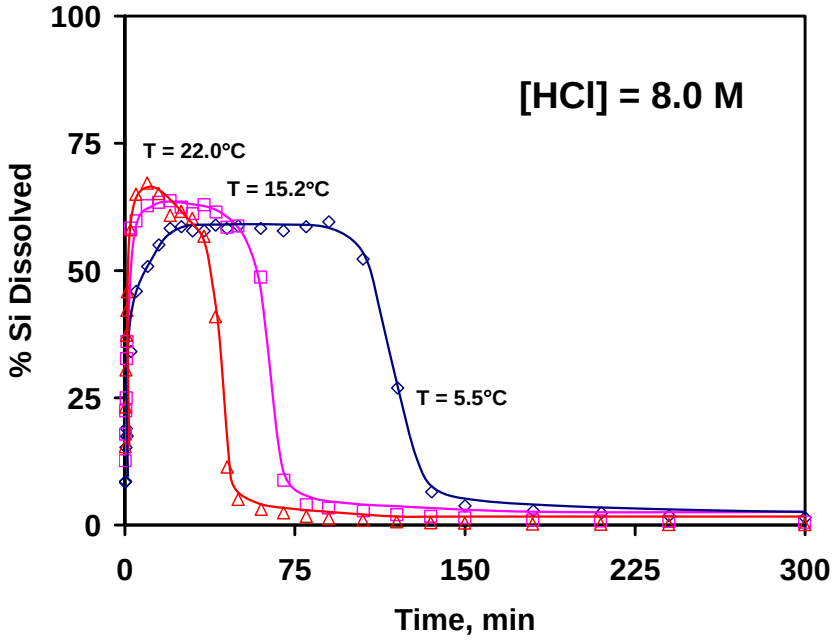

Figure D.1: Dissolution of analcime in 8M HCl at 22.0, 15.2, and 5.5ºC. *8g analcime, 300 mL solution, 500 rpm.* Figure from R. L. Hartman thesis, University of Michigan, Ann Arbor, 2005.

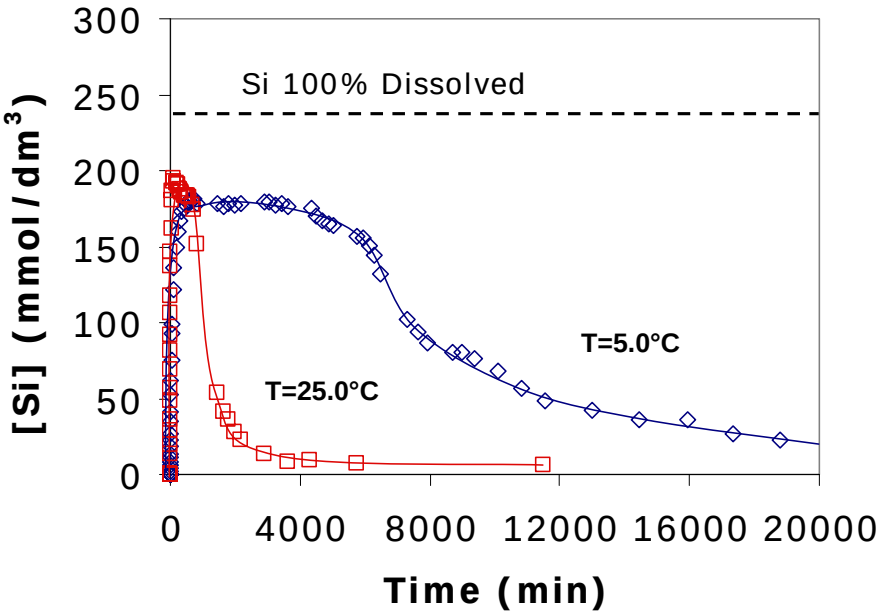

Figure D.2: Dissolution of analcime in 3M citric acid at 25.0 and 5.0ºC. *8g analcime, 300 mL solution, 500 rpm.*

The precipitation time for different HCl concentrations at 5.0°C was measured from data in Figure 3.4. The precipitation time for 3 solutions at 22.0°C and for 1 solution at 15.2°C was estimated from R.L. Hartman's thesis, University of Michigan, Ann Arbor, 2005. The results are graphed in Figure D.3.

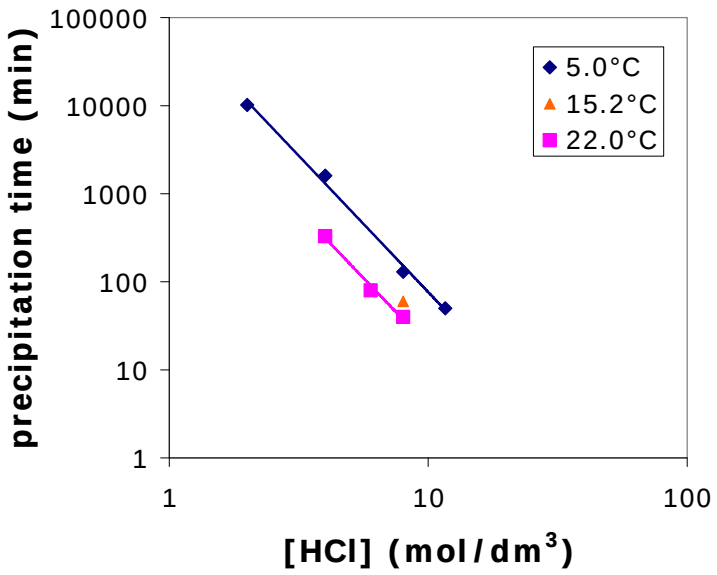

Figure D.3: Precipitation time vs. HCl concentration at 5.0, 15.2, and 22.0 °C.

The precipitation time vs. [HCl] curves were fit to a power law model:

$$\text{5.0°C:} \quad t_p = 95479\,[HCl\,]^{-3.0966}$$

$$\text{22.0°C:} \quad t_p = 22258\,[HCl\,]^{-3.0740}$$

The fit of the power law model was excellent, with R^2 values of 0.9956 and 0.9905 for the 5.0°C and 22.0°C curves, repectively.

$$\frac{t_{p,5.0}}{t_{p,22.0}} \approx \frac{95479[HCl]^{-3}}{22258[HCl]^{-3}} \approx 4.29$$

Thus, the precipitation time at 5.0°C is approximately 4.3 times greater than the precipitation time at 22.0°C. This is linked, of course, to the silicate particle growth, as the precipitation time is the approximate time the particles grow to 0.2 microns in size.

APPENDIX E

HYDRATION OF IONS AND EFFECT OF ANIONS ON SILICA PARITCLE GROWTH

Figure E.1 shows silica particle growth in 4M hydrochloric acid solutions with 1M of sodium salt added. The sodium salts increase the silica particle growth rate in the order NaBr > NaCl ≈ $NaNO_3$.

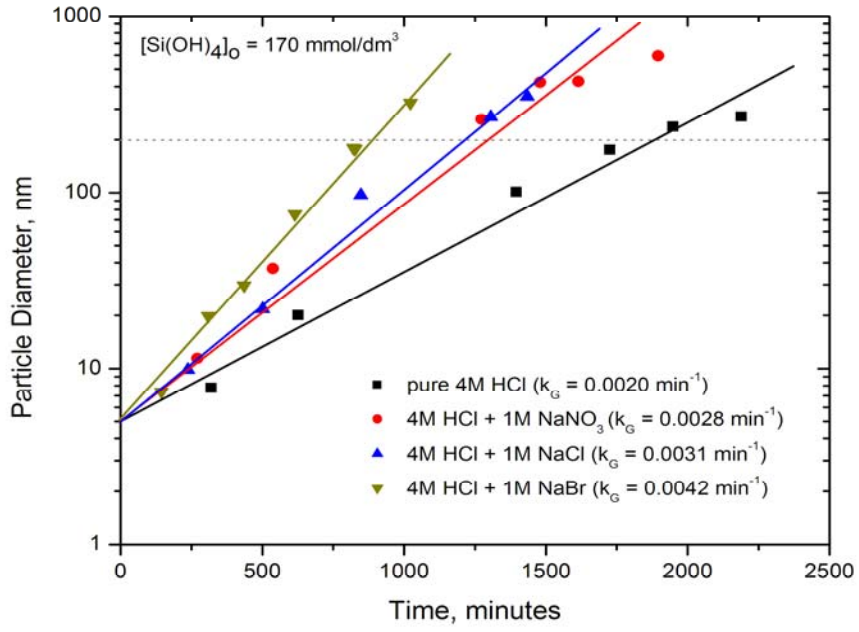

Figure E.1: Mean silica particle diameter measured by DLS in 4M HCl plus 1M sodium salt solutions. *$[Si(OH)_4]_0$=170 mmol/L, 5.0ºC, 500rpm.*

Referring to Table E.1, one observes that aggregation rate constant increases as ion hydration radius increases. It was hypothesized that an increasing ionic radius for the salts could cause faster silica particle growth by 1) disordering the hydration spheres surrounding the silica particle allowing faster flocculation or by 2) excluding silica from their hydration sphere effectively concentrating the silica in solution. However, these mechanisms are up for debate and furthermore, the correlation between particle growth rate and hydration radius does not necessarily mean there is a cause and effect here.

Table E.1: Properties of the 4M HCl plus salt solutions. The particle growth rate constant measured by DLS is tabulated in the second column for each of the solutions.

Chemicals	**Aggregation rate constant, min-1**	**Ionic strength, mol/dm3**	**Hydration number (±1)**	**Hydration radius, nm**	**Bare ion radius, nm**
Base case					
4M HCl	0.0020	4	3	0.28	-
With 1M Chloride salts					
Cs+	0.0020	5	1 – 2	0.33	0.169
Na+	0.0031	5	4 – 5	0.36	0.095
Mg2+	0.0090	7	~6	0.43	0.065
Ca2+	0.0175	7	6	0.41	0.099
Al3+	0.0216	10	~6	0.48	0.050
With 1M Sodium salts					
NO3-	0.0028	5	0	0.34	0.264
Cl-	0.0031	5	1	0.36	0.181
Br-	0.0042	5	1	0.33	0.195

APPENDIX F

MONOSILICIC ACID DISAPPEARANCE: A CLOSER LOOK AT THE SECOND AND THIRD ORDER RATE LAWS

Figure F.1 shows UV-Vis monosilicic acid concentration as the rate function $\frac{1}{2}\left[\frac{1}{[Si(OH)_4]^2} - \frac{1}{[Si(OH)_4]_o^{\ 2}}\right]$ vs. time. Recall that this rate function arises when the rate law $\frac{d[Si(OH)_4]}{dt} = -k_D[Si(OH)_4]^3$ is integrated. Figure F.2 shows the rate function for 6, 4, and 2M HCl in more detail.

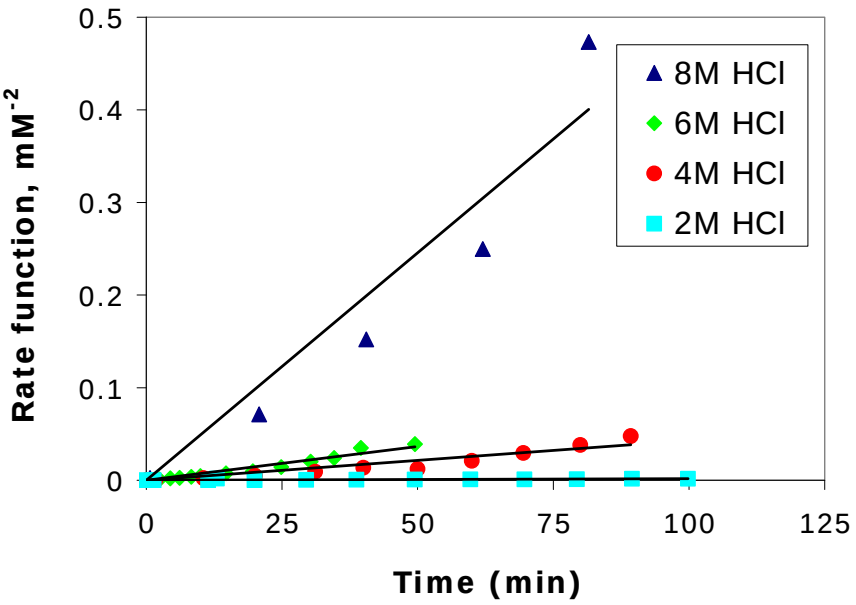

Figure F.1: Rate function for a third-order monosilicic acid disappearance plotted vs. time

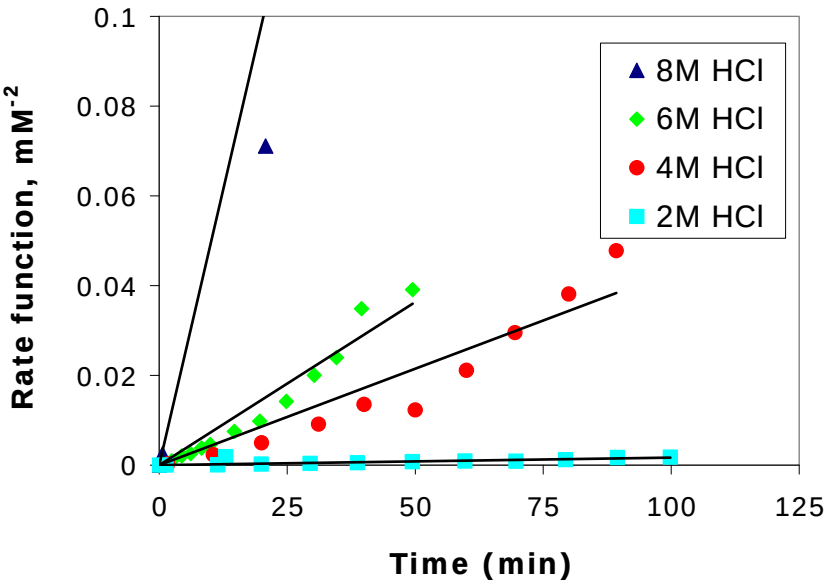

Figure F.2: Rate function for a third-order monosilicic acid disappearance plotted vs. time.

Comparing Figure F.1 and Figure F.2 to Figure 3.8, it is observed that the third-order rate law fits the monosilicic acid disappearance better than a second-order rate law.

Figure F.3 shows UV-Vis monosilicic acid concentration in salt solutions as the rate function $\frac{[Si(OH)_4]_O}{[Si(OH)_4]}$ vs. time. Recall that this rate function arises when the rate law $\frac{d[Si(OH)_4]}{dt} = -k_D[Si(OH)_4]^2$ is integrated.

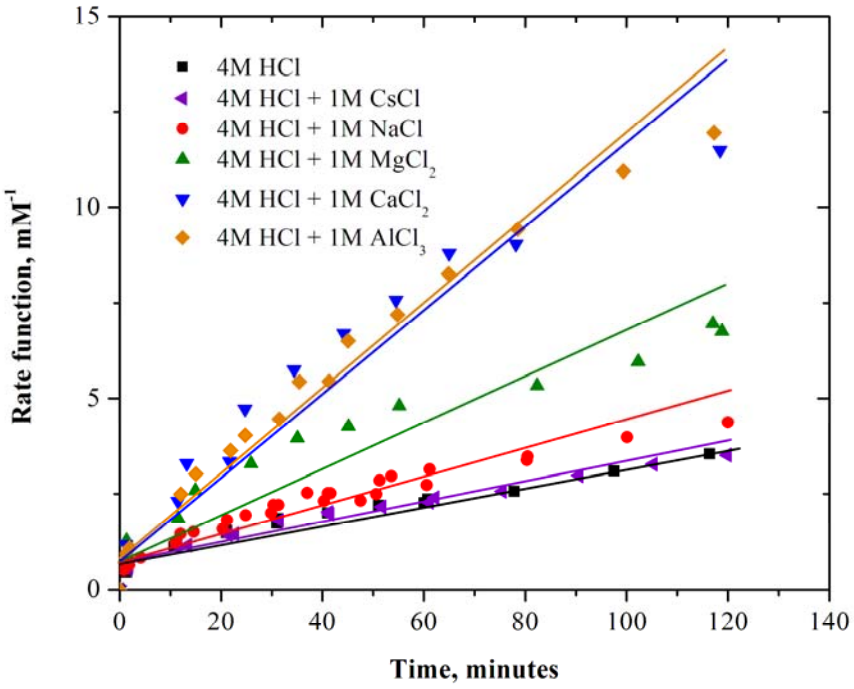

Figure F.3: Rate function for a second-order monosilicic acid disappearance plotted vs. time for salt solutions.

Comparing Figure F.3 to Figure 4.8, it is observed that when salt is present, a third-order rate law for monosilicic acid disappearance is better than a second-order rate law fit.